QUANTIFYING CORN EMERGENCE USING UAV IMAGERY AND MACHINE LEARNING

A Dissertation

presented to

the Faculty of the Graduate School

at the University of Missouri – Columbia

In Partial Fulfillment

of the Requirements for the Degree

Doctor of Philosophy

---

by

CHIN NEE VONG

Dr. Jianfeng Zhou, Dissertation Supervisor

MAY 2022

The undersigned, appointed by the dean of the Graduate School, have examined the dissertation entitled

QUANTIFYING CORN EMERGENCE
USING UAV IMAGERY AND MACHINE LEARNING

presented by Chin Nee Vong,

a candidate for the degree of doctor of philosophy of Food and Hospitality Systems,

and hereby certify that, in their opinion, it is worthy of acceptance.

_____

Dr. Jianfeng Zhou

_____

Dr. Azlin Mustapha

_____

Dr. Leon G. Schumacher

_____

Dr. Kenneth A. Sudduth

_____

Dr. Newell R. Kitchen

DEDICATION

I dedicate my dissertation work to all my beloved family and friends. Expressing my gratitude to my parents, brothers, and sisters-in-law in Malaysia who have supported me all the while not only for my PhD journey but my every single moment from the past 31 years. A special gratitude to my eldest brother in the US who always take good care of me since I came to US. Without them, I will not be who I am now. I will always appreciate their love.

I also dedicate this dissertation work to many of my friends in Malaysia and US, who have been good listeners and supporters to me. They helped me to go through the toughest moments in graduate school journey. Special thanks to the friends I know through Mizzou International Christian Fellowship, whom we have countless of meaningful conversations, yearly Thanksgiving meals, and different activities (hiking, horse-back riding, Independence Day celebration, etc.). I feel so grateful to meet all these friends and always appreciate our friendships.

Last but not least, I dedicate my work to my husband, Dr. Jingkai Wei for his endless love, supports, and encouragements for me to successfully complete my PhD journey. I will always appreciate all of his love.

ACKNOWLEDGEMENT

I would like to express my gratitude to my academic advisor and committee chair, Dr. Jianfeng Zhou for his continued advice, guidance, and support throughout my dissertation projects. He provided me a great opportunity to study and work in Mizzou Precision and Automated Agriculture Lab (PAAL), which helped me in gaining more research experiences to solve agricultural problems and improve agricultural productivity using engineering approaches and techniques. Furthermore, he is always willing to connect me with other research groups, which helped me to complete my dissertation projects successfully as well as expanded my networks. These projects would not have been possible without her supervision and support.

I would also like to extend my gratitude to my committee members, Dr. Newell R. Kitchen and Dr. Kenneth A. Sudduth, who have provided me great suggestions, guidance, supports, and resources such as experiment sites, data collection and analysis, and manuscript preparation for my dissertation projects. Their passions in research from different perspectives (agronomy and engineering) will lead me to be a 'keep learning, keep improving' future researcher to keep working on projects relating to agricultural field. I am also extremely grateful to my other two committee members, Dr. Azlin Mustapha and Dr. Leon G. Schumacher for spending time and efforts in checking my academic and research progress and providing recommendations for my projects. Their different expertized focuses had led me to think more broadly and creatively for various possible insights about my current and future research projects. A special thanks to Dr. Allen L. Thompson, who showed me great techniques in teaching and interacting with students when I worked as teaching assistant with him. His passion in teaching had

enhanced my teaching philosophy not just towards students in a class but also towards anyone who I will be supervised on in the future.

I would like to express my sincere thanks to all my past and present co-workers especially Dr. Jing Zhou, Dr. Aijing Feng, Dr. Dandan Fu, Lance S. Conway, Stirling A. Stewart, and Shagor Sarkar for their generous assistance in data collection, data analysis, and manuscript preparation. They have been always my great supports, mentors, and friends for me to complete my doctoral program. It is a great pleasure working with them.

Completing a dissertation is a tough journey but I am so grateful to have all my professors, families, and friends as dedicated and acknowledged for helping me in going through the PhD journey and stay strong for my future.

TABLE OF CONTENTS

LIST OF ILLUSTRATIONS

LIST OF TABLES

LIST OF ABBREVIATIONS

ANOVA	Analysis OF Variance
ARS	Agricultural Research Service
CA	Conservation Agriculture
CART	Classification And Regression Tree
CEC	Cation Exchange Capacity
CNN	Convolutional Neural Network
CS	Cropping System
CV	Coefficient of Variation
DAE	Days After Emergence
DAEmean	Mean Days to Imaging After Emergence
DAP	Days After Planting
DL	Deep Learning
DVI	Difference Vegetation Index
EC	Electrical Conductivity
EC_a	Apparent Electrical Conductivity
ExG	Excess Green
ExR	Excess Red
FPS	Frame Per Second
GDD	Growing Degree Day
GDU	Growing Degree Units
GDVI	Green Difference Vegetation Index
GLI	Green Leaf Index

GNDVI	Green Normalized Difference Vegetation Index
GOSAVI	Green Optimized Soil Adjusted Vegetation Index
GRVI	Green Ratio Vegetation Index
GSAVI	Green Soil Adjusted Vegetation Index
GSD	Ground Sampling Distance
HSD	Honest Significant Difference
HSV	Hue, Saturation, Value
ISO	International Organization for Standardization
LAI	Leaf Area Index
LTAR	Long-Term Agroecosystem Research
MAPE	Mean Absolute Percentage Error
ML	Machine Learning
MNVI	Difference between Excess Green and Excess Red
MTCS	Minimum-Till Corn-Soybean Rotation
N	Nitrogen
NGRDI	Normalized Green minus Red Difference Index
NDRE	Normalized Difference Red-edge
NDVI	Normalized Difference Vegetation Index
NormG	Normalized Green
NormNIR	Normalized Near-infrared
NormR	Normalized Red
NTCC	No-Till Corn-Corn Rotation with Cover Crop Implementation
NTCS	No-Till Corn-Soybean Rotation

OSAVI	Optimized Soil Adjusted Vegetation Index
PA	Precision Agriculture
PS	Plant Spacing
PSstd	Plant Spacing Standard Deviation
R	Replication
R^2	Coefficient of Determination
R-CNN	Region based Convolutional Neural Networks
ReLU	Rectified Linear Unit
RF	Random Forest
RGB	Red-Green-Blue
RMSE	Root Mean Square Error
ROI	Region Of Interest
RVI	Ratio Vegetation Index
SAVI	Soil Adjusted Vegetation Index
SD	Standard Deviation
SHT	Standard Hough Transformation
VIF	Variance Inflation Factor
VIRE	Vegetation Index Red-edge
VIs	Vegetation indices
UAV	Unmanned Aerial Vehicle
USDA	United States Department of Agriculture
YOLO	You Only Look Once

QUANTIFYING CORN EMERGENCE
USING UAV IMAGERY AND MACHINE LEARNING

Chin Nee Vong

Dr. Jianfeng Zhou, Dissertation Supervisor

ABSTRACT

Corn (*Zea mays* L.) is one of the important crops in the United States for animal feed, ethanol production, and human consumption. To maximize the final corn yield, one of the critical factors to consider is to improve the corn emergence uniformity temporally (emergence date) and spatially (plant spacing). Conventionally, the assessment of emergence uniformity usually is performed through visual observation by farmers at selected small plots to represent the whole field, but this is limited by time and labor needed. With the advance of unmanned aerial vehicle (UAV)-based imaging technology and advanced image processing techniques powered by machine learning (ML) and deep learning (DL), a more automatic, non-subjective, precise, and accurate field-scale assessment of emergence uniformity becomes possible. Previous studies had demonstrated the success of crop emergence uniformity using UAV imagery, specifically at fields with simple soil background. There is no research having investigated the feasibility of UAV imagery in the corn emergence assessment at fields of conservation agriculture that are covered with cover crops or residues to improve soil health and sustainability.

The overall goal of this research was to develop a fast and accurate method for the assessment of corn emergence using UAV imagery, ML and DL techniques. The pertinent information is essential for corn production early and in-season decision making as well as agronomy research. The research comprised three main studies, including

Study 1: quantifying corn emergence date using UAV imagery and a ML model; Study 2: estimating corn stand count in different cropping systems (CS) using UAV images and DL; and Study 3: estimating and mapping corn emergence under different planting depths. Two case studies extended Study 3 to field-scale applications by relating emergence uniformity derived from the developed method to planting depths treatments and estimating final yield. For all studies, the primary imagery data were collected using a consumer-grade UAV equipped with a red-green-blue (RGB) camera at a flight height of approximate 10 m above ground level. The imagery data had a ground sampling distance (GSD) of 0.55 – 3.00 mm $pixel^{-1}$ that was sufficient to detect small size seedlings. In addition, a UAV multispectral camera was used to capture corn plants at early growth stages (V4, V6, and V7) in case studies to extract plant reflectance (vegetation indices, VIs) as plant growth variation indicators. Random forest (RF) ML models were used to classify the corn emergence date based on the days after emergence (DAE) to time of assessment and estimate yield. The DL models, U-Net and ResNet18, were used to segment corn seedlings from UAV images and estimate emergence parameters, including plant density, average DAE (DAEmean), and plant spacing standard deviation (PSstd), respectively.

Results from Study 1 indicated that individual corn plant quantification using UAV imagery and a RF ML model achieved moderate classification accuracies of 0.20 - 0.49 that increased to 0.55 – 0.88 when DAE classification was expanded to be within a 3-day window. In Study 2, the precision for image segmentation by the U-Net model was ≥ 0.81 for all CS, resulting in high accuracies in estimating plant density ($R^2 \geq 0.92$; RMSE ≤ 0.48 plants m^{-1}). Then, the ResNet18 model in Study 3 was able to estimate

emergence parameters with high accuracies (0.97, 0.95, and 0.73 for plant density, DAEmean, and PSstd, respectively). Case studies showed that crop emergence maps and evaluation in field conditions indicated an expected trend of decreasing plant density and DAEmean with increasing planting depths and opposite results for PSstd. However, mixed trends were found for emergence parameters among planting depths at different replications and across the N-S direction of the fields. For yield estimation, emergence data alone did not show any relation with final yield (R^2 = 0.01, RMSE = 720 kg ha^{-1}). The combination of VIs from all the growth stages was only able to estimate yield with R^2 of 0.34 and RMSE of 560 kg ha^{-1}.

In summary, this research demonstrated the success of UAV imagery and ML/DL techniques in assessing and mapping corn emergence at fields practicing all or some components of conservation agriculture. The findings give more insights for future agronomic and breeding studies in providing field-scale crop emergence evaluations as affected by treatments and management as well as relating emergence assessment to final yield. In addition, these emergence evaluations may be useful for commercial companies when needing justification for developing new technologies relating to precision planting to crop performance. For commercial crop production, more comprehensive emergence maps (in terms of temporal and spatial uniformity) will help to make better replanting or early management decisions. Further enhancement of the methods such as more validation studies in different locations and years as well as development of interactive frameworks will establish a more automatic, robust, precise, accurate, and ‘ready-to-use’ approach in estimating and mapping crop emergence uniformity.

CITATION OF PUBLISHED WORK

Three chapters of this dissertation have been published/accepted as follows:

Chapter 2

Vong, C. N., Stewart, S. A., Zhou, J., Kitchen, N. R., & Sudduth, K. A. (2021). Corn emergence date estimation using UAV imagery. *Transactions of the ASABE*, *64(4)*, 1173-1183. https://doi.org/10.13031/trans.14145.

Chapter 3

Vong, C. N., Conway, L. S., Zhou, J., Kitchen, N. R., & Sudduth, K. A. (2021). Early corn stand count of different cropping systems using UAV-imagery and deep learning. *Computers and Electronics in Agriculture*, *186*, 106214. https://doi.org/10.1016/j.compag.2021.106214.

Chapter 4

Vong, C. N., Conway, L. S., Feng, A., Zhou, J., Kitchen, N. R., & Sudduth, K. A. (2022). Corn emergence uniformity estimation and mapping using UAV imagery and a deep learning model. *Computers and Electronics in Agriculture*. Accepted paper.

CHAPTER ONE

INTRODUCTION

1.1 Background and Problem Statement

Corn (*Zea mays L.*) is one of the vital crops in the United States with about 37.8 million hectares planted area and 11.11 metric tons of grain yield per hectare in 2021 (USDA, 2022). The usage of corn in US was mostly for animal feed (nearly half) as it provides a good source of energy, followed by ethanol production, export to other countries, and human consumption (USDA, 2015). Achieving a high corn yield is usually the ultimate goal for production, yet, reducing negative impacts to the environment such as reducing excess runoff of chemical applications is also critical to ensure long-term sustainable production to provide adequate food for the future population (Hunt et al., 2019).

One of the initial factors affecting the final yield is the corn emergence uniformity, which can be evaluated temporally (by emergence date) and spatially (by plant spacing). Corn plants that emerge uniformly at about the same time and sufficient distance between them reduce competition for available water, nutrients, and sunlight as well as limit weed intrusion (Karayel & Özmerzi, 2008; Zhang et al., 2018). Previous research indicated that temporal variation in emergence causes consistent yield reductions. For example, Nafziger et al. (1991) indicated that with delayed planting of 10 to 12 and 22 days, the average yield decreased by 6% and 12%, respectively. Another study showed an average yield reduction by 4.3% and 8.7% when planting was delayed for 12 and 21 days, respectively (Liu et al., 2004a). Moreover, Andrade and Abbate (2005) also illustrated that the average yield difference between plots with emergence

variability of three days was about 12% less than that of control plots with uniform emergence.

On the other hand, mixed results were found on the effects of spatial variability in plant spacing on yield. For instance, Lauer and Rankin (2004) showed a decrease of 5% to 18% in relative yield when plant spacing standard deviation was above 12 cm. A separate study showed an average yield decrease of 62 kg ha^{-1} for each centimeter increase in plant spacing standard deviation when it was greater than 5 cm (Nielsen, 2001). However, Liu et al. (2004b) indicated that there was no strong correlation between plant spacing standard deviation and yield ($R^2 = 0.06$).

With these studies showing negative effects of emergence uniformity on yield, early assessment of emergence parameters, including stand count, emergence date, and plant spacing variability, become valuable for early and in-season management decisions, such as replanting, post-emerge herbicide applications, and fertilizers applications (Vong et al., 2021). Furthermore, these assessments can be used to evaluate spatial yield variability as shown in yield maps. However, these measurements were seldom conducted in commercial fields, which is mostly due to the time-consuming and labor-intensive manual measurements needed especially for large fields (Varela et al., 2018). These manual measurements can only be done by field scouting at multiple sites, which is subjective and may not be representative of whole fields with variable soil conditions and landscape positions that affect the seed germination and emergence.

With the advent of unmanned aerial vehicle (UAV)-based imaging and advanced image processing techniques, a more automatic, non-subjective, precise, and accurate assessment of emergence is now feasible. Many studies have shown the usage of high-

resolution red-green-blue (RGB) UAV imagery for evaluating crop emergence such as plant density, emergence rate, coefficient of variation of emergence region, canopy cover, and spacing uniformity of corn, wheat, cotton, and potato with a high coefficient of determination of $R^2 > 0.80$ (Feng et al., 2020; Jin et al., 2017; Li et al., 2019; Liu et al., 2017; Shirzadifar et al., 2020; Shuai et al., 2019). Moreover, some studies also indicated success of mapping corn and wheat emergence and status at a field scale using an orthomosaic generated from the sequential images captured by an UAV (Shirzadifar et al., 2020; Sona et al., 2016; Torres-Sánchez et al., 2014). These maps are beneficial in visualizing the crop emergence and status in the field and to examine emergence variability due to different environment or treatment factors and relating to spatial yield variability.

Among the studies of UAV applications in estimating corn emergence, none of them had detected corn at a much earlier stage (before V2) and determined the corn emerged date and temporal emergence uniformity. Most of the studies were focused on estimating corn stand count at V2 to V8 vegetative growth stages in fields under conventional agriculture (with conventional tillage or minimum tillage forming a simple image background dominated by soil) (Gnädinger & Schmidhalter, 2017; Kitano et al., 2019; Shuai et al., 2019; Varela et al., 2018). They were not applied to corn fields practicing conservation agriculture (CA) with more complex background containing a mixture of soil and crop residue from previous crops and cover crops. In recent years, CA with principles of crop planting with minimum soil disturbance (i.e., no-till), permanent soil cover from crop residues or cover crops, and crop rotation has become popular in practice as it can mitigate negative environmental impacts while maintaining desired

yield (Conway et al., 2018; Hobbs et al., 2008; Yost et al., 2016). Meanwhile, limited studies have demonstrated corn emergence uniformity mapping (Shirzadifar et al., 2020) and studied the relationship between emergence uniformity and early growth as well as final yield using UAV imagery at a field scale.

There is a need in further discovering the potential of UAV imagery in evaluating corn emergence uniformity and the effects on early growth and final yield at a field scale in fields practicing CA. To accomplish this, new methods such as machine learning and deep learning techniques are needed.

1.2 Literature Review

1.2.1 Corn Emergence Parameters

One of the corn emergence parameters is plant density, defined as the number of plants per unit area. It is also one of the grain yield components (i.e., ear number per unit area, seed number per ear, and seed weight) in maximizing the final corn yield (Assefa et al., 2016). A higher plant density increases yield as there are more plants per unit area. However, it increases the interplant competition for sunlight, water, and nutrients resulting in increased stem lodging and barrenness (Sangoi, 2001). Subsequently, the number of ears produced per plant and kernels set per ear will decrease and reduce the final grain yield. On the other hand, a lower plant density will not secure a good yield as modern corn hybrids usually produce only one ear per plant (Sangoi, 2001). Hence, an optimum plant density is required when planting corn in different conditions.

The other corn emergence parameters describing emergence uniformity are emergence time (temporal) and plant spacing (spatial). Uniform emergence is desired as it reduces competition for the available resources among plants and increases yield.

Factors affecting this uniform emergence include soil environment, planting depths, planter performance, management practices, and their interactions (Andrade & Abbate, 2005; Pommel et al., 2002; Rutto et al., 2014). A good seed-soil contact is critical for successful germination, where the ideal condition is when the soil temperature is between 20 to 30 °C and moisture is near field capacity (Schneider & Gupta, 1985). These factors will be influenced by planting depths and management practices, for instance, a deeper depth and surface residue (from no-till) lowers the soil temperature and increases the time for the coleoptile elongation to the soil surface (Pommel et al., 2002). At the same time, seeds should not be planted too shallow (<1.9 cm) to attain a strong nodal system for plant structural support and increased resistance to drought stress. Meanwhile, planters with low precision in placing seeds and careless planting operations (traveling at high speed) also result in non-uniform emergence (Andrade & Abbate, 2005). These factors will not just induce seeds to emerge at different times but also result in missing plants when seeds do not germinate or experience early death, subsequently resulting in higher plant spacing (average and standard deviation) and lower plant density.

1.2.2 Conservation Agriculture (CA)

Conservation agriculture (CA) has been known as a strategy to manage agro-ecosystems with the aims to increase or maintain productivity, profits, and food security as well as conserving and enhancing the resource base and environment (Friedrich et al., 2012). It is composed of three cropping management principles, which are crop planting with continuous zero or minimum soil disturbance (e.g., no-till and minimum disturbance from farm traffic), permanent organic soil cover from previous crop residues or cover crops, and crop rotation to diversify the crop species grown (Friedrich et al., 2012; Hobbs

et al., 2008; Pittelkow et al., 2015). Studies demonstrated that CA with no-till, crop rotation, and cover crop implementation improved soil health (e.g., increased soil organic matter) when compared to minimum-till or plow-till while maintaining or increasing yield (Conway et al., 2018; Nunes et al., 2018). This improved soil health lowers the overall fertilizer inputs, increasing crop productivity and reducing negative environmental impacts such as excess fertilizer runoff (Conway et al., 2018; Johnston et al., 2009). Moreover, with the same crop rotation (corn-soybean), corn yield was similar between no-till and mulch tillage and yield stability was higher in no-till (Yost et al., 2016). These results collectively indicated that CA could achieve the goal of long-term sustainable agricultural production, which is to produce more food from limited lands by using natural resources efficiently with minimal impact on the environment (Hobbs et al., 2008). This can then provide sufficient food for our future generations.

1.2.3 UAV System in Assessing Crop Emergence

An UAV can be defined as a space-traversing vehicle operated by remote control or flying autonomously without needing a human crew on board (Cai et al., 2014). The two common types of UAV are fixed-wing and rotary-wing (Radoglou-Grammatikis et al., 2020). The former has a predefined airfoil and fixed wings to enable lift based on the UAV forward airspeed while the later (also known as multirotor UAV) has more than two rotors to produce appropriate power for the propellers to create lift for take-off and active flight. A rotary-wing UAV has the advantage over fixed wing UAV that they are easier to fly, take-off, and land as operation by controllers and autonomous flight is feasible (Thamm et al., 2015). Furthermore, they do not need a landing strip (as needed by a fixed-wing UAV), which is more convenient in field conditions. However, they have

the limitation of shorter flight time (12 to 30 mins) and restricted speeds to cover a large area (Cai et al., 2014). Despite of the disadvantages of rotary-wing UAV, they are still widely utilized in studies for agricultural applications due to their more user-friendly and developed features.

Numerous studies used the rotary-wing UAV to assess crop emergence such as corn (Gnädinger & Schmidhalter, 2017; Shirzadifar et al., 2020; Shuai et al., 2019; Varela et al., 2018), wheat (Jin et al., 2017; Liu et al., 2017), cotton (Chen et al., 2018; Feng et al., 2020), rapeseed (Zhao et al., 2018), and potato (Li et al., 2019). The emergence assessment consisted of stand count or plant density (Chen et al., 2018; Feng et al., 2020; Gnädinger & Schmidhalter, 2017; Jin et al., 2017; Shirzadifar et al., 2020; Shuai et al., 2019; Varela et al., 2018; Zhao et al., 2018), spacing uniformity (Shirzadifar et al., 2020), emergence rate (Li et al., 2019), coefficient of variation (CV) of emergence region (Liu et al., 2017), and canopy cover (Feng et al., 2020; Li et al., 2019). The rotary-wing UAV used, as categorized based on number of rotors, included quadcopters (e.g., DJI Mavic Pro, DJI Phantom 2 and 4, and DJI 1 Inspire) (Chen et al., 2018; Feng et al., 2020; Liu et al., 2017; Shirzadifar et al., 2020; Shuai et al., 2019), hexacopters (e.g., Atechsys) (Jin et al., 2017), and octocopters (e.g., DJI S1000 and DJI Matrice 600) (Varela et al., 2018; Zhao et al., 2018).

In these crop emergence assessment studies, a high-resolution red, green, and blue (RGB) camera with at least 12 megapixels was mounted on the rotary-wing UAV to take RGB color images. Their flight heights (above ground level) were between 3 to 20 m to achieve a ground sampling distance of 0.60 – 8.91 mm pixel^{-1} so that small size seedlings can be detected for further emergence estimation and assessment. The images were

mostly taken at the very early emergence time such as 6 to 16 days after planting (DAP) for cotton (Chen et al., 2018; Feng et al., 2020), vegetative growth stage V2 for corn before overlapping plants occurred (Shuai et al., 2019; Varela et al., 2018), and 1.0 to 2.5 visible leaves for wheat (Jin et al., 2017).

The typical procedure to process the UAV RGB images collected to estimate the emergence parameters comprised: 1) segment them into target (each plant) and background (soil, residue, and weeds) to detect each plant; 2) extract direct information (stand count or plant density) or image features to estimate emergence parameters (plant spacing, canopy area, emergence rate, and CV of emergence region). For image segmentation, most of the studies used vegetation indices (VIs) such as excess green (ExG), excess red (ExR), difference between excess green and excess red (MNVI), normalized green minus red difference index (NGRDI), and green leaf index (GLI) (Jin et al., 2017; Li et al., 2019; Liu et al., 2017; Shirzadifar et al., 2020; Shuai et al., 2019; Varela et al., 2018; Zhao et al., 2018) to first signify the green pixels in the image. A few studies used image contrast enhancement such as the decorrelation stretch procedure for signifying the green pixels (Feng et al., 2020; Gnädinger & Schmidhalter, 2017). Next, a threshold value determined based on pixel distribution in a histogram (Shirzadifar et al., 2020), visual inspection (Shuai et al., 2019), or Otsu algorithm (Jin et al., 2017; Li et al., 2019; Liu et al., 2017; Varela et al., 2018; Zhao et al., 2018) was used to segment the plants from background. Occasionally, threshold values determined from other color spaces including HSV and L*a*b, especially after image enhancement, were used to perform the image segmentation (Gnädinger & Schmidhalter, 2017; Shirzadifar et al., 2020).

The final output of the image segmentation was a binary image with white color (pixel value = 1) as plants and black color (pixel = 0) as background. Sometimes, weeds which has a similar green color as plants were detected as plants. Further processing such as removing detected objects with size less than a certain value (small size weeds and noise) and merging two objects (individual plant separated into two parts when certain parts were segmented as background as affected by sunlight and view angle) (Shirzadifar et al., 2020; Shuai et al., 2019; Varela et al., 2018; Zhao et al., 2018).

The second step of information or image feature extraction included directly counting the detected objects in a specific image area to determine the stand count or plant density. For plant spacing estimation, generally, the centroid of each object was extracted and used in the Euclidean distance method (Shirzadifar et al., 2020; Shuai et al., 2019; Zhang et al., 2018). Certain crops such as wheat, cotton, rapeseed, and potato have multiple seedlings in one individual plant or overlapped plants, hence, image features were extracted to correlate with the plant density (Chen et al., 2018; Jin et al., 2017; Li et al., 2019; Zhao et al., 2018). The common image features extracted included area, convex area, perimeter, major axis length, minor axis length, eccentricity, and solidity. Then, a statistical model was developed to estimate the emergence parameter using multiple linear regression (e.g., multiple stepwise regression) (Zhao et al., 2018) and machine learning (ML) methods (e.g., support vector machine and random forest) (Jin et al., 2017; Li et al., 2019). This typical procedure is usually feasible for fields with simple soil background but not for complex background especially with the combination of soil, crop residue, and weeds. Therefore, more advanced techniques using ML and deep learning

(DL) are required and will be discuss in more detail in section 1.2.3. Moreover, DL can be used directly to extract information from images without needing image segmentation.

To evaluate the capability of the UAV system and models in assessing the crop emergence, several statistical measures were used to compare the actual and estimated emergence parameters in these studies. The most widely used measure is coefficient of determination (R^2) to show the agreement between the actual and estimated parameters (Feng et al., 2020; Gnädinger & Schmidhalter, 2017; Jin et al., 2017; Li et al., 2019; Liu et al., 2017; Shirzadifar et al., 2020; Shuai et al., 2019; Zhao et al., 2018). The second most widely used measure is the root-mean-square-error (RMSE), which is the standard deviation of the residuals (difference between actual and estimated values) to show the deviation of the estimated parameters from the actual ones (Jin et al., 2017; Li et al., 2019; Shuai et al., 2019). The other measures consisted of precision, recall, accuracy, and F-measure when the analysis involved image classification (instead of regression) or single plant estimation in small plots (Chen et al., 2018; Varela et al., 2018; Zhao et al., 2018). The studies' results showed high R^2 when estimating stand count or plant density (0.72 – 0.95) for corn, cotton, and wheat; plant spacing (0.89 – 0.94) for corn; and canopy area (0.93 – 0.99) for cotton and potato. Meanwhile, a low RMSE was shown for corn plant spacing estimation (1.70 – 2.56 cm) (Shuai et al., 2019). Other measures showed high precision and accuracy (> 0.71) in estimating stand count or plant density for corn and cotton (Chen et al., 2018; Shuai et al., 2019; Varela et al., 2018). All these results illustrated the feasibility of a UAV system in estimating and assessing crop emergence.

1.2.4 Machine Learning (ML) and Deep Learning (DL) in UAV Imagery for Crop Emergence Assessment

Machine learning can be defined as providing the ability for machines to learn without strictly being programmed, which involves a learning process to learn from "experience" (training data) to perform a specific task (Liakos et al., 2018). The general procedures of ML techniques are building a model using training data (data with features as independent variables and responses or labels as dependent variables) and testing the model performance using testing data. The tasks performed can be regression (usually for numeric value estimation or prediction), classification (for categorical data), and clustering (for finding natural groupings of data). The learning process of ML can be divided into supervised and unsupervised learning. Supervised learning requires both the features and label data for learning in order to match the features with the label and uses the trained model for prediction or classification in testing data. On the other hand, unsupervised learning uses the feature data without label data in order to discover hidden patterns.

Deep learning is a kind of ML, which has different functions (e.g., convolutions, pooling layers, and fully connected layers) to transform the data in a hierarchical way and form a "deeper" neural network model (Kamilaris & Prenafeta-Boldú, 2018). A significant advantage of DL over conventional ML is its ability for feature learning, which extracts features automatically from raw data through the different functions (LeCun et al., 2015). One type of DL model extensively used for pattern recognition in image data is convolutional neural network (CNN) (Albawi et al., 2017). It possesses a convolution layer for extracting features automatically from each input image, a pooling layer for reducing the dimensionality of the extracted features (Amara et al., 2017), and a

fully-connected layer at the end for classification of the input images with the learned features. The following paragraphs will demonstrate ML and DL techniques in UAV imagery for crop emergence assessment.

For ML techniques, several studies first used VIs (e.g., ExG) and thresholding (e.g., Otsu) methods to segment the plants from the background (Banerjee et al., 2021; Jin et al., 2017; Li et al., 2019; Varela et al., 2018). Image features such as size (e.g., area, convex area, perimeter, major axis length, and minor axis length), shape (e.g., eccentricity, solidity, and elongation), and reflectance (i.e., different VIs) were extracted. These features were used to either classify plants and non-plants (soil and weeds) in corn (Varela et al., 2018) or estimate the plant density of wheat (Banerjee et al., 2021; Jin et al., 2017) and potato (Li et al., 2019) with ML models such as support vector regression, Gaussian process regression, decision tree, and random forest. On the other hand, a few studies used k-means clustering and supervised maximum likelihood classifier ML techniques to directly classify the images into plants and non-plants followed by plant counting in corn (Shirzadifar et al., 2020) and cotton (Chen et al., 2018). Results showed that the image classification using ML methods had higher accuracies than that of VIs and thresholding method (0.86 – 0.96 vs. 0 – 0.86) when estimating corn stand count (Shirzadifar et al., 2020).

Most of the studies used DL models in detecting individual plants in a bounding box for further stand count or plant density in corn (Hosseiny et al., 2020; Velumani et al., 2021), cotton (Oh et al., 2020), soybean (Habibi et al., 2021), and potato (Mhango et al., 2021). The common type of DL model used for this application is region based convolutional neural networks (R-CNN) with the widely used version as faster R-CNN in

detecting corn (Hosseiny et al., 2020; Velumani et al., 2021) and potato (Mhango et al., 2021). The other type is YOLO (You Only Look Once) with the general version used as YOLOv3 in detecting cotton (Oh et al., 2020) and soybean (Habibi et al., 2021). Both of these types of DL models used a deep feature extractor backbone, derived from available DL models to extract features from images. For faster R-CNN, the DL models used include ResNet (Hosseiny et al., 2020; Velumani et al., 2021) and VGG (Mhango et al., 2021) while for YOLOv3, the DL model used was DarkNet (Habibi et al., 2021). These studies showed high accuracy or R^2 when estimating stand count or plant density (accuracy > 0.64; R^2 > 0.82).

Moreover, several studies used DL models in image classification to detect the exact area of an individual plant and/or its center point (i.e., stem) in sugar-beet, corn, strawberry (Barreto et al., 2021), and rapeseed (Zhang et al., 2020). Barreto et al. (2021) used a fully convolutional network (FCN) with encoder-decoder structure while Zhang et at. (2020) used an image analysis software known as eCognition Developer 9.3 with CNN module for image classification. Detecting the exact area of each plant helps for further analysis, for instance, relating plant responses (e.g., leaf area and plant reflectance) to emergence parameters such as emergence date. Detecting the center point of plants can determine more accurate plant stand count especially when there are overlapping plants and for more precise plant spacing estimation, subsequently increasing accuracy in estimating spacing uniformity. Lastly, a study by Feng et al. (2020) used a pre-trained CNN model, ResNet18 to estimate emergence parameters including plant density and canopy area directly from RGB images. The results from these studies indicated a low MAPE of less than 4.5% when estimating plant density and canopy area

for sugar beet, corn, strawberry, and cotton. Overall, all the studies indicated the feasibility of using ML and DL and UAV imagery for assessing crop emergence parameters.

1.2.5 Mapping of Crop Emergence using UAV Imagery

Conventionally, studies have focused on the different image processing, ML and DL techniques in UAV imagery for detecting individual plants and estimating different crop emergence parameters. Limited studies further applied the estimation at field scale, which is critical in investigating the emergence variability in fields as affected by soil properties and landscape position. Precision agriculture (PA) involves the observation of field spatial variability and management according to the principle of right practice at the right place and the right time (Mulla, 2013). Field-scale mapping is needed to identify spatial variability, which is usually affected by variable soil conditions,. One of the methods used to measure and map the soil properties such as soil salinity, clay content, and moisture content was soil apparent electrical conductivity (EC_a) measured by proximal soil sensors (Corwin & Lesch, 2003; Doolittle et al., 1994; Sudduth et al., 2005). The patterns estimated from the EC_a measurement are used to define management zones (Mulla, 2013). Moreover, yield maps available from yield monitors could also be used as to define the management zones (King et al., 2005).

There are some available software to stitch UAV imagery to generate an orthomosaic such as Agisoft Metashape (Agisoft LLC, St. Petersburg, Russia) or Pix4D mapper (Pix4D S.A., Lausanne, Switzerland). This orthomosaic can then be used to produce the crop emergence maps (Feng et al., 2020; Mhango et al., 2021; Shirzadifar et al., 2020). These maps showing the emergence distribution in a field can give some

insight on the field spatial variability as demonstrated by Feng et al. (2020). The cotton emergence maps showed similar patterns with yield and EC_a maps, i.e., regions of field with low canopy area had low EC_a and yield. Hence, crop emergence mapping is beneficial to investigate the field spatial variability as affected by soil properties and can be related to early crop growth and final yield.

1.3 Goal and Objectives

The overall goal of this research was to apply ML and DL techniques in UAV imagery processing to provide corn emergence information, essential for early and in-season decision-making in corn production as well as agronomy research. The emergence parameters include emergence time (which had not been widely determined in other studies), plant density, and spatial variability based on plant spacing standard deviation, critical for replanting decisions and post-emergence management as well as for relating to early growth and final yield. The assessment was conducted in CA fields of different cropping systems, which could show the capability of UAV imagery with ML and DL techniques in estimating the corn emergence in CA. The research comprised three studies with these specific objectives:

Study 1: To estimate corn emergence date using ML technique in UAV imagery. Since corn emerges across a range of days, early and late emerging seedlings have different size and shape characteristics. Image features extracted from UAV seedling images were used in a ML model to estimate the corn emergence date based on days after emergence (DAE) on the imaging date.

Study 2: To estimate corn early stand count in different cropping systems (CS) using a DL technique with UAV imagery. With a complex background containing soil, residue from the previous crop and cover crop, and weeds existing in corn of different CS, a DL model was used to segment the UAV imagery and identify individual plants for further stand count estimation.

Study 3: To estimate and map temporal and spatial emergence uniformity of corn planted at different planting depths. With the promising results from objective 1 and 2, another DL technique was applied to UAV imagery to estimate more emergence parameters temporally and spatially. Maps of these emergence parameters were produced to visualize the emergence uniformity between planting depth treatments.

The descriptions of Studies 1 to 3 are detailed in the following dissertation chapters 2 to 4. Chapter 5 demonstrates example applications of studying the relationship between corn emergence at field scale (mapping from Study 3) and early corn growth with final yield under different planting depths.

References

Albawi, S., Mohammed, T. A., & Al-Zawi, S. (2017). *Understanding of a convolutional neural network.* Paper presented at the 2017 International Conference on Engineering and Technology (ICET).

Amara, J., Bouaziz, B., & Algergawy, A. (2017). A deep learning-based approach for banana leaf diseases classification. *Datenbanksysteme für Business, Technologie und Web (BTW 2017)-Workshopband*.

Andrade, F. H., & Abbate, P. E. (2005). Response of maize and soybean to variability in stand uniformity. *Agronomy Journal, 97*(4), 1263-1269.

Assefa, Y., Vara Prasad, P., Carter, P., Hinds, M., Bhalla, G., Schon, R., . . . Ciampitti, I. A. (2016). Yield responses to planting density for US modern corn hybrids: A synthesis-analysis. *Crop Science, 56*(5), 2802-2817.

Banerjee, B. P., Sharma, V., Spangenberg, G., & Kant, S. (2021). Machine learning regression analysis for estimation of crop emergence using multispectral uav imagery. *Remote Sensing, 13*(15), 2918.

Barreto, A., Lottes, P., Yamati, F. R. I., Baumgarten, S., Wolf, N. A., Stachniss, C., . . . Paulus, S. (2021). Automatic UAV-based counting of seedlings in sugar-beet field and extension to maize and strawberry. *Computers and Electronics in Agriculture, 191*, 106493.

Cai, G., Dias, J., & Seneviratne, L. (2014). A survey of small-scale unmanned aerial vehicles: Recent advances and future development trends. *Unmanned Systems, 2*(02), 175-199.

Chen, R., Chu, T., Landivar, J. A., Yang, C., & Maeda, M. M. (2018). Monitoring cotton (Gossypium hirsutum L.) germination using ultrahigh-resolution UAS images. *Precision Agriculture, 19*(1), 161-177.

Conway, L. S., Yost, M. A., Kitchen, N. R., Sudduth, K. A., & Veum, K. S. (2018). Cropping system, landscape position, and topsoil depth affect soil fertility and nutrient buffering. *Soil Science Society of America Journal, 82*(2), 382-391.

Corwin, D., & Lesch, S. M. (2003). Application of soil electrical conductivity to precision agriculture: theory, principles, and guidelines. *Agronomy Journal, 95*(3), 455-471.

Doolittle, J., Sudduth, K., Kitchen, N., & Indorante, S. (1994). Estimating depths to claypans using electromagnetic induction methods. *Journal of Soil and Water Conservation, 49*(6), 572-575.

Feng, A., Zhou, J., Vories, E., & Sudduth, K. A. (2020). Evaluation of cotton emergence using UAV-based imagery and deep learning. *Computers and Electronics in Agriculture, 177*, 105711.

Friedrich, T., Derpsch, R., & Kassam, A. (2012). Overview of the global spread of conservation agriculture. *Field Actions Science Reports. The journal of field actions*(Special Issue 6).

Gnädinger, F., & Schmidhalter, U. (2017). Digital counts of maize plants by unmanned aerial vehicles (UAVs). *Remote Sensing, 9*(6), 544.

Habibi, L. N., Watanabe, T., Matsui, T., & Tanaka, T. S. (2021). Machine learning techniques to predict soybean plant density using UAV and satellite-based remote sensing. *Remote Sensing, 13*(13), 2548.

Hobbs, P. R., Sayre, K., & Gupta, R. (2008). The role of conservation agriculture in sustainable agriculture. *Philosophical Transactions of the Royal Society B: Biological Sciences, 363*(1491), 543-555.

Hosseiny, B., Rastiveis, H., & Homayouni, S. (2020). An Automated Framework for Plant Detection Based on Deep Simulated Learning from Drone Imagery. *Remote Sensing, 12*(21), 3521.

Hunt, N. D., Hill, J. D., & Liebman, M. (2019). Cropping System Diversity Effects on Nutrient Discharge, Soil Erosion, and Agronomic Performance. *Environmental science & technology, 53*(3), 1344-1352.

Jin, X., Liu, S., Baret, F., Hemerlé, M., & Comar, A. (2017). Estimates of plant density of wheat crops at emergence from very low altitude UAV imagery. *Remote Sensing of Environment, 198*, 105-114.

Johnston, A. E., Poulton, P. R., & Coleman, K. (2009). Soil organic matter: its importance in sustainable agriculture and carbon dioxide fluxes. *Advances in agronomy, 101*, 1-57.

Kamilaris, A., & Prenafeta-Boldú, F. X. (2018). Deep learning in agriculture: A survey. *Computers and electronics in agriculture, 147*, 70-90.

Karayel, D., & Özmerzi, A. (2008). Evaluation of three depth-control components on seed placement accuracy and emergence for a precision planter. *Applied Engineering in Agriculture, 24*(3), 271-276.

King, J., Dampney, P., Lark, R., Wheeler, H., Bradley, R., & Mayr, T. (2005). Mapping potential crop management zones within fields: use of yield-map series and

patterns of soil physical properties identified by electromagnetic induction sensing. *Precision Agriculture, 6*(2), 167-181.

Kitano, B. T., Mendes, C. C., Geus, A. R., Oliveira, H. C., & Souza, J. R. (2019). Corn Plant Counting Using Deep Learning and UAV Images. *IEEE Geoscience and Remote Sensing Letters*.

Lauer, J. G., & Rankin, M. (2004). Corn response to within row plant spacing variation. *Agronomy Journal, 96*(5), 1464-1468.

LeCun, Y., Bengio, Y., & Hinton, G. (2015). Deep learning. *Nature, 521*(7553), 436-444.

Li, B., Xu, X., Han, J., Zhang, L., Bian, C., Jin, L., & Liu, J. (2019). The estimation of crop emergence in potatoes by UAV RGB imagery. *Plant Methods, 15*(1), 1-13.

Liakos, K. G., Busato, P., Moshou, D., Pearson, S., & Bochtis, D. (2018). Machine learning in agriculture: A review. *Sensors, 18*(8), 2674.

Liu, T., Li, R., Jin, X., Ding, J., Zhu, X., Sun, C., & Guo, W. (2017). Evaluation of seed emergence uniformity of mechanically sown wheat with UAV RGB imagery. *Remote Sensing, 9*(12), 1241.

Liu, W., Tollenaar, M., Stewart, G., & Deen, W. (2004a). Response of corn grain yield to spatial and temporal variability in emergence. *Crop Science, 44*(3), 847-854.

Liu, W., Tollenaar, M., Stewart, G., & Deen, W. (2004b). Within-row plant spacing variability does not affect corn yield. *Agronomy Journal, 96*(1), 275-280.

Mhango, J. K., Harris, E. W., Green, R., & Monaghan, J. M. (2021). Mapping potato plant density variation using aerial imagery and deep learning techniques for precision agriculture. *Remote Sensing, 13*(14), 2705.

Mulla, D. J. (2013). Twenty five years of remote sensing in precision agriculture: Key advances and remaining knowledge gaps. *Biosystems engineering, 114*(4), 358-371.

Nafziger, E. D., Carter, P. R., & Graham, E. E. (1991). Response of corn to uneven emergence. *Crop Science, 31*(3), 811-815.

Nielsen, R. (2001). Stand establishment variability in corn. *Dept. of Agronomy publication# AGRY-91-01. Purdue University, West Lafayette, IN*.

Nunes, M. R., van Es, H. M., Schindelbeck, R., Ristow, A. J., & Ryan, M. (2018). No-till and cropping system diversification improve soil health and crop yield. *Geoderma, 328*, 30-43.

Oh, S., Chang, A., Ashapure, A., Jung, J., Dube, N., Maeda, M., . . . Landivar, J. (2020). Plant counting of cotton from UAS imagery using deep learning-based object detection framework. *Remote Sensing, 12*(18), 2981.

Pittelkow, C. M., Liang, X., Linquist, B. A., Van Groenigen, K. J., Lee, J., Lundy, M. E., . . . Van Kessel, C. (2015). Productivity limits and potentials of the principles of conservation agriculture. *Nature, 517*(7534), 365-368.

Pommel, B., Mouraux, D., Cappellen, O., & Ledent, J.-F. (2002). Influence of delayed emergence and canopy skips on the growth and development of maize plants: a plant scale approach with CERES-Maize. *European Journal of Agronomy, 16*(4), 263-277.

Radoglou-Grammatikis, P., Sarigiannidis, P., Lagkas, T., & Moscholios, I. (2020). A compilation of UAV applications for precision agriculture. *Computer Networks, 172*, 107148.

Rutto, E., Daft, C., Kelly, J., Chim, B. K., Mullock, J., Torres, G., & Raun, W. (2014). Effect of delayed emergence on corn (Zea mays L.) grain yield. *Journal of Plant Nutrition, 37*(2), 198-208.

Sangoi, L. (2001). Understanding plant density effects on maize growth and development: an important issue to maximize grain yield. *Ciência rural, 31*(1), 159-168.

Schneider, E., & Gupta, S. (1985). Corn emergence as influenced by soil temperature, matric potential, and aggregate size distribution. *Soil Science Society of America Journal, 49*(2), 415-422.

Shirzadifar, A., Maharlooei, M., Bajwa, S. G., Oduor, P. G., & Nowatzki, J. F. (2020). Mapping crop stand count and planting uniformity using high resolution imagery in a maize crop. *Biosystems Engineering, 200*, 377-390.

Shuai, G., Martinez-Feria, R. A., Zhang, J., Li, S., Price, R., & Basso, B. (2019). Capturing Maize Stand Heterogeneity Across Yield-Stability Zones Using Unmanned Aerial Vehicles (UAV). *Sensors, 19*(20), 4446.

Sona, G., Passoni, D., Pinto, L., Pagliari, D., Masseroni, D., Ortuani, B., & Facchi, A. (2016). *UAV multispectral survey to map soil and crop for precision farming applications.* Paper presented at the Remote Sensing and Spatial Information Sciences Congress: International Archives of the Photogrammetry Remote Sensing and Spatial Information Sciences Congress: 19 July.

Sudduth, K., Kitchen, N., Wiebold, W., Batchelor, W., Bollero, G., Bullock, D., . . . Schuler, R. (2005). Relating apparent electrical conductivity to soil properties

across the north-central USA. *Computers and Electronics in Agriculture, 46*(1-3), 263-283.

Thamm, H.-P., Brieger, N., Neitzke, K., Meyer, M., Jansen, R., & Mönninghof, M. (2015). SONGBIRD-an innovative UAS combining the advantages of fixed wing and multi rotor UAS. *International Archives of the Photogrammetry, Remote Sensing & Spatial Information Sciences, 40*.

Torres-Sánchez, J., Pena, J. M., de Castro, A. I., & López-Granados, F. (2014). Multi-temporal mapping of the vegetation fraction in early-season wheat fields using images from UAV. *Computers and Electronics in Agriculture, 103*, 104-113.

USDA. (2015). *USDA Coexistence Fact Sheets Corn*. Retrieved from https://www.usda.gov/sites/default/files/documents/coexistence-corn-factsheet.pdf

USDA. (2022). *Crop Production*. Retrieved from https://downloads.usda.library.cornell.edu/usda-esmis/files/tm70mv177/h415qd68b/6m312r896/crop0322.pdf

Varela, S., Dhodda, P., Hsu, W., Prasad, P., Assefa, Y., Peralta, N., . . . Ciampitti, I. (2018). Early-season stand count determination in corn via integration of imagery from unmanned aerial systems (UAS) and supervised learning techniques. *Remote Sensing, 10*(2), 343.

Velumani, K., Lopez-Lozano, R., Madec, S., Guo, W., Gillet, J., Comar, A., & Baret, F. (2021). Estimates of maize plant density from UAV RGB images using Faster-RCNN detection model: impact of the spatial resolution. *Plant Phenomics, 2021*.

Vong, C. N., Conway, L. S., Zhou, J., Kitchen, N. R., & Sudduth, K. A. (2021). Early corn stand count of different cropping systems using UAV-imagery and deep learning. *Computers and Electronics in Agriculture, 186*, 106214.

Yost, M. A., Kitchen, N. R., Sudduth, K. A., Sadler, E. J., Baffaut, C., Volkmann, M. R., & Drummond, S. T. (2016). Long-term impacts of cropping systems and landscape positions on claypan-soil grain crop production. *Agronomy Journal, 108*(2), 713-725.

Zhang, J., Basso, B., Price, R. F., Putman, G., & Shuai, G. (2018). Estimating plant distance in maize using Unmanned Aerial Vehicle (UAV). *PloS one, 13*(4), e0195223.

Zhang, J., Zhao, B., Yang, C., Shi, Y., Liao, Q., Zhou, G., . . . Zhang, D. (2020). Rapeseed Stand Count Estimation at Leaf Development Stages With UAV Imagery and Convolutional Neural Networks. *Frontiers in Plant Science, 11*, 617.

Zhao, B., Zhang, J., Yang, C., Zhou, G., Ding, Y., Shi, Y., . . . Liao, Q. (2018). Rapeseed seedling stand counting and seeding performance evaluation at two early growth stages based on unmanned aerial vehicle imagery. *Frontiers in plant science, 9*, 1362.

CHAPTER TWO

CORN EMERGENCE DATE ESTIMATION USING UAV IMAGERY

2.1 Abstract

Assessing corn (Zea Mays L.) emergence uniformity soon after planting is important for relating to grain production and making replanting decisions. Unmanned aerial vehicle (UAV) imagery has been used for determining corn densities at vegetative growth stage 2 (V2) and later, but not as a tool for quantifying emergence date. The objective of this study was to estimate days after corn emergence (DAE) using UAV imagery and a machine learning method. A field experiment was designed with four planting depths to obtain a range of corn emergence dates. UAV imagery was collected during the first, second and third weeks after emergence. Acquisition height was approximately 5 m above ground level, which resulted in a ground sampling distance of 1.5 mm pixel^{-1}. Seedling size and shape features derived from UAV imagery were used for DAE classification based on a random forest machine learning model. Results showed that 1-day DAE could be distinguished based on image features within the first week after initial corn emergence with a moderate overall classification accuracy of 0.49. However, for the second week and beyond, the overall classification accuracy diminished (0.20 to 0.35). When estimating DAE within a 3-day window (-1 to +1 day), the overall 3-day classification accuracies ranged from 0.54 to 0.88. Diameter, area, and the ratio of major axis length to area were important image features to predict corn DAE. Findings demonstrated that UAV imagery can detect newly-emerged corn plants and estimate their emergence date to assist in assessing emergence uniformity. Additional studies are needed for fine-tuning image collection procedures and image feature identification in order to

improve accuracy.

2.2 Introduction

Corn is one of the most important food crops in the world as well as a vital source for animal feed and biofuel (Klopfenstein et al., 2013; Shiferaw et al., 2011). Based on the latest report from the Food and Agriculture Organization of the United Nations (2020), total global corn (maize) production in year 2018 was more than 1.1 billion tons, with a harvested area of close to 200 million ha. To maximize corn grain yield, management is needed to optimize seedling emergence uniformity (i.e., emergence time) and seedling spatial uniformity (i.e., plant spacing). Temporal variation in seedling emergence leads to consistent yield reductions (Andrade & Abbate, 2005; Liu et al., 2004; Nafziger et al., 1991). The study by Nafziger et al. (1991) showed that the average harvested yield of corn decreased by 6% and 12% when the plant date was delayed 10 to 12 days and 22 days, respectively. Meanwhile, Liu et al. (2004) found that the average yield decreased 4.3% and 8.7% with delayed planting of 12 and 21 days. In a separate investigation, the average yield of corn with an emergence difference of three days was about 12% less than that of the corn in control plots with uniform emergence (Andrade & Abbate, 2005).

Evaluating the temporal variation in seedling emergence is also necessary for making replanting decisions, by assessing the effect of the variation both in time of emergence and proportion of delay plants on final grain yield (Nafziger et al., 1991). As stated by (Lauer & Rankin, 2004), the first step to make the replanting decision is crop scouting at multiple regions of the field to determine the plant population and its uniformity. However, this method is labor intensive, subjective, and spatially inadequate

for fields with variable soil conditions that influence seed germination and emergence. With the advantages of unmanned aerial vehicles (UAV), optical sensors, advanced image processing, and analytic technologies, time and labor needed for crop scouting can be greatly reduced (Shuai et al., 2019), and a more precise and accurate estimation of plant density can be acquired.

Research has shown the usefulness of UAV red-green-blue (RGB) imagery in determining corn plant density and spacing estimation at early stages. Gnädinger & Schmidhalter (2017) used aerial images to determine corn post-emergence plant density at their vegetative growth stages of V3 to V5 (with three to five visible leaves, Ransom et al., 2013) and achieved an accuracy of $R^2 = 0.89$. In other work, Varela et al. (2018) demonstrated the potential of using high–resolution RGB images with a spatial resolution of 2.4 mm $pixel^{-1}$ to estimate corn stand count at the V2 to V3 growth stages based on supervised learning techniques. In addition, UAV imagery was used to estimate corn plant spacing (Zhang et al., 2018) and corn plant density at about two weeks after emergence (Shuai et al., 2019). The results from Shuai et al. (2019) showed at least 96% of precision when estimating the number of plants and R^2 of 0.89 to 0.91 when estimating the plant spacing. All the stated studies showed promising results of using UAV imagery in detecting and counting the corn seedlings as well as estimating plant spacing. However, none of them used UAV imagery for detecting corn emergence at much earlier stages (i.e., pre-growth stage V2) and quantifying emergence date of seedlings.

Previous research has also used UAV-derived image features, including size and shape (e.g., area, diameter, major axis length, minor axis length, solidity, and eccentricity) to estimate wheat density (Jin et al., 2017) and detect corn at an early

growth stage (Varela et al., 2018). Jin et al. (2017) used these features in a support vector machine to estimate the wheat density and achieved R^2 from 0.80 to 0.91 at different experiment sites. Varela et al. (2018) used image features in a decision tree to classify corn and non-corn objects (weeds) and found that image features of aspect ratio, axis-diameter ratio, convex area, thinness, and solidity were significant in the classification. In addition, image features of size and shape utilized in artificial neural network modeling were effective in distinguishing different varieties of corn seed (accuracy from 0.88 to 0.92, Chen et al., 2010) and rice seed (accuracy from 0.70 to 0.95, Chaugule & Mali, 2014).

Our review of the literature did not reveal any previous research to determine plant emergence date based on image features. Since corn emerges across a range of days, early and late emerging seedlings have different size and shape characteristics. These characteristics could be identified using image features, and would be useful in classifying the number of days after emergence (DAE) for each individual plant seedling. The overall objective of this study was to estimate the DAE using size and shape features extracted from UAV imagery. Specific objectives were: 1) to extract size and shape features from corn plant images, 2) to build a random forest (RF) machine learning model to predict corn plant DAE, and 3) to identify important image features in predicting plant DAE.

2.3 Materials and Methods

2.3.1 Experimental Site and Setup

The experiment was conducted at the Bay Farm Research Facility, University of Missouri, Columbia, MO, USA (38°52’ 45.3” N, 92°12’15.3” W) with 18 plots arranged

in a randomized complete block design as illustrated in Fig. 2-1a. Treatments included four planting depths (3.8, 5.1, 6.4, and 7.6 cm) with four replications (with an additional replication for 5.1 and 7.6 cm depths). This range of depths produced variability in corn emergence date. Each plot was 3.0 m long and included four rows of corn with an inter-row spacing of 0.76 m and average intra-row spacing of 17.7 cm. Only the middle two rows were selected for manual measurement and image analysis as shown in Fig. 2-1b. All corn was planted on 9 April 2019 with no-tillage using a custom-built John Deere four-row planter, equipped with MaxEmerge XP row units (Deere & Co., Moline, IL, USA) adjusted to plant seeds at the four defined depths. Seed-firmer sensors (SmartFirmer, Precision Planting, Tremont, IL, USA) were also mounted on the planter to estimate the soil conditions while planting. Corn emergence was checked daily between 8 to 10 am beginning on 22 April (first emergence) until complete emergence (29 April), with newly emerged plants marked with unique color stakes for each day. Emergence was not checked on 28 April due to time constraint and the plants emerged on 28 April were therefore grouped with the plants emerged on 29 April.

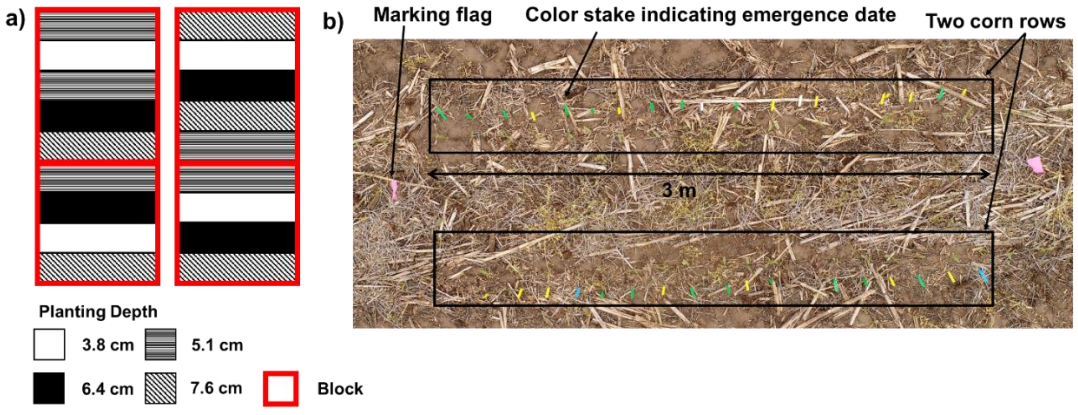

Figure 2-1. a) Schematic diagram of the plots arranged in randomized complete block design and b) an example UAV image of one study plot captured at about 5 m height on 3 May 2019 (DAE 5 to 12).

2.3.2 UAV Image Collection

Aerial images were collected using a Phantom 4 Advanced UAV imaging system (DJI, Shenzhen, Guangdong, China) with an onboard camera that has a field-of-view (FOV) of 84° and an image size of 4864 by 3648 pixels (20M pixels). The DJI Go 4 app was used to set the UAV height at 5 m above ground level (AGL) resulting a ground sampling distance (GSD) of 1.5 mm pixel^{-1}. The GSD is the distance between two consecutive pixel centers measured on the ground (Orych, 2015). The camera was adjusted to vertically facing down to the field, i.e., nadir view (Lillesand et al., 2004), to manually acquire images for each plot. The images were taken manually using default camera settings (auto white balance and ISO range). Aerial image data were collected on 26 April and 3, 11, and 15 May between 10 am and 2 pm local time (i.e., minimum changes in the solar zenith angle). The aerial image collected on 26 April was to test the capability of the UAV images to detect corn within the first week after first emergence (DAE 1 to 5 in this study). Aerial images collected on later dates represented five to 12, 13 to 20, and 17 to 24 days after the first emergence. Figure 2-2 summarizes a timeline of corn emergence and dates of aerial image collection.

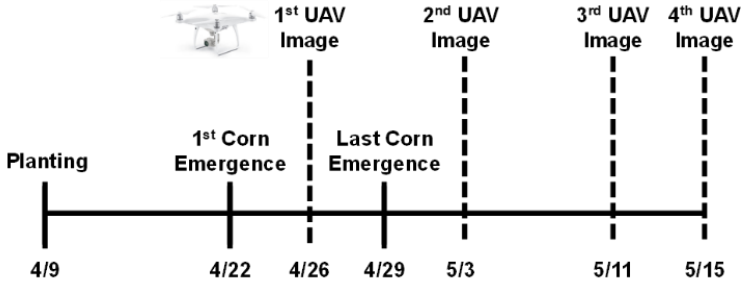

Figure 2-2. Summary of corn emergence dates and UAV image collection dates.

2.3.3 Image Data Processing and Image Feature Extraction

Small corn seedlings from DAE 1 to 5 were difficult to identify due to the small size. Additionally, identifying seedlings was particularly difficult on the no-till research site as abundant ground residue and patches of winter annual weeds obscured seedlings (Fig. 2-1). Therefore, each corn seedling was manually cropped from the UAV images to simplify the image processing procedure. To signify corn seedlings in images, a contrast enhancement procedure based on linear contrast stretch was performed on each image using the '*decorrstretch*' function from MATLAB (R2017b, MathWorks, Inc., Natick, MA, USA) (Gnädinger & Schmidhalter, 2017). Linear contrast stretch expands the original pixel value in the image linearly into a new distribution (Chandpa et al., 2014). The *decorrstretch* function in MATLAB transforms the pixel values of each band into the color eigenspace of the 3-by-3 (three bands of R, G, and B) correlation matrix followed by stretching them to equalize the band variances and transformed the color range to a normalized interval between 0.01 and 0.99 (used 'Tol', '0.01' arguments in '*decorrstretch'* function in Matlab). This function is able to enhance the color differences between corn seedlings and their background (soil or residue) (Fig. 2-3) to segment corn seedlings accurately. Contrast enhanced images in RGB color space were converted to HSV (hue, saturation, value) color space to eliminate the luminance effect. The "Color Thresholder App" from MATLAB was used to determine the threshold value for each band in HSV color space to segment the image (Fig. 2-3). Size and shape features were then extracted using the '*regionprops*' function from MATLAB or computed using equations listed in Table 2-1.

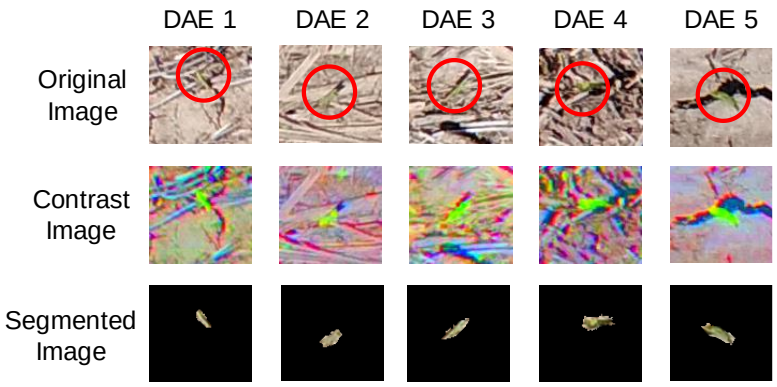

Figure 2-3. Illustration of segmented corn images at different DAE using contrast enhancement and segmentation with a threshold value from HSV color space.

Table 2-1. Description of size and shape features (SF) extracted from each single corn image.

Feature	Description or Equation	Reference
Area	Total pixel number of a segmented seedling in images.	MATLAB*
Perimeter	The pixel number around the boundary of a segmented seedling.	MATLAB*
Diameter	The pixel number of the diameter of an equivalent circle with the same area as the segmented seedling.	MATLAB*
Major Axis Length	The pixel number of the major axis of an equivalent ellipse of the segmented seedling.	MATLAB*
Minor Axis Length	The pixel number of the minor axis of an equivalent ellipse to the segmented seedling.	MATLAB*
Eccentricity	The ratio of the distance between the foci of the ellipse and its major axis length (ellipse with eccentricity 0 is a circle and 1 is a line segment).	MATLAB*
Solidity	Proportion of the pixels in the convex hull that are also in the region.	MATLAB*
Aspect Ratio	$\frac{Major\ Axis\ Length}{Minor\ Axis\ Length}$	(Najafabadi & Farahani, 2012)
Roundness	$\frac{4\pi \times Area}{Perimeter}$	(Najafabadi & Farahani, 2012)
Compactness	$\frac{Perimeter^2}{Area}$	(Najafabadi & Farahani, 2012)
SF1	$\frac{1}{Compactness}$	(Chaugule & Mali, 2014)
SF2	$\frac{Major\ Axis\ Length}{Area}$	(Chaugule & Mali, 2014)
SF3	$\frac{Area}{Major\ Axis\ Length^3}$	(Chaugule & Mali, 2014)
SF4	$\frac{Area}{(\frac{Major\ Axis\ Length}{2})^2 \times \pi}$	(Chaugule & Mali, 2014)
SF5	$\frac{Area}{\frac{Major\ Axis\ Length}{2} \times \frac{Minor\ Axis\ Length}{2} \times \pi}$	(Chaugule & Mali, 2014)
SF6	$\frac{Minor\ Axis\ Length}{Area}$	
SF7	$\frac{Area}{Minor\ Axis\ Length^3}$	

* Image features extracted using image regions function (‘*regionprops’*) from MATLAB (R2017b).

The actual values (in mm or mm^2) of the calculated image features listed in Table 2-1 were computed using the product of the number of pixels of the stated image features and the GSD. The GSD of each image was determined using reference boards with known dimensions and the length of color stakes in each UAV image. This GSD determination is useful to show the needed GSD ranges for detecting the small newly-emerged plants.

2.3.4 Random Forest Machine Learning Modeling

A Random Forest (RF) modeling method was used to predict corn plant DAE. The RF model is a type of classification and regression tree (CART) machine learning method employing ensembles of classifications (James et al., 2013; Rodriguez-Galiano et al., 2012). Advantages offered by an RF model include its fast training, higher accuracy, less potential of overfitting (when using a large number of trees), measures of variable importance, ability to capture non-linear correlation between the variables and predictors, and no requirement for data distribution assumptions such as normality (Belgiu & Drăguţ, 2016; Gareth, 2010; O’Brien & Ishwaran, 2019; Rodriguez-Galiano et al., 2012). To develop the RF model, a dataset consisting of the response variable (DAE) and 17 image features (Table 2-1) was established with 70% of the images as training data and 30% of the images as testing data. The number of observations for image dates 26 April and 3 May was 310 and 627, and the number was 624 for 11 and 15 May. For every tree branch built in the RF model, only four features were randomly selected instead of using the full set of features to decorrelate the trees and build a reliable model (Gareth, 2010). Since the RF model will not overfit even using a large number of trees, studies have

suggested the ideal number of trees ranging from 64 to 500 (Belgiu & Drăguţ, 2016; Gareth, 2010; Oshiro et al., 2012). In this study, an open source software RStudio (ver. 1.2.1335, RStudio, Boston, MA, USA.) was utilized for conducting RF modeling using the '*randomForest'* package (Breiman & Cutler, 2018). The default value of 500 trees in the package was used.

The model performance was evaluated using the test data with two metrics, i.e., accuracy of each class and overall accuracy for the classification (Kuhn, 2019). The accuracy of each class was defined as the ratio of the number of seedlings correctly classified to each DAE class to the total number of actual samples (seedlings) in each DAE class. The overall accuracy was defined as the ratio of the number of correctly classified seedling in all DAE classes to the total number of actual seedlings in all DAE classes. An additional metric, i.e., 3-day accuracy, was also defined to study the potential of UAV imagery in predicting the DAE within a 3-day window. The 3-day accuracy was the ratio of the number of samples predicted one day before and after the actual DAE (-1 to +1 DAE) to the total number of actual samples in each DAE class. To clarify, 1-day accuracy in DAE means that the predicted DAE was the same as the actual DAE, while 3-day accuracy in DAE means that the predicted DAE was within a 3-day window centered on the actual DAE.

The importance of the image features to the DAE prediction was evaluated using the mean decrease in the Gini index (Belgiu & Drăguţ, 2016; Gareth, 2010). The Gini index is used to measure the variance impurity (purity), i.e., the variance of a distribution associated with each class, where a small value implies a node has observations predominantly from a single class (Gareth, 2010). The mean decrease in Gini index was

defined as the ratio of the total decrease in Gini index from all the nodes when the feature was used to the number of trees used (Gareth, 2010). A large value in the mean decrease in Gini index implied an important feature. This approach was used in this study to identify the important features in predicting DAE. An analysis of variance (ANOVA) test (Sawyer, 2009) at a 0.05 significance level ($\alpha = 0.05$) was performed to determine the significance in the difference between DAE of the two top-ranked features identified at earlier image dates (first and second weeks of emergence). When the ANOVA test showed a significant result, a pairwise comparison technique known as Tukey's Honest Significant Difference (HSD, $\alpha = 0.05$) test (Abdi & Williams, 2010) was computed to compare the feature mean difference between DAEs. The statistical analysis was performed using the '*aov*' and '*TukeyHSD*' functions in RStudio. All the image data processing and ML modeling were performed in a laptop configured as Intel Core i7-7600U 2.80 GHz CPU, a Intel HD Graphics 620 GPU with 7.9 GB memory, 16 GB RAM, and a 463 GB hard disk drive.

2.4 Results and Discussion

2.4.1 Ground Sampling Distance (GSD)

The ground sampling distance (GSD) in each image was different due to the variation of actual flight heights. Although the UAV was set to fly at a nominal height of 5.0 m, the actual height varied based on the launch location of the UAV and the field slope. The computed GSD ranged from 0.55 to 1.54 mm pixel^{-1} in different plots for UAV images captured on different days. Figure 2-4 shows images taken on 26 April for two plots with the lowest (0.55 mm pixel^{-1}) and highest (0.94 mm pixel^{-1}) computed GSD. The small sized plants at DAE 1 and 2 were detectable using the described image

processing workflow. This result supports the conclusion that a range of GSD from 0.55 to 0.94 mm pixel^{-1} can be used to detect corn at DAE 1 and 2.

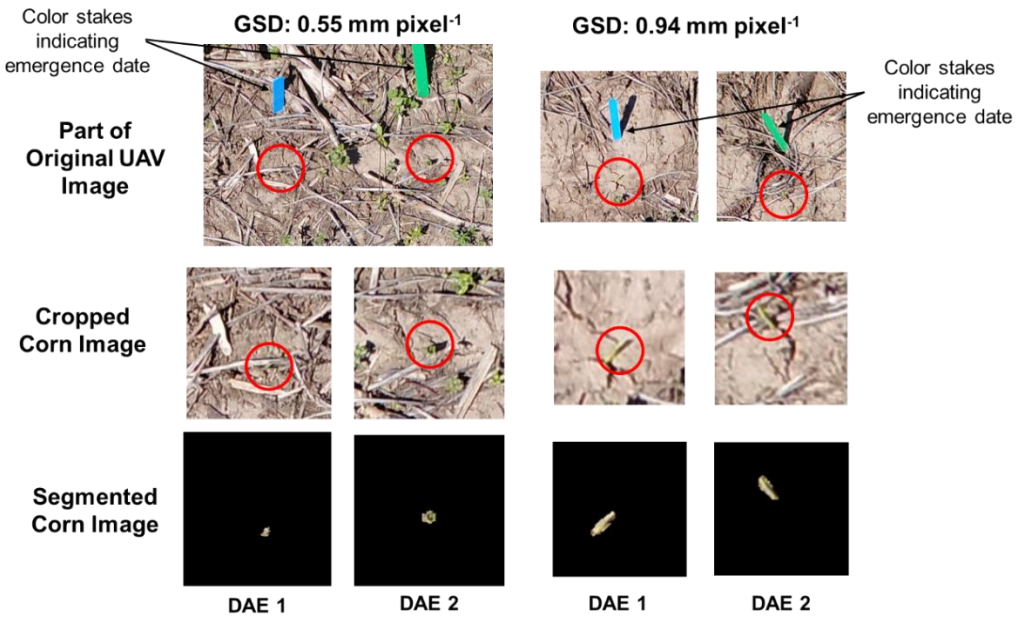

Figure 2-4. UAV images captured on 26 April at two different computed ground sampling distances (GSD). Blue and green color stakes indicate emergence dates of 26 April (DAE 1) and 25 April (DAE 2), respectively.

2.4.2 Classification Accuracy for Each Image Date

The classification accuracies of the RF model using data of different imaging dates are shown in Fig. 2-5. The digit in each grid indicates the ratio between the predicted number of samples for each DAE and the actual number of samples for the DAE with darker blue color indicating a higher ratio. Diagonal grids show the classification accuracy for each DAE while grids at the bottom indicate 3-day accuracy. As presented in Fig. 2-5a, i.e., during the first week of emergence, approximately half of the samples for all the DAE classes were predicted correctly. The classification accuracy ranged from 0.45 to 0.56, with the exception of the DAE 5 that had an accuracy of only 0.20. Figure 2-5a also shows that 36% of DAE 1 plants were predicted as DAE 2 plants, and more than 20% of DAE 2 plants were predicted as plants of either DAE 1 or DAE 3.

Figure 2-6 illustrates representative plants for each DAE to analyze the potential reasons for the low classification accuracy. It can be seen that plants of both DAE 1 and DAE 2 could be described as ‘through surface’ or ‘spike’ (Poncet et al., 2019), having similar morphological appearance in size and shape. The similarity in size and shape of newly emerged plants may cause the misclassification of plants between DAE 1 and DAE 2.

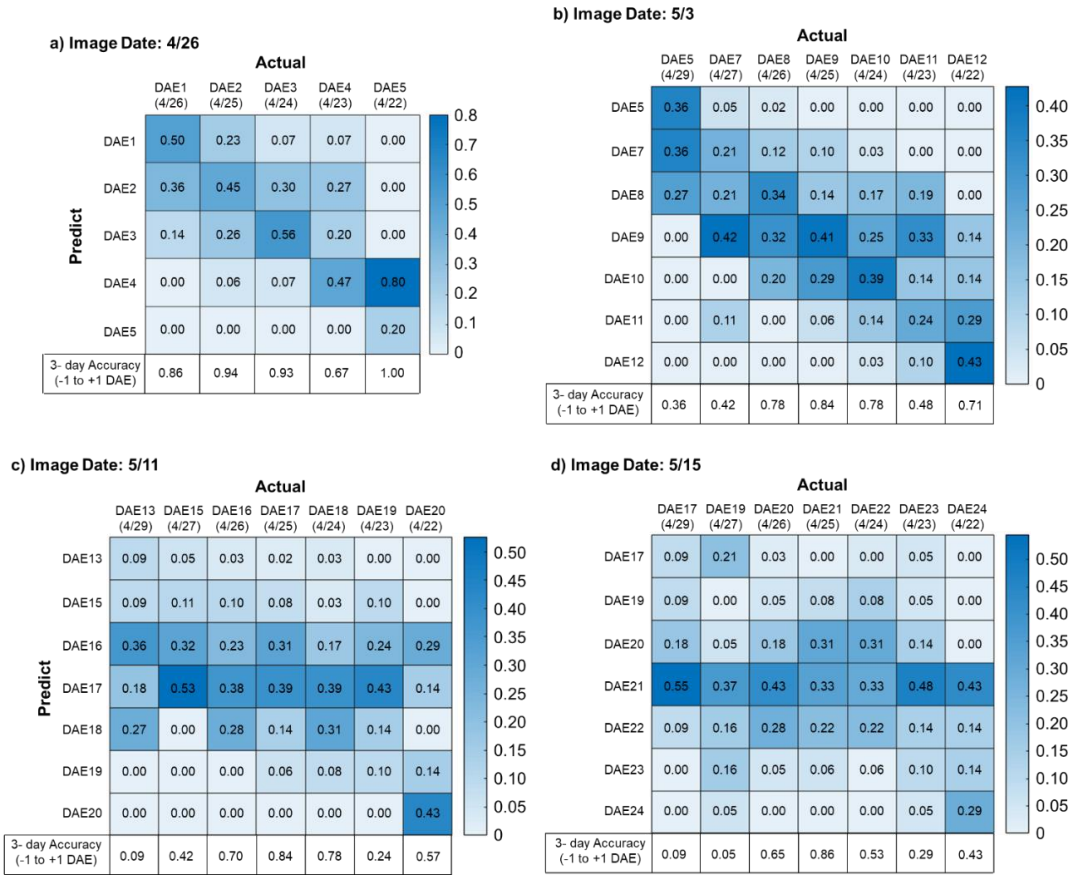

Figure 2-5. Heat maps of the classification accuracy and 3-day accuracy (-1 to +1 DAE) of each DAE class on each image date (emergence date in parentheses).

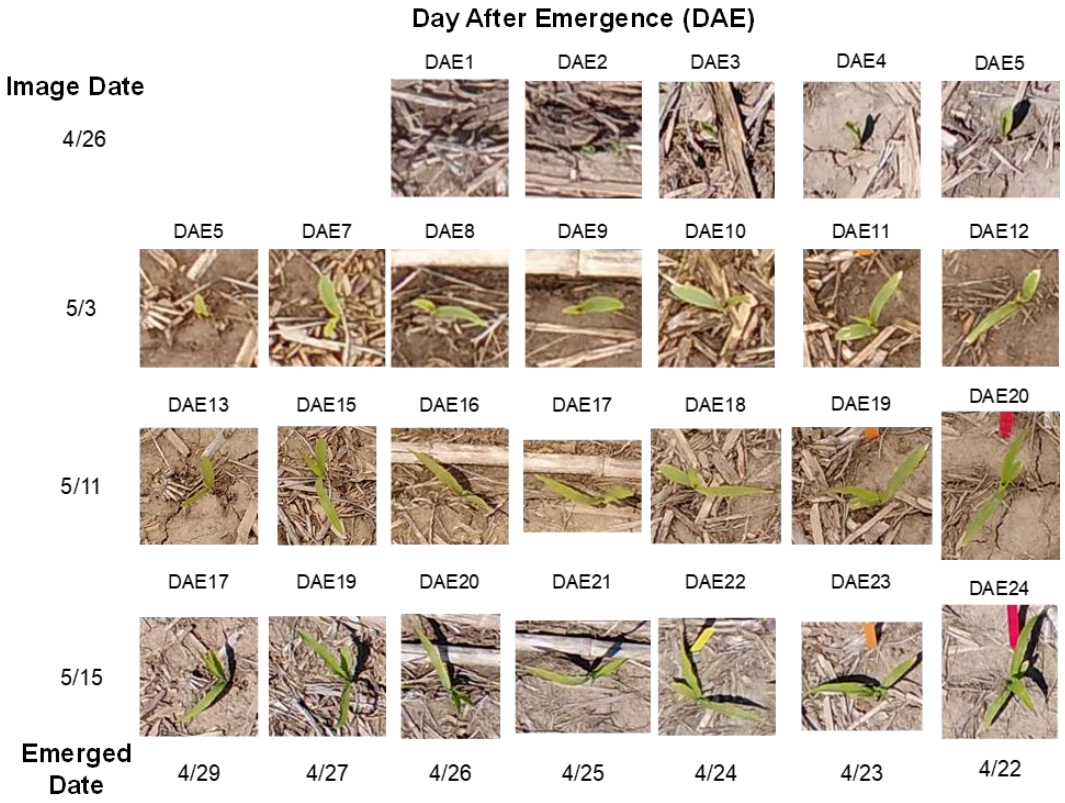

Figure 2-6. Example cropped corn images from UAV images of different DAE on each image date.

On the other hand, plants in DAE 3 could be described as having the first leaf opened, which increases the distinction in size and shape when compared to those in DAE 1 and DAE 2, and might be reason for slightly improved accuracy in DEA 3 (56%). Another possible reason for the low accuracy was that some of the plants in DAE 3 were in the transition stage from 'spike' to first leaf, causing 30% of the plants in DAE 3 to be predicted as those in DAE 2. Similar results were shown for DAE 4 (about 50% of the samples were predicted as DAE 2 and 3) and DAE 5 (80% of the samples were predicted as DAE 4), which the second leaf was becoming visible, but the plant size and shape were similar in both DAEs.

Figure 2-5b illustrates the classification accuracy for the second week of emergence (DAE 5 to DAE 12), showing that less than half of the samples for all DAE

classes were predicted correctly with accuracy ranging from 0.21 to 0.43. About 30% of DAE 5 plants were predicted as DAE 7 and DAE 8, which had two leaves opened (Fig. 2-6). The low classification accuracy might be due to the lack of distinctive features for some plants transitioning from one to two leaf, i.e., some DAE 5 plants may have transitioned to two leaf plants. Similarly, about 75% of DAE 7 plants were predicted to have emerged earlier. The prediction for 1-day DAE was best from DAE 8 through 10, but still not better than about 40%. There was a combination of over- and under-prediction for these DAEs that could be due to the similar characteristics during these days with two opened leaves without substantial differences (Fig. 2-6). Meanwhile, both DAE 11 and DAE 12 had the third leaf visible (Fig. 2-6), which could help improve the classification (the highest classification accuracy of 0.43 for DAE 12 among the other DAEs). However, more than half of them were classified as earlier DAEs because they were transitioning from two to three leaves.

Accuracy of predicting 1-day DAE for the third and fourth image dates (Fig. 2-5c and d; image dates 5/11 and 5/15) was generally worse than the earlier image dates, ranging from 0.00 to 0.43 accuracy. The poor classification accuracy in these DAEs might be due to emergence of the third leaf and its expansion over a three- to four-day window (DAE 15 to 19 in Fig. 2-6) with an insignificant increase in size. Although the third leaf provides additional features for image analysis, the fact that its emergence and expansion occurs over about four to five days diminishes the ability of nadir-view images to accurately classify DAE. Similarly, the fourth leaf emerged and expanded over many days (DAE 20 to 24 in Fig. 2-6) confounded the 1-day DAE prediction. Additionally, at the fourth leaf stage, older leaves on the lower part of plants were blocked by newer

leaves, which caused image features to be less sensitive in differentiating plants at different DAEs. In general, these results support that 1-day DAE prediction will be best from emergence through the two-leaf stage, and after that the sensitivity in predicting DAE classes getting weak.

Another reason for DAE misclassification was the limited number of plants being evaluated. The total number of plants emerged between 22 to 29 April was 627. The plant number ranged from 120 to 170 for emergence dates 24 to 26 April but was less than 70 for other dates. The small datasets for training and testing potentially skewed model sensitivity (O'Brien & Ishwaran, 2019). Additionally, although the camera was adjusted to obtain nadir images, seedlings that were not at the center of images had a somewhat oblique view resulting in errors due to image distortion (Seifert et al., 2019).

Occasionally, emergence and growth of each individual seedling may not be uniform due to soil and residue conditions, which causes some variability in the image features from plant to plant. One of the most vital factors affecting the corn emergence and seedling growth in the first six weeks is soil temperature (Alessi & Power, 1971). Studies showed that lower soil temperature caused by residue from no-till (similar to the field in our study) delayed corn emergence, early growth and development (Al-Darby & Lowery, 1987; Bollero et al., 1996). Figure 2-7a and b illustrate the two examples of residue distribution and their influence on growth rate from plants that emerged on the same day, DAE 5. In Fig. 2-7a, a DAE 5 plant was classified correctly with the common feature of the second visible leaf (Fig. 2-6). On the other hand, Fig. 2-7b shows a DAE 5 plant but this plant was growing in low residue surroundings and was misclassified as a DAE 7. The low residue environment (i.e., more darker soil absorbing light) enabled

higher soil temperatures and more rapid growth. Figure 2-7c and d show another example of image feature variability caused by the coleoptile (a protective sheath covering the first leaf) orientation. In Fig. 2-7c, a DAE 1 plant was classified correctly with the coleoptile emerged vertically from the soil surface. In Fig. 2-7d, the coleoptile did not emerge vertically from the soil surface but instead was forced to grow horizontally as it encountered surface residue, and was misclassified as a DAE 2 plant.

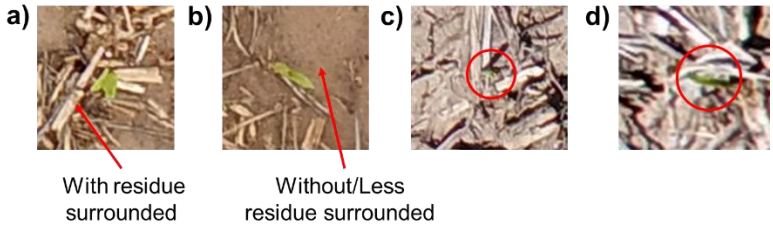

Figure 2-7. Example images showing correctly classified and misclassified plants. (a) A correctly classified DAE 5 plant surrounded by the average residue for the field; (b) a DAE 5 plant misclassified as a DAE 7 plant surrounded with less residue; (c) a correctly classified DAE 1 plant with coleoptile emerged vertically from the soil surface (red circle) and (d) a DAE 1 plant misclassified as a DAE 2 plant with the coleoptile growing horizontally (red circle).

2.4.3 Three-day Classification Accuracy for Each Image Date and Overall Classification Accuracy

During the first week of emergence, the 3-day accuracy was high for each DAE (> 0.85) except for DAE 4 (0.67) (Fig. 2-5a). For the second image date (Fig. 2-5b), 3-day accuracy was not as good as the first week, but still ranged from 0.36 to 0.84, with no consistent trend from day to day. Similar results were indicated for the last two image dates (Fig. 2-5c and d). Figure 2-8 shows the overall prediction accuracies of the 1-day DAE and 3-day DAE for each image date. On average, UAV imagery predicted the 1-day DAE with moderate overall accuracy (i.e., < 0.5), but accuracy was greatly improved when the performance measure for DAE was expanded to be within a 3-day window. As with predicting 1-day DAE, DAE classification sensitivity using the 3-day window was

reduced as plants matured. Prediction of plant emergence in a 3-day period is useful for studies about corn emergence uniformity. Previous studies on the effects of delayed emergence on yield used wider day ranges such as one to three weeks (Andrade & Abbate, 2005; Liu et al., 2004; Nafziger et al., 1991). Only one study investigated the effects of delayed planting of 2, 5, 8 and 12 days on yield (Lawles et al., 2012). Moreover, indication of delayed days was based on delayed planting days without documenting the exact emergence day. This might be due to the time-consuming and labor-intensive field work needed to record the exact emergence day. Therefore, this study shows proof of concept of using high-resolution UAV images for predicting DAE within a 3-day period. Additional automation in data processing procedure would be needed to extend the scale of this process.

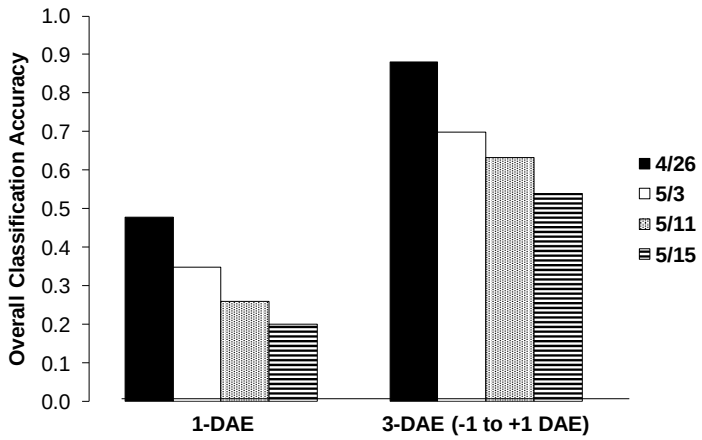

Figure 2-8. Overall accuracies of exact DAE and DAE within a three-day window for each image date.

2.4.4 Identification of Important Image Features

It is useful to evaluate the importance of different image features on the performance of estimation of DAEs. Figure 2-9 demonstrates the variable importance plots for the important features determined using the mean decrease in Gini index. As can

be seen, three features, i.e., diameter, area, and SF2 (ratio of major axis length to area) were consistently within the top five of the 17 features across all image dates. Diameter was within the top three for all dates. The fact that these three features were consistently strong contributors for predicting DAE suggests their importance, and therefore should be focused on in future studies. Figure 2-10 illustrates the mean diameter and area for the first two image dates (26 April and 3 May) at different DAEs. The diameter and area increased with increasing DAE, which corresponded to the plant growth with increasing leaf size and additional visible leaves. These morphological features captured through UAV images provide phenological information that may be useful for crop growth modeling (Dodig et al., 2019; Wang et al., 2018). Interestingly, for the first image date, minor axis length ranked as the most important feature, but was much less important in the subsequent image dates. Figure 2-11 depicts the minor and major axis length of the ellipse region of the corn plant at different DAEs. During the first week of emergence (Fig. 2-11a), the ellipse region of the plant covered the complete area of the first leaf. Thus, minor axis length increased with increasing leaf size. On the other hand, for the second week onwards (Fig. 2-11b to 2-11d), the ellipse region depicted the overall nadir view of the plant, which the minor axis length sometimes represented the width of one leaf or the center region of the plant (at the whorl or nearby it, Fig. 2-11d). This uncertainty caused inconsistent trends in this feature at different DAEs.

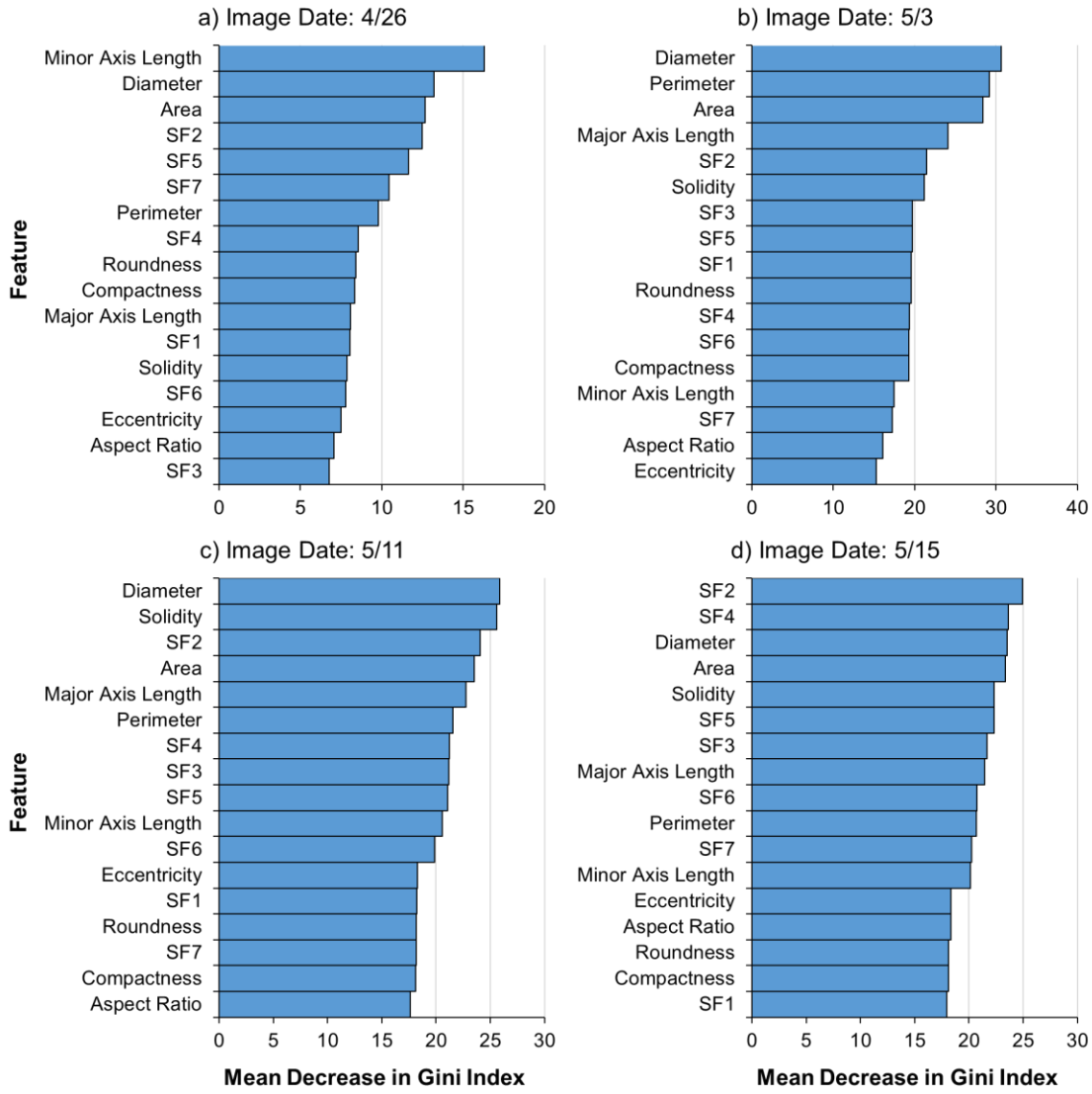

Figure 2-9. Variable importance plots indicating important features based on mean decrease in the Gini index for image date a) 26 April, b) 3 May, c) 11 May, and d) 15 May.

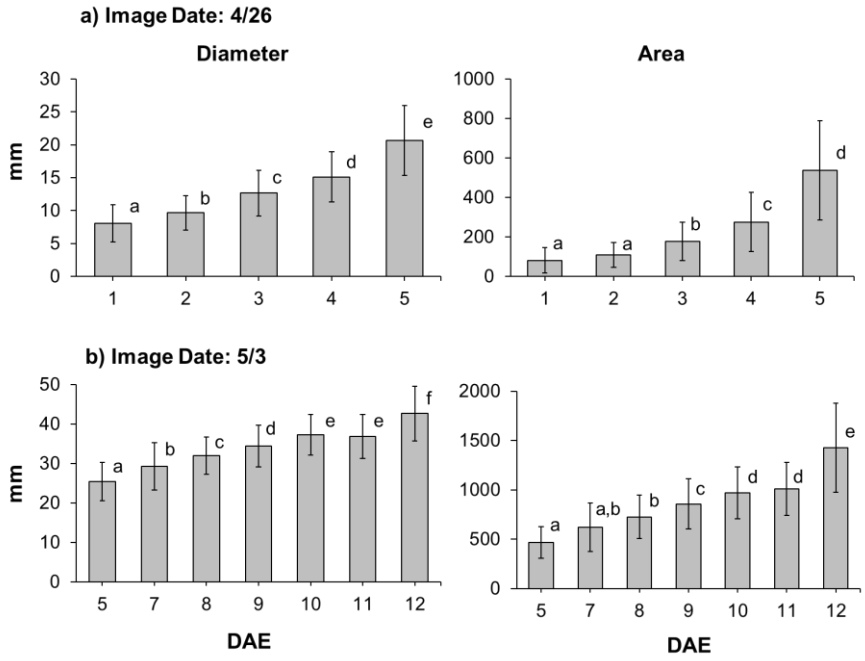

Figure 2-10. Mean diameter and area for image date a) 26 April and b) 3 May (different letters in each chart show significant differences in the mean at p-value less than 0.05 for the Tukey HSD test).

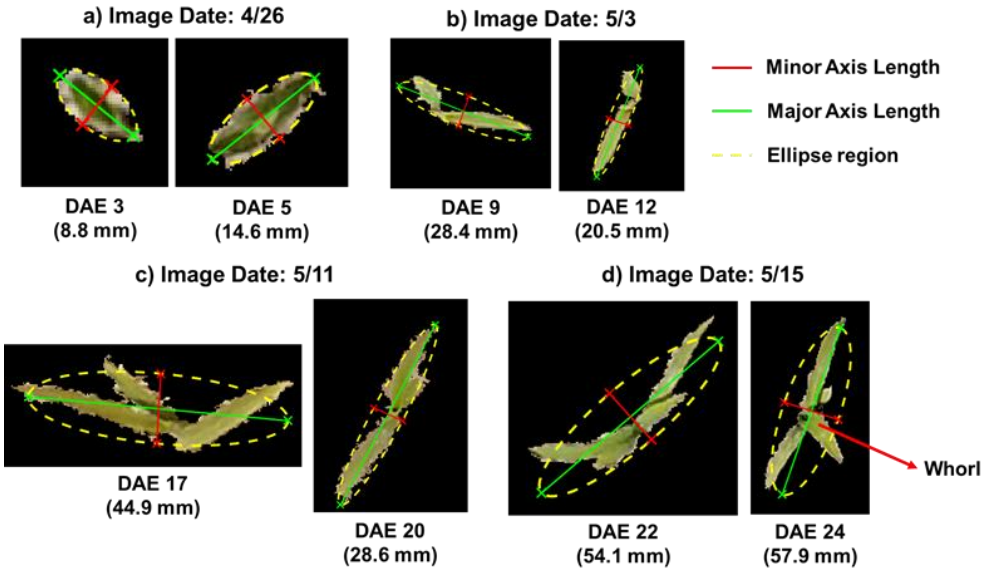

Figure 2-11. Minor and major axis length representation for corn plants at different DAEs in image date a) 26 April, b) 3 May, c) 11 May, and d) 15 May (value in parentheses is minor axis length).

2.4.5 Future Study and Applications

This study provided meaningful estimates of post-emergence DAE using UAV images. In order to achieve this, it is necessary to fly the imaging system at a low altitude (~5 m) to acquire sufficient GSD, which will require higher resolution cameras to achieve the equivalent GSD with larger areas per scene. In addition, manual identification of corn plants was required for this study because of the presence of winter annual weeds growing alongside the emerging corn plants. Also, plant residues from the previous growing season added a challenge with image processing for predicting DAE. However, since conservation and no-tillage systems are often encouraged for soil conservation and health, this issue needs to be resolved. Future work should include more advanced image processing or deep learning (DL) models to automate the background removal (weeds and residues) such as using DL models to detect and segment single plants from each image.

As automation of image processing is developed and refined, time and labor needed for collecting field-scale UAV imagery for this type of analysis will be reasonable. As a bridge to that, more large-scale field experiments on emergence uniformity evaluation using UAV images should be conducted. These studies might include other soil and crop management factors, such as investigating the effects of emergence uniformity due to tillage systems (Lithourgidis et al., 2005), different planting depths (Hussen et al., 2013; Molatudi & Mariga, 2009), and seed size (Molatudi & Mariga, 2009). In addition, plant morphological features may be affected by environmental factors including soil and weather conditions, which may cause bias of DAE estimation using only image features. Therefore, in future work, the DAE

estimation model should also include environmental information such as growing degree day (GDD), soil apparent electricity conductivity (ECa), and soil information from a real-time planting sensor (SmartFirmer, Precision Planting, Tremont, IL, USA).

To improve the classification accuracy, different approaches of UAV data collection could be tested. For example, collecting a sequence of multiple images captured with varied "sufficient overlaps", such as 85% front and 70% side overlap for field-scale experiments as suggested by aerial image stitching software, Pix4D (Pix4D Inc. Denver, CO, USA) to produce an orthomosaic (Lin & Medioni, 2007). This will reduce the variability of image features caused by imaging plants at an oblique angle. In addition, orthomosaic generation can be useful for mapping emergence uniformity for the entire field and the proportion of early and delayed emergence. This would be beneficial in making replanting decisions (Nafziger et al., 1991). Another UAV data collection approach could be collecting a series of nadir and oblique (camera adjusted to vertical angle of 45° and 135°) images to generate a 3D dense point clouds (Che et al., 2020; Karpina et al., 2016; Zhou et al., 2018). These 3D dense point clouds may be useful to extract other features such as plant height and total number of leaves.

2.5 Conclusion

This research demonstrated UAV imagery can be used to detect newly-emerged corn plants and estimate emergence date, which will be valuable for evaluating plant emergence uniformity and replanting decisions. The required GSD to detect the small corn seedlings (DAE 1 to 5) during the first week after emergence ranged from 0.55 to 0.94 mm $pixel^{-1}$. Unmanned aerial vehicle imagery was not able to predict the 1-day DAE with high overall accuracies, but was capable of predicting DAE within a 3-day window

(-1 to +1 DAE) with higher overall accuracies. DAE prediction was best for the first two weeks after emergence (from emergence through two-leaf stage). Afterward, sensitivity in predicting DAE was reduced. Diameter, area and SF2 (i.e., minor axis length/area) were important features identified to differentiate DAE for all image dates with one additional feature of minor axis length for the first week of emergence. Further studies should acquire multiple images and generate an orthomosaic to reduce image feature variability. More plant samples at each DAE should be included to obtain a more robust model and subsequently, increase the actual DAE prediction accuracy. Furthermore, additional environmental data should be included in the prediction model to reduce the DAE estimation bias. To conclude, this study serves as the very first approach in estimating corn emergence date in field conditions using UAV imagery with a high overall 3-day estimation accuracy. The methods and results of this study may provide baseline information for researchers who will conduct similar projects in the future.

References

Abdi, H., & Williams, L. J. (2010). Tukey's honestly significant difference (HSD) test. *Encyclopedia of research design, 3*, 583-585.

Al‐Darby, A., & Lowery, B. (1987). Seed zone soil temperature and early corn growth with three conservation tillage systems. *Soil Science Society of America Journal, 51*(3), 768-774.

Alessi, J., & Power, J. (1971). Corn emergence in relation to soil temperature and seeding depth 1. *Agronomy Journal, 63*(5), 717-719.

Andrade, F. H., & Abbate, P. E. (2005). Response of maize and soybean to variability in stand uniformity. *Agronomy Journal, 97*(4), 1263-1269.

Belgiu, M., & Drăguţ, L. (2016). Random forest in remote sensing: A review of applications and future directions. *ISPRS Journal of Photogrammetry and Remote Sensing, 114*, 24-31.

Bollero, G. A., Bullock, D. G., & Hollinger, S. E. (1996). Soil temperature and planting date effects on corn yield, leaf area, and plant development. *Agronomy Journal, 88*(3), 385-390.

Breiman, L., & Cutler, A. (2018). *Breiman and Cutler's random forests for classification and regression*. Retrieved from https://cran.r-project.org/web/packages/randomForest/randomForest.pdf

Chandpa, K. R., Jani, A. M., & Prajapati, G. I. (2014). Comparative Study of Linear and Non-linear Contrast Enhancement Techniques. *International Journal of Research and Scientific Innovation, 1*, 37-41.

Chaugule, A., & Mali, S. N. (2014). Evaluation of texture and shape features for classification of four paddy varieties. *Journal of Engineering, 2014*.

Che, Y., Wang, Q., Xie, Z., Zhou, L., Li, S., Hui, F., . . . Ma, Y. (2020). Estimation of maize plant height and leaf area index dynamic using unmanned aerial vehicle with oblique and nadir photography. *Annals of Botany*.

Chen, X., Xun, Y., Li, W., & Zhang, J. (2010). Combining discriminant analysis and neural networks for corn variety identification. *Computers and electronics in agriculture, 71*, S48-S53.

Dodig, D., Božinović, S., Nikolić, A., Zorić, M., Vančetović, J., Ignjatović-Micić, D., . . . Altmann, T. (2019). Image-Derived Traits Related to Mid-Season Growth Performance of Maize Under Nitrogen and Water Stress. *Frontiers in Plant Science, 10*, 814.

Food and Agriculture Organization of the United Nations. (2020). FAOSTAT statistical database. Retrieved from http://www.fao.org/faostat/en/#data/QC/visualize

Gareth, J. (2010). *An introduction to statistical learning: with applications in R*: Springer Verlag.

Gnädinger, F., & Schmidhalter, U. (2017). Digital counts of maize plants by unmanned aerial vehicles (UAVs). *Remote Sensing, 9*(6), 544.

Hussen, S., Alemu, B., & Ahmed, F. (2013). Effect of planting depth on growth performance of maize (Zea mays) at the experimental site of Wollo University, Dessie, Ethiopia. *International Journal of Sciences: Basic and Applied Research, 8*(1), 10-15.

James, G., Witten, D., Hastie, T., & Tibshirani, R. (2013). *An introduction to statistical learning*: New York: Springer.

Jin, X., Liu, S., Baret, F., Hemerlé, M., & Comar, A. (2017). Estimates of plant density of wheat crops at emergence from very low altitude UAV imagery. *Remote Sensing of Environment, 198*, 105-114.

Karpina, M., Jarząbek-Rychard, M., Tymków, P., & Borkowski, A. (2016). UAV-based automatic tree growth measurement for biomass estimation. *International Archives of the Photogrammetry, Remote Sensing and Spatial Information Sciences, 8*.

Klopfenstein, T., Erickson, G., & Berger, L. (2013). Maize is a critically important source of food, feed, energy and forage in the USA. *Field Crops Research, 153,* 5-11.

Kuhn, M. (2019). Package 'caret': RStudio. Retrieved from https://cran.r-project.org/web/packages/caret/caret.pdf

Lauer, J. G., & Rankin, M. (2004). Corn response to within row plant spacing variation. *Agronomy Journal, 96*(5), 1464-1468.

Lawles, K., Raun, W., Desta, K., & Freeman, K. (2012). Effect of delayed emergence on corn grain yields. *Journal of plant nutrition, 35*(3), 480-496.

Lin, Y., & Medioni, G. (2007). *Map-enhanced UAV image sequence registration and synchronization of multiple image sequences.* Paper presented at the 2007 IEEE Conference on Computer Vision and Pattern Recognition.

Lithourgidis, A. S., Tsatsarelis, C. A., & Dhima, K. V. (2005). Tillage effects on corn emergence, silage yield, and labor and fuel inputs in double cropping with wheat. *Crop Science, 45*(6), 2523-2528.

Liu, W., Tollenaar, M., Stewart, G., & Deen, W. (2004). Response of corn grain yield to spatial and temporal variability in emergence. *Crop Science, 44*(3), 847-854.

Molatudi, R., & Mariga, I. (2009). The effect of maize seed size and depth of planting on seedling emergence and seedling vigour. *Journal of applied sciences research, 5*(12), 2234-2237.

Nafziger, E. D., Carter, P. R., & Graham, E. E. (1991). Response of corn to uneven emergence. *Crop Science, 31*(3), 811-815.

Najafabadi, S. S. M., & Farahani, L. (2012). Shape analysis of common bean (Phaseolus vulgaris L.) seeds using image analysis. *International Research Journal of Applied and Basic Sciences, 3*(8), 1619-1623.

Nations, F. a. A. O. o. t. U. (2020). FAOSTAT statistical database. Retrieved from http://www.fao.org/faostat/en/#data/QC/visualize

O'Brien, R., & Ishwaran, H. (2019). A random forests quantile classifier for class imbalanced data. *Pattern recognition, 90*, 232-249.

Orych, A. (2015). REVIEW OF METHODS FOR DETERMINING THE SPATIAL RESOLUTION OF UAV SENSORS. *International Archives of the Photogrammetry, Remote Sensing & Spatial Information Sciences, 40*.

Oshiro, T. M., Perez, P. S., & Baranauskas, J. A. (2012). *How many trees in a random forest?* Paper presented at the International workshop on machine learning and data mining in pattern recognition.

Poncet, A. M., Fulton, J. P., McDonald, T. P., Knappenberger, T., & Shaw, J. N. (2019). Corn emergence and yield response to row-unit depth and downforce for varying field conditions. *Applied Engineering in Agriculture, 35*(3), 399-408.

Ransom, J., Endres, G., & McWilliams, D. (2013). Corn Growth and Management Quick Guide A1173. *Available at Web site http://www. ag. ndsu. edu/pubs/plantsci/crops/a1173. pdf (verified April 2017)*.

Rodriguez-Galiano, V. F., Ghimire, B., Rogan, J., Chica-Olmo, M., & Rigol-Sanchez, J. P. (2012). An assessment of the effectiveness of a random forest classifier for land-cover classification. *ISPRS Journal of Photogrammetry and Remote Sensing, 67*, 93-104.

Sawyer, S. F. (2009). Analysis of variance: the fundamental concepts. *Journal of Manual & Manipulative Therapy, 17*(2), 27E-38E.

Seifert, E., Seifert, S., Vogt, H., Drew, D., van Aardt, J., Kunneke, A., & Seifert, T. (2019). Influence of Drone Altitude, Image Overlap, and Optical Sensor Resolution on Multi-View Reconstruction of Forest Images. *Remote Sensing, 11*(10), 1252.

Shiferaw, B., Prasanna, B. M., Hellin, J., & Bänziger, M. (2011). Crops that feed the world 6. Past successes and future challenges to the role played by maize in global food security. *Food Security, 3*(3), 307.

Shuai, G., Martinez-Feria, R. A., Zhang, J., Li, S., Price, R., & Basso, B. (2019). Capturing Maize Stand Heterogeneity Across Yield-Stability Zones Using Unmanned Aerial Vehicles (UAV). *Sensors, 19*(20), 4446.

Varela, S., Dhodda, P., Hsu, W., Prasad, P., Assefa, Y., Peralta, N., . . . Ciampitti, I. (2018). Early-season stand count determination in corn via integration of imagery from unmanned aerial systems (UAS) and supervised learning techniques. *Remote Sensing, 10*(2), 343.

Wang, N., Wang, E., Wang, J., Zhang, J., Zheng, B., Huang, Y., & Tan, M. (2018). Modelling maize phenology, biomass growth and yield under contrasting temperature conditions. *Agricultural and Forest Meteorology, 250*, 319-329.

Zhang, J., Basso, B., Price, R. F., Putman, G., & Shuai, G. (2018). Estimating plant distance in maize using Unmanned Aerial Vehicle (UAV). *PloS one, 13*(4), e0195223.

Zhou, J., Fu, X., Schumacher, L., & Zhou, J. (2018). Evaluating geometric measurement accuracy based on 3d reconstruction of automated imagery in a greenhouse. *Sensors, 18*(7), 2270.

CHAPTER THREE

EARLY CORN STAND COUNT OF DIFFERENT CROPPING SYSTEMS USING UAV-IMAGERY AND DEEP LEARNING

3.1 Abstract

Optimum plant stand density and uniformity is vital in order to maximize corn (*Zea mays* L.) yield potential. Assessment of stand density can occur shortly after seedlings begin to emerge, allowing for timely replant decisions. The conventional methods for evaluating an early plant stand rely on manual measurement and visual observation, which are time-consuming, subjective because of the small sampling areas used, and unable to capture field-scale spatial variability. This study aimed to evaluate the feasibility of an unmanned aerial vehicle (UAV)-based imaging system for estimating early corn stand count in three cropping systems (CS) with different tillage and crop rotation practices. A UAV equipped with an on-board RGB camera was used to collect imagery of corn seedlings (~14 days after planting) of CS, i.e., minimum-till corn-soybean rotation (MTCS), no-till corn-soybean rotation (NTCS), and no-till corn-corn rotation with cover crop implementation (NTCC). An image processing workflow based on a deep learning (DL) model, U-Net, was developed for plant segmentation and stand count estimation. Results showed that the DL model performed best in segmenting seedlings in MTCS, followed by NTCS and NTCC. Similarly, accuracy for stand count estimation was highest in MTCS (R^2 = 0.95), followed by NTCS (0.94) and NTCC (0.92). Differences by CS were related to amount and distribution of soil surface residue cover, with increasing residue generally reducing the performance of the proposed method in stand count estimation. Thus, the feasibility of using UAV imagery and DL

modeling for estimating early corn stand count is influenced by soil and crop management practices.

3.2 Introduction

Optimum plant density and uniformity are critical crop management parameters to maximize crop production and yield, especially for corn (*Zea mays* L.) (Sangoi, 2001). Optimal plant density is determined based on a number of factors, such as hybrid, maturity, length of growing season, and planting date (Sangoi, 2001). For example, higher planting density is suggested for early planting where there is a risk of yield loss due to the lower soil and air temperature (Bollero et al., 1996; Sangoi, 2001; Stanger & Lauer, 2006). In addition, higher planting density is utilized to increase the stress-tolerance of corn hybrids to maximize yield (Assefa et al., 2016; Van Roekel & Coulter, 2011). Although seeds may be planted at the optimum density, spatial variation of the plant density can occur due to poor seed germination (including emergence delays and/or failed emergence), planter performance problems, and early-season plant death due to stress (Thorp et al., 2007). Collectively, this variability affects final corn grain yield. Therefore, early assessment of plant density by quantifying stand count is valuable for subsequent management decisions (e.g., replanting and post-emerge herbicide applications) and for evaluating spatial yield variability as shown in yield maps.

The conventional method for an early stand count is usually based on manually counting the number of seedlings at multiple sites within a given field (Nielsen, 2003). Manual assessment of stand count is time consuming, labor intensive, subjective due to small sampling areas used, and may not be representative of whole fields (Varela et al., 2018). In addition, sensors mounted on the row-dividers of a combined head have been

developed to count and map plant density at harvest, resulting in more information for crop management recommendations for the next growing season (Birrell & Sudduth, 1995; Sudduth et al., 2000). However, this measurement has no value for guiding in-season management.

Recently, UAV-based imaging systems have shown the potential of capturing high-resolution red-green-blue (RGB) images for detecting and estimating stand counts of different crops including corn (Gnädinger & Schmidhalter, 2017; Kitano et al., 2019; Shuai et al., 2019; Varela et al., 2018), wheat (*Triticum aestivum* L.) (Jin et al., 2017), cotton (*Gossypium* L.) (Chen et al., 2018), rapeseed (*Brassica napus* L.) (B. Zhao et al., 2018), and sorghum (*Sorghum bicolor* L.) (Ghosal et al., 2019; Guo et al., 2018). These studies acquired images using high-resolution RGB cameras at a low altitude (3 to 20 m) that resulted in a ground sampling distance (GSD) of 0.20 to 8.9 mm pixel^{-1}. Studies showed that UAV-based methods could estimate stand counts accurately with coefficients of determination (R^2) of 0.80 to 0.91, 0.56 to 0.84, 0.72 to 0.89, and 0.89 for wheat (Jin et al., 2017), sorghum (Ghosal et al., 2019; Guo et al., 2018), rapeseed (B. Zhao et al., 2018), and corn (Gnädinger & Schmidhalter, 2017), respectively.

One of the most important steps in the assessment of crop stand count using UAV imagery is to segment plants from images. The crop segmentation can be conducted using vegetation indices to signify the difference between crop and background. For example, a simple excess green vegetation index was used to segment corn plants from UAV images where there were only small amounts of residue on the soil surface (Shuai et al., 2019; Varela et al., 2018). (Gnädinger & Schmidhalter, 2017) used contrast enhancement and threshold value in two color spaces (i.e., HSV and L*a*b) for image segmentation to

detect plants at the 3- to 5-leaf development stage, while (Kitano et al., 2019) used a deep learning (DL) method to estimate plant density with different treatments (plant densities, flying heights and growth stages). Although these studies demonstrated the potential of detecting plants and determining corn stand count at early growth stages using global thresholds, they focused on fields under traditional agriculture practices that included conventional or minimum tillage, where the image background was simple and dominated by soil. In recent years, conservation agriculture has become popular due to its potential for mitigating negative environmental impacts while maintaining desired yield (Conway et al., 2018; Hobbs et al., 2008; Nunes et al., 2018; Pittelkow et al., 2015; Yost et al., 2016). Conservation agriculture fields that include no-till (crop planting with minimum soil disturbance), cover crops, and diverse crop rotations (Hobbs et al., 2008; Pittelkow et al., 2015) have plant residues that make it difficult to identify early-stage plants for accurate evaluation of stand count. For UAV imagery stand count methods to be widely adoptable, the stand count assessment methods need to be evaluated for corn fields where conservation agriculture is practiced and where there is a more complex background. Based on our best knowledge, the performance of UAV-based method in stand count assessment for crops managed using conservation agriculture has not been evaluated.

Due to advances in image processing and deep learning (DL) techniques, it is now possible to process images with more complex backgrounds. Deep learning is a kind of machine learning (ML), which is composed of different functions (e.g., convolutions, pooling layers, and fully connected layers) to transform data in a hierarchical way, forming a “deeper” neural network model (Kamilaris & Prenafeta-Boldú, 2018). Deep

learning techniques are more effective than conventional ML in the identification of subtle differences in images due to their ability for feature learning from raw data and automatic feature extraction in the model. Deep learning has shown great potential in segmenting plants from the soil background using low-altitude UAV images (Fan et al., 2018; Fawakherji et al., 2019; Kitano et al., 2019; Trujillano et al., 2018; Zhang et al., 2020; Zhuang et al., 2018). The RGB color and multispectral images captured from a UAV have been used in a DL model to segment tobacco (*Nicotiana tabacum* L.) (Fan et al., 2018), corn (Fawakherji et al., 2019; Kitano et al., 2019; Trujillano et al., 2018), sugar beet (*Beta vulgaris* L.) (Fawakherji et al., 2019) and purple rapeseed leaves (Zhang et al., 2020). Moreover, RGB images collected from a camera mounted on an agricultural robot were used in a DL model to segment corn and sugar beet plants under different light conditions (Zhuang et al., 2018). All these studies used the same type of DL model known as a convolutional neural network (CNN), which is primarily used for pattern recognition within images (Albawi et al., 2017). The main architecture of CNN is formed by stacked layers of convolution, pooling, and fully-connected layers. The convolution layer extracts features automatically from each input image and the pooling layer reduces the dimensionality of the extracted features (Amara et al., 2017). Then, the fully-connected layer at the end utilizes the learned features to classify the input images. Examples of the CNN models used include U-Net for corn and purple rapeseed leaves segmentation (Kitano et al., 2019; Zhang et al., 2020), Segnet and VGG-UNet for corn and sugar beet classification (Fawakherji et al., 2019), and LeNet for corn classification (Trujillano et al., 2018).

With the promising results from using UAV imagery and DL modeling for segmenting images, the present study aimed to evaluate the feasibility of UAV-based imagery and a DL model for estimating early corn stand count in different cropping systems (CS). The specific objectives included: 1) to build a DL model for segmenting corn plants in different CS from UAV images; and 2) to build an image processing workflow for corn early stand count estimation.

3.3 Material and Methodology

3.3.1 Experimental Site

This study was conducted in 2019 at a research farm in the United States Department of Agriculture, Agricultural Research Service (USDA-ARS) Long-Term Agroecosystem Research (LTAR) network (Sadler et al., 2015) near Centralia, MO (39°13’48” N, 92°7’14” W). A detailed description and research history of the site have been reported previously (Conway et al., 2018; Yost et al., 2016). In the present study, a large-plot area (12 ha) and an adjacent 4-ha field were used (Fig. 3-1). The replicated plot area had 10 CS main plots with three replications. Each plot was 190 m by 20 m (0.4 ha). As indicated in Table 3-1, this study included two of the 10 CS, i.e., minimum-tillage corn-soybean rotation (MTCS, Fig. 1) and no-till corn-soybean rotation (NTCS, Fig. 1). These have been managed in this same rotation for > 25 years. A third CS, no-till continuous corn with cover crops (NTCC) was implemented in the adjacent 4-ha field (Fig. 3-1). For MTCS and NTCS, the plots were planted with soybean (*Glycine max*) in 2018, resulting in low to medium amounts of residue in the plots when planting corn in 2019 (Fig. 3-2a to d). Meanwhile, in the spring of 2018, corn was planted in the NTCC, followed by a cover crop seeding in the fall. The cover crop consisted of cereal rye

(*Secale cereale L.*) and hairy vetch (*Vicia villosa Roth*), causing a higher percentage of residue cover when planting in 2019 (Fig. 3-2e and f). The cover crops were terminated using 32 oz. of glyphosate (Roundup) and 32 oz. of glufosinate (Liberty) herbicides.

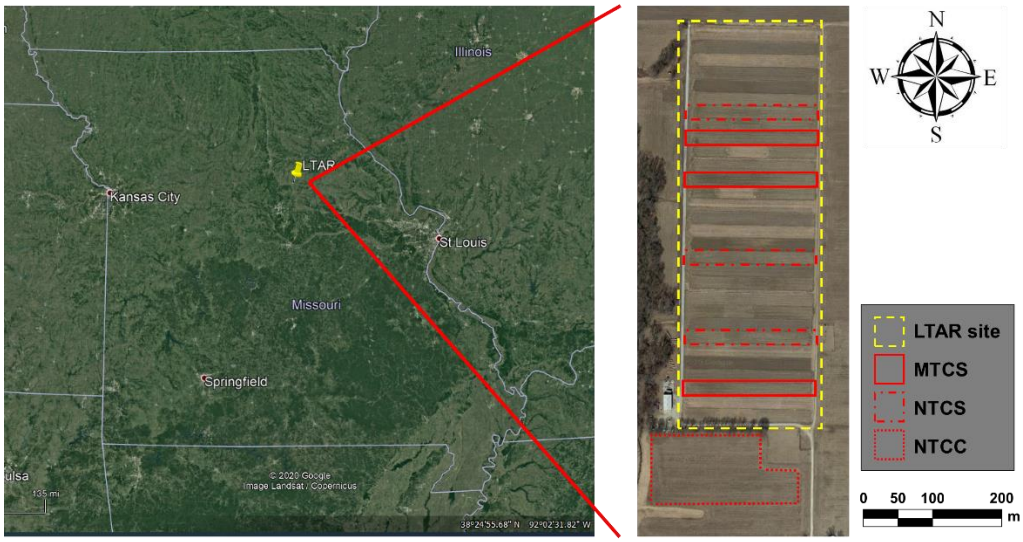

Figure 3-1. Long-Term Agroecosystem Research (LTAR) experimental site used for this study with different cropping systems (MTCS: minimum-till corn-soybean; NTCS: no-till corn-soybean; NTCC: no-till corn-corn including cover crop) identified.

Table 3-1. Cropping system description, date of planting, and UAV image acquisition date in 2019 at the study site near Centralia, MO.

Cropping System	Description	Residue Cover	Planting Date	UAV Image Date
MTCS	Minimum-till; Corn following soybean	None/Low	May 15th	May 28th
NTCS	No-till; Corn following soybean	Medium	May 15th	May 28th
NTCC	No-till; Corn following corn with cover crops	High	May 31st	June 14th

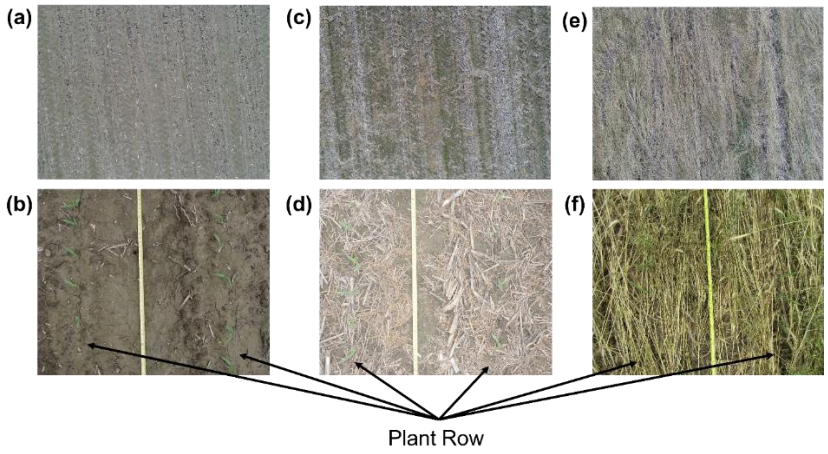

Figure 3-2. Images of the three cropping systems with different types and amounts of residue cover. Images (a), (c) and (e) were taken using the UAV system, and (b), (d) and (f) were taken using a camera from the ground. Images (a) and (b) are minimum-till corn-soybean rotation (MTCS) with no or low residue; (c) and (d) are no-till corn-soybean rotation (NTCS) with medium residue; and (e) and (f) are no-till continuous corn including cover crops (NTCC) with high residue. Images were acquired at 13 (MTCS and NTCS) or 14 (NTCC) days after planting.

A 4-row planter with John Deere *MaxEmerge XP* row units (Deere & Co., Moline, IL, USA) was used for planting corn (hybrid Pioneer 0589, Corteva Agriscience, Wilmington, DE, USA) in all plots at a row spacing of 0.76 m and a travel speed of 1.9 m s^{-1}. In 2019, MTCS and NTCS plots were planted on May 15, while the NTCC field was planted on May 31 (Table 3-1). Seeding rate was set as 81,510 seeds ha^{-1} across the site, which was equivalent to a plant spacing of 16 cm. Additionally, the planter was outfitted with a Precision Planting hydraulic downforce system (DeltaForce®), finger-pickup seed meters (Precision Planting, LLC., Tremont, IL, USA), and seed-firmer sensors (SmartFirmer, Precision Planting, Tremont, IL, USA). No planter residue management (e.g., row cleaners and no-till coulters) was used during the seeding operation.

3.3.2 UAV Data Collection

Aerial image data was collected using a Phantom 4 Advanced UAV (DJI, Shenzhen, Guangdong, China) equipped with an on-board RGB camera. The camera had a field-of-view (FOV) of 84° and the selected image size was 4864 by 3648 pixels (20 M

pixels). Imagery was taken about two weeks after planting when the corn was at the second leaf vegetative growth stage (V2) or earlier. Specifically, data were collected for the MTCS and NTCS plots on May 28 and the NTCC field on June 14, 2019 (Table 3-1) between 10 am and 2 pm local time when the changes in the solar zenith angle are minimal. Sequential images were taken at 0.5 frames per second (fps) at a 10-m flight height and a speed of 2 m s^{-1}, which were set by planning the mission waypoints using the UAV control app Litchi (VC Technology Ltd, London, U.K.) to ensure image overlap of 75% in both forward and sideward directions. Each image frame had a calculated ground sampling distance (GSD) of 0.3 cm $pixel^{-1}$ and covered an area of approximately 159.1 m^2 (14.6 m × 10.9 m). This resulted in about 19 corn rows per image.

3.3.3 Image Processing and Data Analysis

Due to the complexity of images with small corn plants and heavy residues, as well as cover crops in the NTCC CS, an image processing method based on deep learning (DL) was used in this study to segment corn seedlings from UAV imagery. The image processing method included three major steps of 1) developing a DL model for image segmentation; 2) pre-processing UAV image data to prepare the input images for the DL model; 3) post-processing the segmented images from the DL model to obtain final segmented images with the background removed.

3.3.3.1 Development of the Deep Learning Model

The DL model used in this study was the U-Net model, which is a type of convolutional neural network and was first introduced for image segmentation in biomedical applications (Livne et al., 2019; Ronneberger et al., 2015). Recently, it has been widely used in agricultural applications for segmenting and classifying plants,

weeds, and ground straw coverage (Fawakherji et al., 2019; Kitano et al., 2019; Zhang et al., 2020; X. Zhao et al., 2019; Zhou et al., 2020). The U-net model is able to extract global features and context information from small-sized images and does not require a large training dataset (Zhou et al., 2020), making it feasible for this study. These features make it suitable for object segmentation with low resolution, uncertain size, and complex backgrounds (Zhang et al., 2020). Studies also showed that the image segmentation accuracy (pixel-to-pixel comparison) was higher as compared to other DL models such as SegNet (Fawakherji et al., 2019; Zhang et al., 2020).

In this study, the U-Net model was built using the 'unetLayers' function in Matlab with an encoder and a decoder as illustrated in Fig. 3-3. The encoder learned image features from input images, and reduced its dimension (width × height) by the max pool operation (2 × 2 filter size). The decoder identified the localization of the object-of-interest based on the corresponding reference feature map from the encoder part (depth concatenation). The depth concatenation also restored the image to its original dimension by up-convolution (2 × 2 filter size) and up-ReLU (Rectified Linear Unit) operations. The bridge section connected the encoder and decoder parts. All convolution operations had a filter size of 3 by 3, except for the final convolution layer before the output segmented image, which had a filter size of 1 by 1. The dropout operation selected a probability (0.5 in this study) at which input elements were dropped out randomly to prevent overfitting when training the neural network. Fig. 3-3a to 3-3g visualize some channels from the multi-channel feature map of the step-by-step image segmentation from the model. Training options as indicated in Table 3-2 were used.

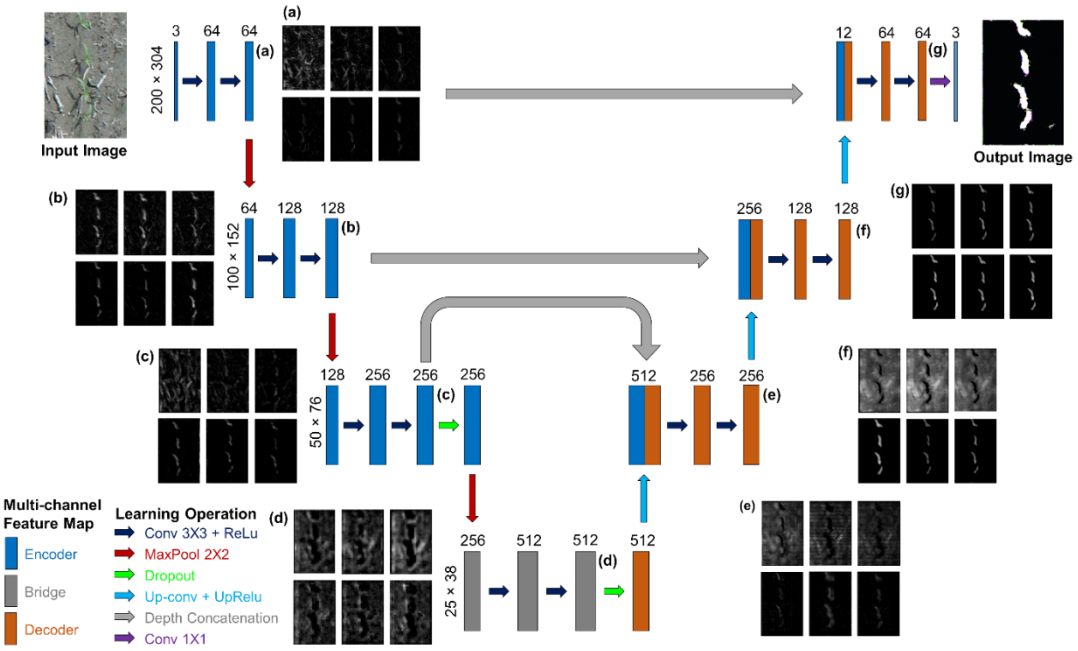

Figure 3-3. The architecture of the U-net deep learning model used in the study with legend at the bottom left. Each rectangle represents a multi-channel feature map with the number of channels given above. Image dimension (width × height) is indicated at the left edge. (a) to (g) show example channels from the feature map.

Table 3-2. Training option values used to train the model.

Training Option Name	Value
Solver	'adam'
Learning Rate	0.0001
Max Epoch	50
Mini Batch Size	64

3.3.3.2 Pre-processing UAV Images

Ten UAV images were randomly selected from each CS to train the U-Net model for image segmentation. Images were rotated to ensure plant rows were vertical based on visual inspection. Each plant row image was subsequently cropped to 200 pixels wide by the height of the rotated image (Fig. 3-4a to 3-4c) using Matlab (R2019b, MathWorks, Natick, MA, USA). The image width of 200 pixels (equivalent to 60 cm based on the average GSD of 0.3 cm pixel^{-1}) was selected to include one corn row in the middle and an adequate background. Then, smaller-sized images with a dimension of 200 by 304 pixels

were cropped from the plant row images, where the 304 pixels of image height covering 91 cm included one to five corn plants in each cropped image (Fig. 3-4d). Theoretically, five plants should have been included in the cropped images based on the 91 cm image length and plant spacing of 16 cm. However, the actual GSD changed during flight due to the variation of flight height caused by field slope and the error of UAV elevation sensor, resulting in fewer plants covered in some images. The cropped images were divided into training (70%), validation (20%), and testing (10%) datasets (Table 3-3). Training and validation datasets were used to build the DL model, and the model was evaluated using the testing dataset. Ground truth images (i.e., binary images of corn plants in white [pixel value = 1] and background in black [pixel value = 0]) of each cropped image were prepared using 'Image Segmenter' apps from the 'Image Processing and Computer Vision' toolbox in Matlab. Regions of interest (i.e., corn plants) were drawn using 'Draw ROIs' in the 'Image Segmenter' apps and the binary image was exported.

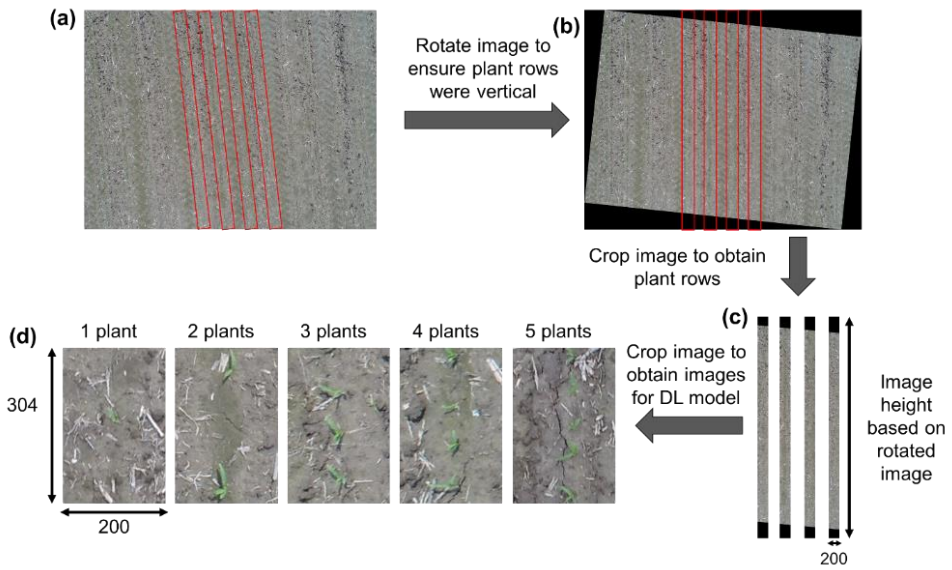

Figure 3-4. Illustration of image data preparation for building the deep learning (DL) model in this study: (a) original UAV image where red boxes indicate plant rows; (b) rotated UAV image; (c) cropped images of plant rows; and (d) cropped images used to build DL model.

Table 3-3. Number of cropped images from each cropping system used in training, validation and testing datasets.

Dataset	MTCS	NTCS	NTCC	Total
Training	1020	1000	1016	3036
Validation	290	280	288	858
Testing	140	130	139	409
Total	1450	1410	1443	

3.3.3.4 Post-processing Segmented Images from DL Model

Followed by the U-Net model, image post-processing steps including an adaptive image thresholding method (Bradley & Roth, 2007) and the morphological operation of image erosion were used to remove the remaining background or any noise in the image. The final segmented binary image was compared with the ground truth binary image to evaluate the image segmentation of the U-Net model using three parameters, namely precision, recall, and F1 (Table 3-4), which were computed by 'bfscore' in Matlab (Csurka et al., 2013). The average of each parameter for all the images in each CS as well as overall (for all CS) was calculated and reported.

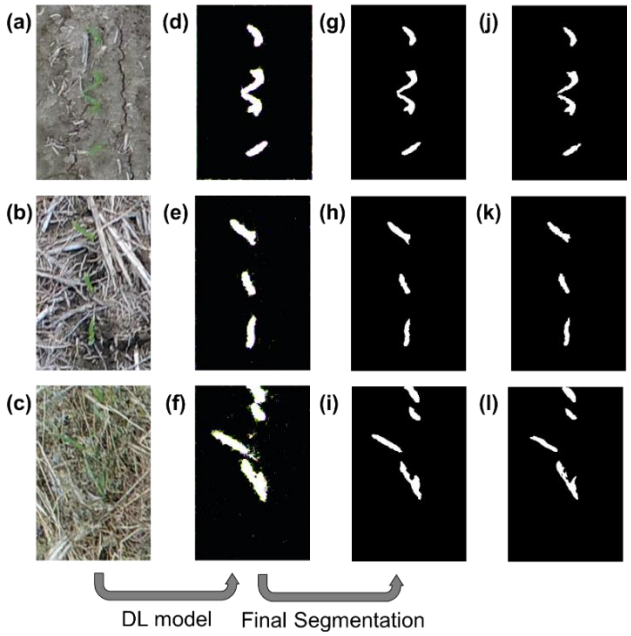

Figure 3-5. Illustration of image segmentation using the proposed deep learning (DL) model and final segmentation results. Images (a) to (c) are the original images; (d) to (f) are output from the proposed DL model; (g) to (i) are final segmented images; (j) to (l) are ground truth binary images prepared using the **'**Image Segmenter**'** apps for each cropping system: minimum-tillage corn-soybean rotation (top row); no-till corn-soybean rotation (middle row); no-till continuous corn including cover crops (bottom row).

Table 3-4. Parameter used to evaluate image segmentation (Csurka et al., 2013).

Parameters	**Description**
Precision	$Precision = \frac{TP}{TP + FP}$ where TP = true positive, number of pixels on the ground truth segmentation boundary that are also on the predicted segmentation boundary; FP = false positive, number of pixels on the predicted segmentation boundary but not on the ground truth segmentation boundary
Recall	$Recall = \frac{TP}{TP + FN}$ where TP = true positive, number of pixels on the ground truth segmentation boundary that are also on the predicted segmentation boundary; FN = false negative, number of pixels on the ground truth segmentation boundary but not on the predicted segmentation boundary
F1	Measures how close the predicted boundary of an object matches the ground truth boundary. $F1 = \frac{2 \times precision \times recall}{recall + precison}$

3.3.4 Image Processing Workflow for Plant Stand Count Estimation

An image processing workflow (Fig. 3-6) was built to estimate plant stand count (number of plant m^{-1}) for each corn row. Firstly, UAV images were cropped to 4800 by 3648 pixels from the original dimension of 4864 ×3648 pixels using the 'imcrop' function in Matlab. This was done so that 288 images could be equally cropped from the UAV image to be used as input images in the U-Net model. The same DL model and post-processing steps as described previously (henceforth referred to as proposed method) were used to segment the cropped images. Then, the cropped images were combined sequentially, followed by a row detection step to prevent counting non-corn objects between rows (Fig. 3-6b to 6e). The row detection step began by first finding the lines (rows) in the binary image using a Hough transformation (Fig. 3-6c), and the angle detected was used to rotate the binary (Fig. 3-6d) and original images. When summing the number of pixels at each image width of the binary image ("1" for plants and "0" for background) and smoothing the data using a Gaussian filter, the detected peaks (red circles in Fig. 3-6e) represented each row (Varela et al., 2018). The image width position of each peak was used to crop each plant row from the rotated original image and binary image. Additionally, the plants in each row were manually counted using the original color image (Fig. 3-6f) and denoted as manual count. Likewise, the plants in the binary image (Fig. 3-6g) were counted by detecting the number of connected components in the image and denoted as UAV count. Since the corn plants were mostly in V2 or earlier growth stages, no plants overlapped. The exception to this was a small number of "double plants", caused by two seeds being released by the planter at the same time.

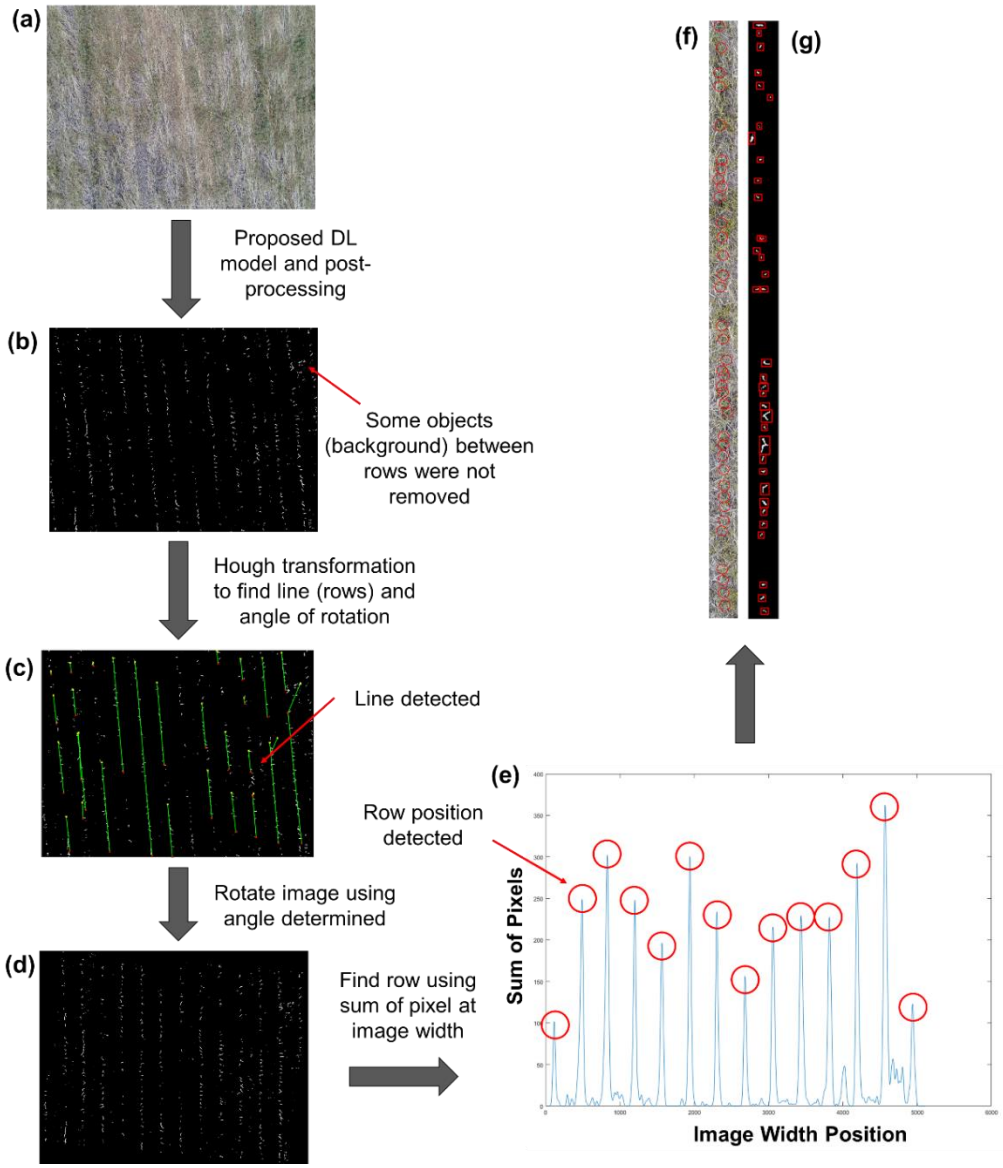

Figure 3-6. Workflow of estimating plant population in each row of a single UAV image captured for the cropping system of no-till continuous corn including cover crops in this study. (a) original UAV image; (b) segmented binary image; (c) segmented binary image with lines in green found by Hough transformation; (d) rotated binary image; (e) smoothed curve with peaks representing plant row positions; (f) cropped original image for manual count (37 plants); (g) cropped binary image for UAV count (36 plants).

Seven to nine UAV images, comprised of about 60 plant rows for each CS were randomly selected for the manual and UAV corn stand count comparison in plants m^{-1}. The stand count in each row was determined using the ratio of the total number of plants in the row to the row length. The GSD for each selected image was different due to the

variability of actual flight height caused by the UAV launch location and field slope. Thus, actual GSD (cm pixel^{-1}) was first calculated using the division of constant planter row spacing (76 cm) by row spacing in pixels from the image. The computed GSD ranged from 0.14 to 0.26 cm pixel^{-1} for the UAV images used in the analyses. Then, the row length was determined by multiplying the number of pixels by the computed GSD. Lastly, scatter plots were created to compare the manual and UAV count. Previous studies used several metrics to describe model performance in estimating stand count, including coefficient of determination (R^2, Gnädinger & Schmidhalter, 2017) and MAPE (Kitano et al., 2019). Thus, these two metrics were utilized to allow for comparison with previous studies, and an additional performance metric of root-mean-square error (RMSE) was also computed. All the data processing and analysis were performed in a laptop configured as Intel Core i7-7600U 2.80 GHz CPU, a Intel HD Graphics 620 GPU with 7.9 GB memory, 16 GB RAM, and a 463 GB hard disk drive.

3.4 Results and Discussion

3.4.1 Image Segmentation Evaluation

Example images of different CS with different precision, recall, and F1 values are shown in Fig. 3-7. The overlay showed a very close agreement between boundaries when the values of all three parameters were equal to one (Fig. 3-7a). Precision values were low when the UAV prediction indicated more plant area than that of the ground truth (Fig. 3-7d), or detected other green objects (Fig. 3-7c) as indicated in the overlay by the green color. Meanwhile, recall values were low when a portion of a plant (Fig. 3-7e and 3-7f) or a complete small-sized plant (Fig. 3-7b) in the ground truth was not included in the prediction as shown in the purple color of the overlay.

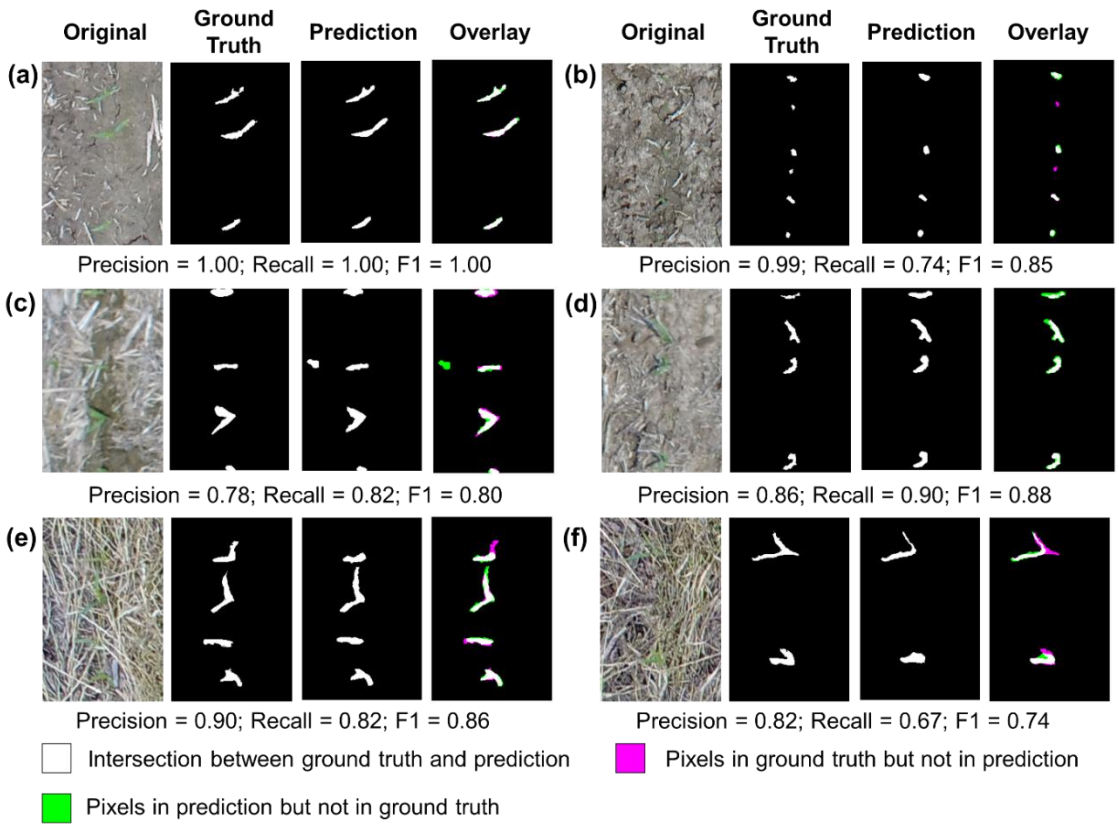

Figure 3-7. Example images showing different precision, recall, and F1 values in three cropping systems: minimum-tillage corn-soybean rotation (a and b), no-till corn-soybean rotation (c and d), and no-till continuous corn including cover crops (e and f). 'Ground Truth' is the binary image prepared by 'Image Segmenter' apps, 'Prediction' is the segmented binary image from the proposed method, and 'Overlay' compares ground truth and segmented binary images.

Results using the proposed method are listed in Table 3-5, including the average precision, recall, and F1 of training, validation and testing datasets for each CS and all the CS (overall). The MTCS had the highest performance with the greatest average precision, recall, and F1 (0.93 – 0.96), followed by NTCS (0.85 – 0.93), and NTCC (0.74 – 0.90). Thus, performance of the proposed method decreased as residue cover increased. Overall, the proposed method was able to segment corn plants from the background in UAV images of different CS with high precision, recall, and F1 for all the datasets (0.86 – 0.92). The MTCS and NTCS had higher average recall than precision for all datasets, suggesting that most prediction images in these CS had plants with larger area than that

of the ground truth images. Nonetheless, the additional area of plants in the ground truth images was usually on the edge of the plants (Fig. 3-7d), and likely did not negatively affect the accuracy of plant stand count estimation. The low precision value also indicated the possibility of detecting other green objects, such as weeds, that were usually found between rows and would cause an over-prediction of stand count. This issue could be addressed by including the row detection step (Fig. 3-6b-e) to avoid counting non-corn objects between rows.

Table 3-5. Average precision, recall and F1 of training, validation and testing datasets for different cropping systems.

Dataset	Parameter	MTCS	NTCS	NTCC	Overall
Training	Precision	0.95	0.89	0.90	0.91
	Recall	0.96	0.93	0.86	0.92
	F1	0.96	0.92	0.88	0.92
Validation	Precision	0.93	0.86	0.78	0.86
	Recall	0.94	0.92	0.74	0.86
	F1	0.94	0.90	0.74	0.86
Testing	Precision	0.94	0.85	0.81	0.87
	Recall	0.96	0.91	0.74	0.86
	F1	0.95	0.90	0.77	0.87

The NTCC had higher average precision than recall, indicating that most of the prediction images had plants with smaller area than that of the ground truth images. The NTCC had the highest amount of residue, with some of the residue covering part of the plant leaves. Hence, this covered part was not included in the prediction image (Fig. 3-7e, f). Additionally, low recall values could be caused by some plants not being detected, which would result in under-prediction during stand count estimation. This issue was especially apparent when the corn plants were surrounded by other green residue (i.e., plants not completely senesced after pre-plant herbicide application) in this NTCC CS, as illustrated in Fig. 3-8.

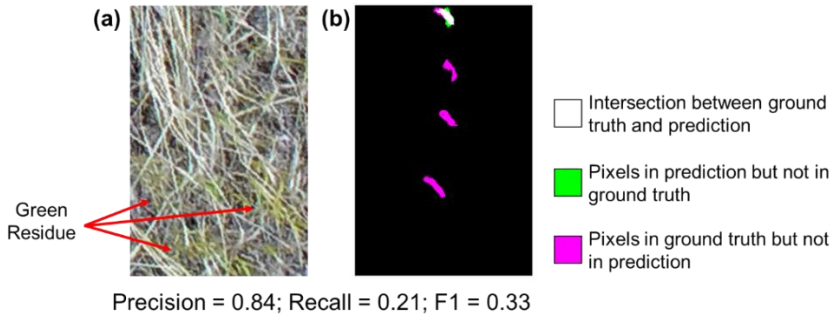

Figure 3-8. Images showing a low recall value in the cropping system with no-till continuous corn including cover crops due to some plants that were not detected when surrounded by green residue. The original image is on the left (a) and the overlaid image between ground truth and segmented binary images is on the right (b).

3.4.2 Plant Stand Count Estimation

Nearly all the background was removed in images from MTCS and NTCS (Fig. 3-9). However, for NTCC, some of the background consisting of green residue was not completely removed (Fig. 3-9i and 3-9l). By introducing the additional step of row detection (Fig. 3-6b to 3-6e), these background objects were not included in the final cropped plant row image (Fig. 3-6f and 3-6g), thus improving the estimation accuracy. Good correspondence was observed between manual and UAV counts of corn for all the CS with R^2 of more than 0.9. (Fig. 3-10). The MTCS had the lowest RMSE and MAPE followed by NTCS and NTCC, suggesting that higher amounts of residue increased the difficulty of counting the correct number of plants.

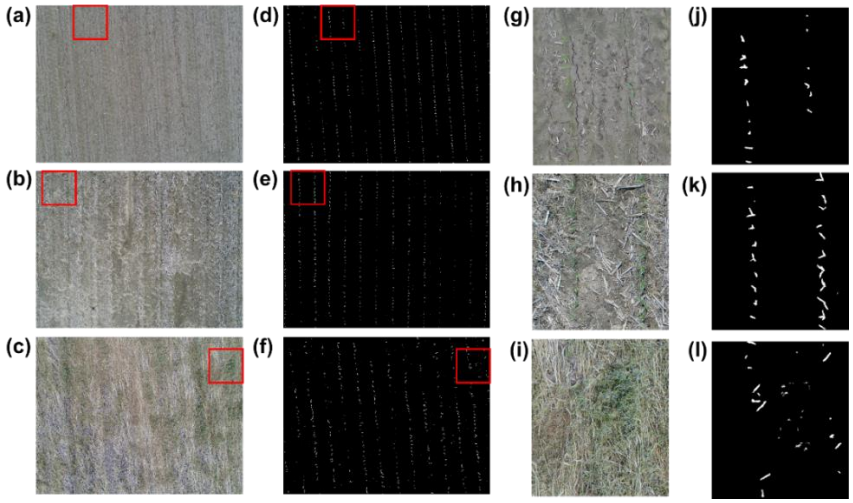

Figure 3-9. Examples of UAV images from cropping systems: minimum-tillage corn-soybean rotation (top row), no-till corn-soybean rotation (middle row), and no-till continuous corn including cover crops (bottom row) used in plant stand count estimation. The original UAV images are in the first column (a-c) and segmented images using the proposed method are in the second column (d-f). Those parts of the original UAV and segmented images in the red boxes are enlarged and shown in the third and fourth columns (g-l).

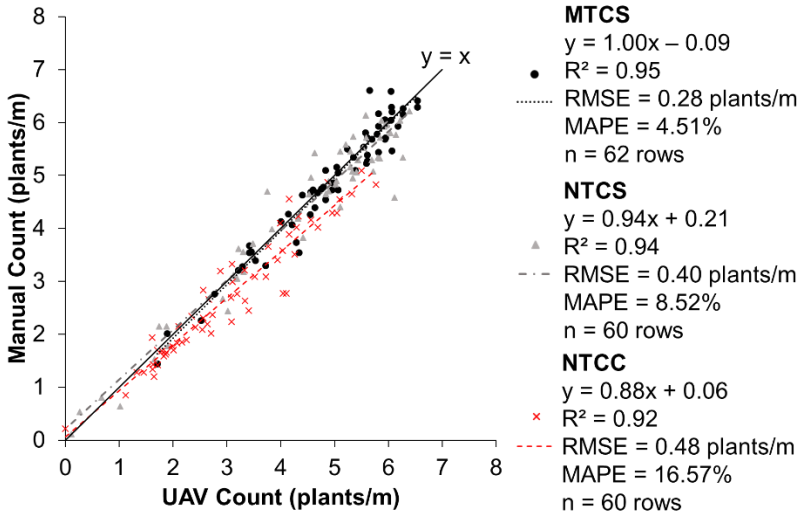

Figure 3-10. Comparison between manual and UAV stand count for each cropping system: minimum-tillage corn-soybean rotation (MTCS), no-till corn-soybean rotation (NTCS), and no-till continuous corn including cover crops (NTCC).

The under-prediction in MTCS and NTCS was attributed to small-sized plants, which were late-emerging plants, and were considered as image noise and removed (Fig.

3-11a to d). Occasionally, the under-prediction was also due to the overlapped leaves of two close plants ("double plants", Fig. 3-11e to h). On the contrary, over-prediction in MTCS and NTCS resulted from a limitation of the image processing workflow when the UAV image was cropped equally into 288 images. Some corn plants were split, with portions appearing in two images (Fig. 3-12a to d), and after the background removal using the proposed method followed by combining the images sequentially, the same plants were divided into two parts (Fig. 3-12e and f). For NTCC, higher amounts of residue resulted in more under- and over-prediction. These residues varied in color from yellow or white dry straw (Fig. 3-13a) to yellow or light green cover crops or weeds (Fig. 3-13c). As indicated in Fig. 3-13a and b, some plants (red circle) were not detected, while in Fig. 3-13c and d, some plants (red box) were divided into two parts.

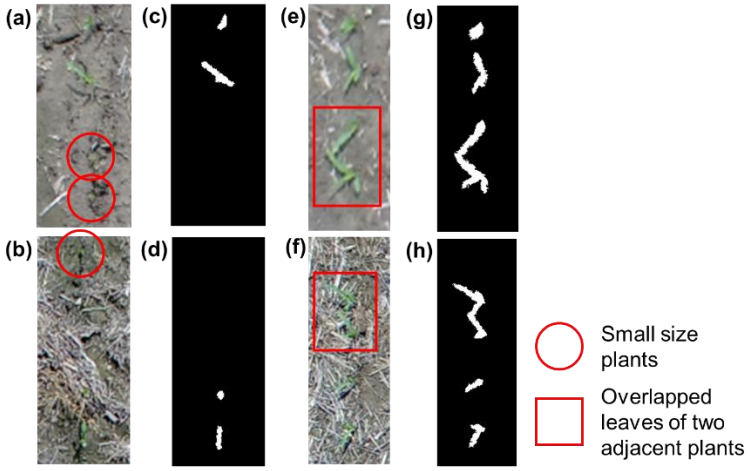

Figure 3-11. Examples of original (a, b, e, and f) and segmented (c, d, g, and h) images showing under-prediction of plant stand count caused by small-sized plants (a-d) and overlapped leaves (e-h) for two cropping systems: minimum-tillage corn-soybean rotation (top row) and no-till corn-soybean rotation (bottom row).

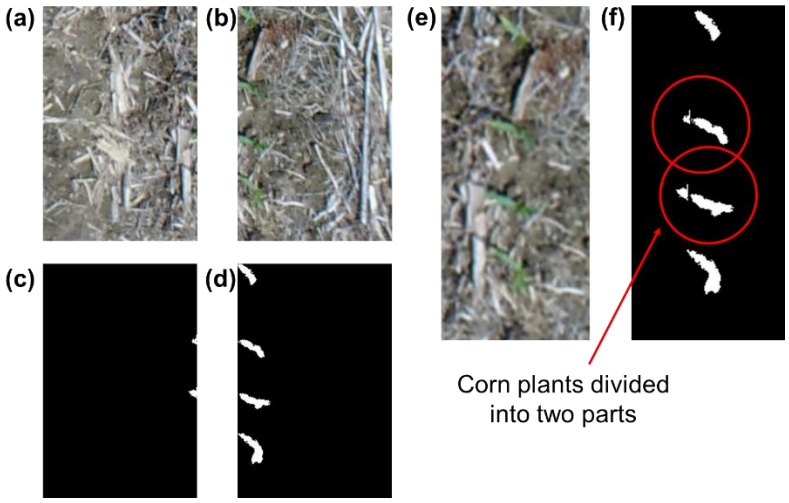

Figure 3-12. Examples of original (a, b, and e) and segmented (c, d and f) images showing corn plants that were divided into two parts, resulting in over-prediction of plant stand count.

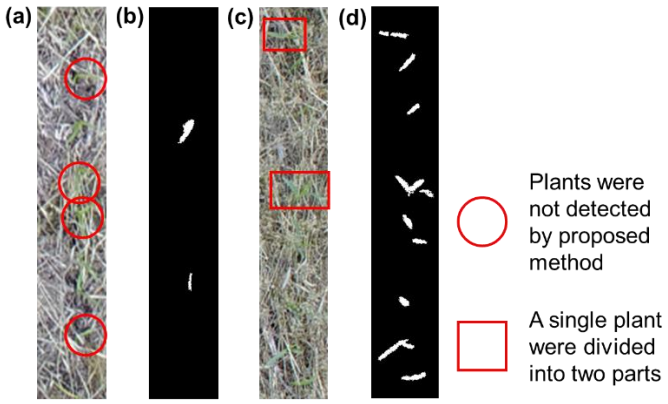

Figure 3-13. Examples of original (a and c) and segmented (b and d) images showing under-prediction (a and b) and over-prediction (c and d) of plant stand count for the cropping system with no-till continuous corn including cover crops.

Although there was some under- and over-prediction for all the CS, our results show better or comparable performance of corn stand count estimation when compared to similar previous studies. For example, our results of $R^2 > 0.90$ for all the CS were higher than the R^2 of 0.89 in the study by (Gnädinger & Schmidhalter, 2017). Although neither the crop growth stage or CS were specificed, the UAV image shown in their article illustrated larger corn plants (3- to 5-leaves) with only soil background, which was

comparable to the MTCS in the present study. Hence, the proposed method attained a higher performance at an earlier growth stage than this previous study.

Similarly, the MAPE results ranged from 4.51% to 16.57% across all CS. This showed comparable or better performance of the proposed method to results from previous research performed by (Kitano et al., 2019), which found MAPE to range from 2.6 to 53.3%. They used DL and UAV images in estimating corn stand counts with different factors such as plant density (45,000, 70,000, and 90,000 plants ha^{-1}), flight height (10, 15, and 20 m), and vegetative growth stage (V4, V6, and V8). When considering the same flight height in our study (10 m), their MAPE ranged from 11.6 to 14.4% when estimating plant stand count at V4 stage. Although the NTCS in our study had MAPE of 16.57%, our proposed method was able to estimate the plant stand count at an earlier stage (V2 compared to V4, which is about 140 growing degree days earlier, Lee et al., 2007). Earlier detection of stand establishment could result in more time to implement management stragies, such as replanting.

Meanwhile, the RMSE in the present study was low for all the CS and ranged from 0.28 to 0.48 plants m^{-1} (Fig. 3-7a to b). A study by Shuai et al. (2019) estimated corn stand count at V2 (UAV images taken 25 DAP at 4 and 5 m flying height) in a field previously planted to wheat and tilled with a vertical tillage implement prior to corn planting. The UAV image in their paper illustrated only soil background, which was similar to MTCS. Their results showed that the model missed two to five plants per plot (129 to 141 plants) in six 5-m rows. An equivalent calculation based on RMSE from our research showed our proposed method missed eight plants per plot. The higher number of missing plants might have been caused by the lower spatial resolution of our study (3.0

mm pixel^{-1}) as compared to theirs (1.1 and 1.4 mm pixel^{-1}). Although our method provided a lower estimation accuracy, it was able to estimate corn stand 11 days earlier than this previous study (14 vs. 25 DAP).

Overall, the proposed method was able to estimate early corn stand count (two weeks after planting, i.e. ~V2) for different CS with R^2 ranging from 0.92 to 0.95, RMSE of 0.28 to 0.48 plants m^{-1}, and MAPE of 4.51 to 16.57%. Further application of the proposed method could produce plant population maps of larger fields using stitched UAV images. This will potentially allow determining the exact location of areas of poor or no emergence in a field. As such, less time and labor will be needed as compared to traditional crop scouting methods.

3.5 Conclusion

This study proposed a method of using UAV imagery and a DL model in estimating early (V2) stand count of corn planted with different CS that varied in soil and residue backgrounds (MTCS, NTCS, and NTCC). Results showed that plant identification by UAV imagery was more difficult as the complexity of the background increased with average precision of 0.94, 0.85, and 0.81 in the testing dataset for MTCS, NTCS, and NTCC CS, respectively. The proposed method using a U-Net DL model and further image processing was able to remove the background from a UAV image and increase plant identification accuracy. For plant stand count estimation, the row detection step improved R^2 to > 0.90 for all CS. Moreover, low RMSE (0.28 to 0.48 plants m^{-1}) and MAPE (4.51 to 16.57%) were attained for all the CS. The proposed method can be extended to estimate plant stand count for larger fields using stitched UAV images to produce plant population maps. These maps would be useful to researchers for making

replanting decisions, estimating yield potential and nutrient recommendations, and evaluating effects of environmental factors on emergence. To test the reliability of the proposed method, future validation work will be needed in plots and fields planted with similar or other soil and crop residue conditions.

References

Albawi, S., Mohammed, T. A., & Al-Zawi, S. (2017). *Understanding of a convolutional neural network.* Paper presented at the 2017 International Conference on Engineering and Technology (ICET).

Amara, J., Bouaziz, B., & Algergawy, A. (2017). A deep learning-based approach for banana leaf diseases classification. *Datenbanksysteme für Business, Technologie und Web (BTW 2017)-Workshopband*.

Assefa, Y., Vara Prasad, P., Carter, P., Hinds, M., Bhalla, G., Schon, R., . . . Ciampitti, I. A. (2016). Yield responses to planting density for US modern corn hybrids: A synthesis-analysis. *Crop Science, 56*(5), 2802-2817.

Birrell, S., & Sudduth, K. A. (1995). *Corn population sensor for precision farming*. ASAE Paper No. 951334. St. Joseph, Michigan: ASAE.

Bollero, G. A., Bullock, D. G., & Hollinger, S. E. (1996). Soil temperature and planting date effects on corn yield, leaf area, and plant development. *Agronomy Journal, 88*(3), 385-390.

Bradley, D., & Roth, G. (2007). Adaptive thresholding using the integral image. *Journal of graphics tools, 12*(2), 13-21.

Chen, R., Chu, T., Landivar, J. A., Yang, C., & Maeda, M. M. (2018). Monitoring cotton (Gossypium hirsutum L.) germination using ultrahigh-resolution UAS images. *Precision agriculture, 19*(1), 161-177.

Conway, L. S., Yost, M. A., Kitchen, N. R., Sudduth, K. A., & Veum, K. S. (2018). Cropping system, landscape position, and topsoil depth affect soil fertility and nutrient buffering. *Soil Science Society of America Journal, 82*(2), 382-391.

Csurka, G., Larlus, D., Perronnin, F., & Meylan, F. (2013). *What is a good evaluation measure for semantic segmentation?* Paper presented at the Proc. British Mac. Vis. Conf.

Fan, Z., Lu, J., Gong, M., Xie, H., & Goodman, E. D. (2018). Automatic tobacco plant detection in UAV images via deep neural networks. *IEEE Journal of Selected Topics in Applied Earth Observations and Remote Sensing, 11*(3), 876-887.

Fawakherji, M., Potena, C., Bloisi, D. D., Imperoli, M., Pretto, A., & Nardi, D. (2019). *UAV Image Based Crop and Weed Distribution Estimation on Embedded GPU Boards* (Vol. 1089): Springer.

Ghosal, S., Zheng, B., Chapman, S. C., Potgieter, A. B., Jordan, D. R., Wang, X., . . . Ninomiya, S. (2019). A weakly supervised deep learning framework for sorghum head detection and counting. *Plant Phenomics, 2019*, 1525874.

Gnädinger, F., & Schmidhalter, U. (2017). Digital counts of maize plants by unmanned aerial vehicles (UAVs). *Remote Sensing, 9*(6), 544.

Guo, W., Zheng, B., Potgieter, A. B., Diot, J., Watanabe, K., Noshita, K., . . . Ninomiya, S. (2018). Aerial imagery analysis–quantifying appearance and number of

sorghum heads for applications in breeding and agronomy. *Frontiers in plant science, 9*, 1544.

Hobbs, P. R., Sayre, K., & Gupta, R. (2008). The role of conservation agriculture in sustainable agriculture. *Philosophical Transactions of the Royal Society B: Biological Sciences, 363*(1491), 543-555.

Jin, X., Liu, S., Baret, F., Hemerlé, M., & Comar, A. (2017). Estimates of plant density of wheat crops at emergence from very low altitude UAV imagery. *Remote Sensing of Environment, 198*, 105-114.

Kamilaris, A., & Prenafeta-Boldú, F. X. (2018). Deep learning in agriculture: A survey. *Computers and electronics in agriculture, 147*, 70-90.

Kitano, B. T., Mendes, C. C., Geus, A. R., Oliveira, H. C., & Souza, J. R. (2019). Corn Plant Counting Using Deep Learning and UAV Images. *IEEE Geoscience and Remote Sensing Letters*.

Lee, C., Herbek, H., Green, J. D., & Martin, J. (2007). *Replanting Options for Corn*. Retrieved from

Livne, M., Rieger, J., Aydin, O. U., Taha, A. A., Akay, E. M., Kossen, T., . . . Frey, D. (2019). A U-Net deep learning framework for high performance vessel segmentation in patients with cerebrovascular disease. *Frontiers in neuroscience, 13*.

Nielsen, R. L. (2003). Estimating Yield and Dollar Returns from Corn Replanting. In: Purdue University Cooperative Extension Service.

Nunes, M. R., van Es, H. M., Schindelbeck, R., Ristow, A. J., & Ryan, M. (2018). No-till and cropping system diversification improve soil health and crop yield. *Geoderma, 328*, 30-43.

Pittelkow, C. M., Liang, X., Linquist, B. A., Van Groenigen, K. J., Lee, J., Lundy, M. E., . . . Van Kessel, C. (2015). Productivity limits and potentials of the principles of conservation agriculture. *Nature, 517*(7534), 365-368.

Ronneberger, O., Fischer, P., & Brox, T. (2015). *U-net: Convolutional networks for biomedical image segmentation.* Paper presented at the International Conference on Medical image computing and computer-assisted intervention.

Sangoi, L. (2001). Understanding plant density effects on maize growth and development: an important issue to maximize grain yield. *Ciência rural, 31*(1), 159-168.

Shuai, G., Martinez-Feria, R. A., Zhang, J., Li, S., Price, R., & Basso, B. (2019). Capturing Maize Stand Heterogeneity Across Yield-Stability Zones Using Unmanned Aerial Vehicles (UAV). *Sensors, 19*(20), 4446.

Stanger, T. F., & Lauer, J. G. (2006). Optimum plant population of Bt and non‐Bt corn in Wisconsin. *Agronomy Journal, 98*(4), 914-921.

Sudduth, K., Birrell, S., & Krumpelman, M. (2000). *Field evaluation of a corn population sensor.* Paper presented at the Proceedings of the 5th International Conference on Precision Agriculture, Bloomington, Minnesota, USA, 16-19 July, 2000.

Thorp, K. R., Steward, B. L., Kaleita, A. L., & Batchelor, W. D. (2007). Using aerial hyperspectral remote sensing imagery to estimate corn plant stand density. *Transactions of the ASABE, 51*(1), 311-320.

Trujillano, F., Flores, A., Saito, C., Balcazar, M., & Racoceanu, D. (2018). *Corn classification using Deep Learning with UAV imagery. An operational proof of concept.* Paper presented at the 2018 IEEE 1st Colombian Conference on Applications in Computational Intelligence (ColCACI).

Van Roekel, R. J., & Coulter, J. A. (2011). Agronomic responses of corn to planting date and plant density. *Agronomy Journal, 103*(5), 1414-1422.

Varela, S., Dhodda, P., Hsu, W., Prasad, P., Assefa, Y., Peralta, N., . . . Ciampitti, I. (2018). Early-season stand count determination in corn via integration of imagery from unmanned aerial systems (UAS) and supervised learning techniques. *Remote Sensing, 10*(2), 343.

Yost, M. A., Kitchen, N. R., Sudduth, K. A., Sadler, E. J., Baffaut, C., Volkmann, M. R., & Drummond, S. T. (2016). Long-term impacts of cropping systems and landscape positions on claypan-soil grain crop production. *Agronomy Journal, 108*(2), 713-725.

Zhang, J., Xie, T., Yang, C., Song, H., Jiang, Z., Zhou, G., . . . Xie, J. (2020). Segmenting Purple Rapeseed Leaves in the Field from UAV RGB Imagery Using Deep Learning as an Auxiliary Means for Nitrogen Stress Detection. *Remote Sensing, 12*(9), 1403.

Zhao, B., Zhang, J., Yang, C., Zhou, G., Ding, Y., Shi, Y., . . . Liao, Q. (2018). Rapeseed seedling stand counting and seeding performance evaluation at two early growth

stages based on unmanned aerial vehicle imagery. *Frontiers in plant science, 9*, 1362.

Zhao, X., Yuan, Y., Song, M., Ding, Y., Lin, F., Liang, D., & Zhang, D. (2019). Use of unmanned aerial vehicle imagery and deep learning unet to extract rice lodging. *Sensors, 19*(18), 3859.

Zhou, D., Li, M., Li, Y., Qi, J., Liu, K., Cong, X., & Tian, X. (2020). Detection of ground straw coverage under conservation tillage based on deep learning. *Computers and electronics in agriculture, 172*, 105369.

Zhuang, S., Wang, P., & Jiang, B. (2018). *Segmentation of green vegetation in the field using deep neural networks.* Paper presented at the 2018 13th World Congress on Intelligent Control and Automation (WCICA).

CHAPTER FOUR

CORN EMERGENCE UNIFORMITY ESTIMATION AND MAPPING USING UAV IMAGERY AND A DEEP LEARNING MODEL

4.1 Abstract

Assessment of corn (*Zea Mays L.*) emergence uniformity is important to evaluate crop yield potential. Previous studies have shown the potential of unmanned aerial vehicle (UAV) imagery and deep learning (DL) models in estimating early stand count and plant spacing uniformity, but few have extended further to field-scale mapping. Additionally, estimation of plant emergence date using UAV imagery in field-scale studies has not been achieved. This study aimed to estimate and map corn emergence uniformity using UAV imagery and DL modeling. Corn emergence uniformity was quantified with plant density, plant spacing standard deviation (PSstd), and mean days to imaging after emergence (DAEmean). Corn was planted at four depths (3.8, 5.1, 6.4, and 7.6 cm). A UAV imaging system equipped with a red, green, and blue (RGB) camera was used to acquire images at 10 m above ground level at 32 days after planting (20 days after the first emergence at V2-V4 growth stage). A pre-trained convolutional neural network, ResNet18, was used to estimate the three emergence parameters. Results showed the estimation accuracies in the testing dataset for plant density, PSstd, and DAEmean were 0.97, 0.73, and 0.95, respectively. The developed method had higher accuracy and lower root-mean-square-error for plant density and DAEmean, indicating better performance than previous studies. A case study was conducted to assess the emergence uniformity of corn at different planting depths using the developed estimation models at field-scale. From this maps were produced. Results showed that the average plant density and

DAEmean decreased and the average PSstd increased with increasing depths, indicating deeper planting depths caused less and later emergence, as well as less spatial uniformity in this field. These emergence uniformity field maps could be used for future field-scale agronomic studies on temporal and spatial crop emergence uniformity and for making planting decisions in commercial production.

4.2 Introduction

The uniformity of corn (*Zea Mays L.*) stand is critical in maximizing yield as it reduces competition between plants for available water, nutrients, and sunlight (Karayel and Özmerzi, 2008). Corn stand uniformity can be assessed temporally and spatially based on emergence date and plant spacing. Pommel et al. (2002) and Rutto et al. (2014) summarized a few factors and their possible interaction that affect crop stand uniformity, including soil environment, planter performance, planting depths, and tillage practices. Seed germination requires adequate water and optimum soil temperature (20 °C to 30 °C) to rupture the seed coat and initiate the seed embryonic tissue development (Poncet et al., 2019; Schneider and Gupta, 1985). Planter configuration and operating parameters often require adjustment for particular soil conditions to facilitate reliable seed placement at a desired depth and spacing (Badua et al., 2018; Poncet et al., 2018). Furthermore, no-tillage practices leave residues on the soil surface that can lower early-season soil temperature and reduce seed germination and emergence (Boomsma et al., 2010; Rutto et al., 2014).

Past research studied the effects of corn emergence uniformity on yield (Kovács and Vyn, 2014; Lawles et al., 2012; Nafziger et al., 1991), using different planting dates to create non-uniform emergence. Other research also investigated the impacts of

different crop management practices such as planter type and settings, tillage, and nitrogen rate on emergence uniformity (Kovács and Vyn, 2014; Liu et al., 2004a; Poncet et al., 2019). The emergence uniformity was quantified by measuring the number of days from planting to 50% plant emergence with more days indicating late emergence (Liu et al., 2004a) and accumulated thermal units or growing degree units (GDU) from planting using 10 and 30°C temperature thresholds, with higher GDU for later emergence (Kovács and Vyn, 2014). Poncet et al. (2019) used Gibb's Index, which determines variability for categorical variables, in predefined seedling categories to quantify emergence uniformity with higher index values indicating more uniformity. A more recent study used days after emergence (DAE) to the time of assessment with lower DAE signifying later emergence (Vong, Stewart, et al., 2021).

For corn spatial uniformity, the parameters most often used include average and standard deviation (SD) of plant spacing (PS) (Lauer and Rankin, 2004; Liu et al., 2004a; Liu et al., 2004b), where higher SD of PS indicates less spatial uniformity. Furthermore, some indices are calculated relative to the theoretical PS, such as the International Organization for Standardization (ISO) multiple index (the percentage of PS with spacing less than 0.5 times the theoretical spacing), ISO miss index (the percentage of PS with spacing more than 1.5 times the theoretical spacing), and coefficient of precision (the percentage of PS with spacing within ± 1.5 cm of the theoretical spacing) (ISO, 1984; Kachman and Smith, 1995; Shirzadifar et al., 2020; Singh et al., 2005). These corn uniformity measurements are conventionally conducted manually in multiple selected sampling plots, which may not be representative of the whole field.

Advances in unmanned aerial vehicle (UAV)-based imaging and image processing technologies provide the ability to efficiently collect high-resolution images of crops at field scale to quantify crop growth conditions. Recent studies have shown the usage of high-resolution red, green, and blue (RGB) UAV imagery for evaluating emergence in corn (Shirzadifar et al., 2020; Shuai et al., 2019; Vong, Conway, et al., 2021), wheat (Jin et al., 2017; Liu et al., 2017), cotton (Feng et al., 2020), and potato (Li et al., 2019). The UAV imagery data can be used to evaluate stand count or plant density (Feng et al., 2020; Jin et al., 2017; Shirzadifar et al., 2020; Shuai et al., 2019; Vong, Conway, et al., 2021), spacing uniformity (Shirzadifar et al., 2019), emergence rate (Li et al., 2019), coefficient of variation (CV) of an emergence region (Liu et al., 2017), and canopy cover (Feng et al., 2020; Li et al., 2019), with relatively high coefficients of determination ($R^2 > 0.80$). In addition, UAV imagery has been used to map and visualize crop emergence and growth status in a large field (Shirzadifar et al., 2020; Sona et al., 2016; Torres-Sánchez et al., 2014).

Previous studies regarding the evaluation of corn emergence using UAV imagery focused on the assessment of stand count (Kitano et al., 2019; Vong, Conway, et al., 2021) and plant spacing uniformity (Shirzadifar et al., 2020; Shuai et al., 2019). Studies analyzing the temporal variation of emergence date are limited (Vong, Stewart, et al., 2021). Some studies used UAV imagery to estimate plant stand count at later vegetative growth stages (e.g., 3 to 8), which is not feasible for early-season decision making, e.g., replanting (Gnädinger and Schmidhalter, 2017; Kitano et al., 2019). In addition, among the published studies that used image processing methods for estimating crop emergence

(Varela et al., 2018; Vong, Conway, et al., 2021; Vong, Stewart, et al., 2021), only one mapped entire fields using UAV imagery (Shirzadifar et al., 2020).

Crop emergence uniformity estimation and mapping in early growth stages are critical for some management decisions, such as replanting and post-emerge herbicide applications (Vong, Conway, et al., 2021). Meanwhile, emergence mapping can also be used to evaluate the spatial variability of yield since non-uniform crop emergence may lead to consistent yield reductions (Andrade and Abbate, 2005; Liu et al., 2004b). Moreover, precision planting, which places seed at a precision spacing and depth to ensure uniform emergence for maximizing final yield, has been facilitated with technologies in today's planter systems. These include hydraulic or pneumatic downforce systems for active in-field adjustment (Poncet, 2019), seed singulation to drop one seed at a time (Iacomi and Papescu, 2015), variable rate seeding based on varying soil conditions (Silva et al., 2021), and variable planting depths based on soil moisture data in real-time (Precision Planting, 2019). Early crop emergence uniformity maps could be critical to evaluate the performance of these technologies up to a field scale level to make necessary adjustments or improvements. The high-resolution data may help understand the constraint factors for better crop emergence.

A challenge of using UAV imagery in assessing crops in early growth stages is the small size of plants and complex background in images. The common procedures of image processing include segmenting the images to remove the soil and residue background and extracting information such as reflectance and morphological appearance of the plants. Generally, conventional image segmentation methods first used vegetation indices (VIs) or contrasting the image to signify the difference between plants and

background (Gnädinger and Schmidhalter, 2017; Shuai et al., 2019; Varela et al., 2018). Then, a threshold value was manually determined based on visual inspection of the images to do the segmentation (Gnädinger and Schmidhalter, 2017; Shirzadifar et al., 2020; Shuai et al., 2019). Meanwhile, an automatic method to determine the threshold value, known as the Otsu threshold, was also widely used (Otsu, 1979; Varela et al., 2018). These methods have been used to process images with a predominantly soil background and are not readily applicable to images with complex backgrounds, i.e., surface residue (Vong, Conway, et al., 2021).

More recently, deep learning (DL) techniques have been widely used to process images with complex backgrounds (Vong, Conway, et al., 2021; Zhang et al., 2019) or extract information directly from the segmented images (Espejo-Garcia et al., 2020; Feng et al., 2020; Yalcin, 2019). The advantage of DL-based image processing methods over conventional approaches is that they can learn the different features from the images or datasets automatically (Vong, Conway, et al., 2021; Yalcin, 2019; Zhang et al., 2019). In addition, DL techniques can be used directly to process raw images to extract novel crop characteristics automatically without human intervention. The DL techniques have been widely used in research related to agriculture, such as assessment of stand count, canopy area and yield (Feng et al., 2020; Yalcin, 2019), weed detection (Milioto et al., 2017), plant growth monitoring (Yalcin, 2019), and leaf disease classification (Deeba and Amutha, 2020).

Deep learning models require significant computing resources and large datasets for training (Espejo-Garcia et al., 2020; Feng et al., 2020). In practice, agriculture-related datasets are usually small due to limited time and resources available for recording

ground truth data. Many DL models have been developed for general-purpose image processing and analytics using the convolutional neural network (CNN), such as AlexNet (Krizhevsky, 2014), VGG (Simonyan and Zisserman, 2014), GoogleNet (Szegedy et al., 2015), ResNet (He et al., 2016), and DenseNet (Huang et al., 2017). These models have been trained and tested on large image datasets for classification, object recognition, and semantic segmentation, and the trained model can be transferred to other similar research. These pre-trained DL models can be fine-tuned to do a specific task by using a smaller training dataset, which is known as transfer learning (Pan and Yang, 2009). In recent years, many studies have used transfer learning for agricultural purposes, such as estimating stand count and canopy area (Feng et al., 2020), classifying plant leaf diseases (Deeba and Amutha, 2020; Subetha et al., 2021), and detecting weeds in fields (Ahmad et al., 2021; Espejo-Garcia et al., 2020).

This study aimed to evaluate the potential of UAV imagery and a DL model to estimate and map temporal and spatial emergence uniformity. In this study, the temporal uniformity referred to stand count and different emergence dates while spatial uniformity was related to evenness of plant spacing. Specific objectives consisted of 1) implementing a pre-trained DL model to estimate corn emergence uniformity, and 2) demonstrating the applicability of the model to estimate and map emergence uniformity at field-scale with corn planted at different depths.

4.3 Materials and Methodology

4.3.1 Study Site and Ground Data Collection

The study was conducted at a 2.6-ha sub-field located at the western portion of a 14-ha corn field near Columbia, MO, USA (38°56’45.7” N, 92°07’57.4” W) as shown in

Fig. 4-1. The dimensions of the study area were 320 m (N-S direction) by 81 m (E-W direction). The study included four planting depths (i.e., 3.8, 5.1, 6.4, and 7.6 cm) with three replications. Each planting depth of each replication included eight rows (6.1 m) of corn along the entire length of the field (~320 m) that resulted in a total of 96 rows of corn with 24 rows per seeding depth.

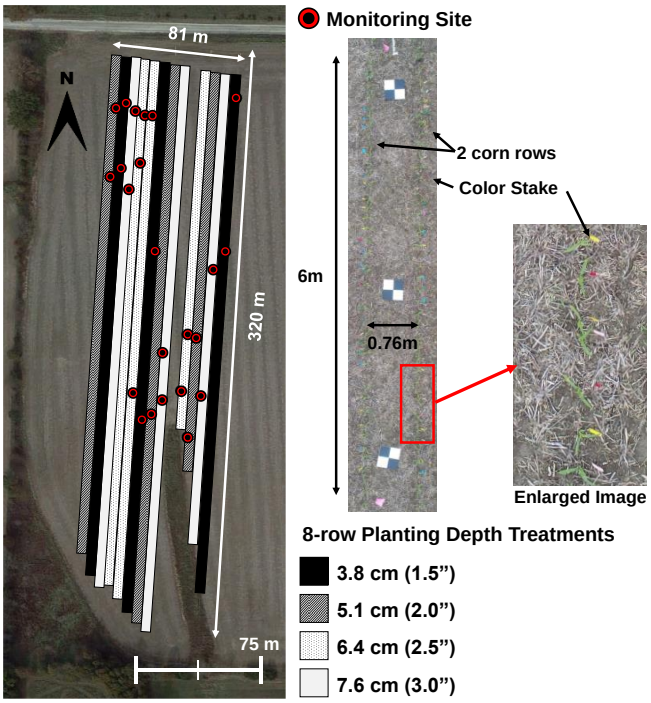

Figure 4-1. Study site with a schematic diagram of 8-row corn planting depth treatments and an example image of a monitoring site taken on 22 May 2020.

The corn hybrid used in the study was Pioneer 0589 (Corteva Agriscience, Wilmington, DE, USA). This corn hybrid had a stress emergence rating of "7" on a 1 to 9 scale according to Corteva's evaluation, with 1 being poor emergence and 9 being high emergence rates (Corteva Agriscience, 2021). The site was planted on 20 April 2020 using a custom-built four-row planter equipped with MaxEmerge XP row units (Deere & Co., Moline, IL, USA) at a 0.76-m row spacing travelling at a speed of 2.0 ms^{-1}. Seed-firmer sensors (SmartFirmer, Precision Planting, Tremont, IL, USA) were also mounted

on the planter to estimate the soil conditions while planting. The corn seeds were no-tilled into soybean stubble from the previous crop in 2019. No row-cleaners or no-till coulters were used on the planter row units. Seeds were planted at the four defined depths at a seeding rate of 81,510 seeds ha^{-1}, which was equivalent to an average plant intra-row seed spacing of 16 cm. The planter was also equipped with a hydraulic downforce system (DeltaForce®) on each row unit and finger-pickup seed meters (Precision Planting, LLC., Tremont, IL, USA).

A total of 23 monitoring sites (five for the 5.1-cm depth and six for each other depth) were marked with flags for ground data collection. Each monitoring site consisted of two 6.0-m long adjacent corn rows (Fig. 4-1a). Corn emergence was checked daily between 8 to 10 am and the newly emerged plants were marked with unique color stakes for each day. The first and last emergence checks in the monitoring sites were 2 and 12 May 2020, equivalent to 12 and 22 days after planting (DAP). Cumulative emergence percentage was also calculated as the cumulative percentage of the number of plants emerged from the first to the last emergence. The different color stakes were used to determine the DAEs on the day when UAV data was collected and to calculate the mean DAE (DAEmean) in 1-m row of the images (details in section 4.3.3.1). The PS was measured using a measuring tape on 15 June 2020 (56 DAP) and used to correlate with the PS estimated using image pixels (details in section 4.3.3.1)

4.3.2 UAV Data Collection

The UAV aerial image data was collected on 22 May 2020 (32 DAP or 20 days after first emergence) when the plants were at vegetative growth stage V2 to V4. The image data collection time was between 10 am and 2 pm local time, coinciding minimum

changes in the solar zenith angle. Aerial images were acquired using a Phantom 4 Advanced UAV imaging system (DJI, Shenzhen, Guangdong, China) with an onboard RGB camera with a field-of-view (FOV) of 84° and image size of 4864 by 3648 pixels. Images were taken sequentially for the whole field at 0.5 frames per second (fps) at a flight height of 10 m and speed of 2 m s^{-1}. The flight mission plan with targeted waypoints was set up through the UAV control app Litchi (VC Technology Ltd, London, UK). This setup ensured an image overlap of 75% in both forward and sideward directions and resulted in a calculated ground sampling distance (GSD) of 0.3 cm $pixel^{-1}$ for each frame.

4.3.3 Image Processing and Data Analysis

4.3.3.1 DL Model Implementation for Plant Emergence Parameters Estimation

The images collected in this study were processed using a previously developed DL technique (Feng et al., 2020) based on a CNN model (ResNet18; He et al., 2016). The model was previously used to estimate the stand count and canopy size of cotton seedlings. The ResNet18 model was selected among other well-known pre-trained CNN models (e.g., AlexNet, VGG, SqueezeNet, and DenseNet) because it achieved a similar or higher accuracy and required fewer computational resources (Feng et al., 2020). Hence, a similar framework was adapted in this study to estimate three corn emergence parameters in a 1-m row segment: plant density, DAEmean, and PS standard deviation (PSstd).

Figure 4-2 summarizes the workflow of the required sizing and normalization step applied to the original images to create an input image in the ResNet18 model for emergence parameter estimation. The required image size for the model is 224 by 224

pixels (Fig. 4-2a). Since the ResNet18 model was trained and tested using the ImageNet dataset (Russakovsky et al., 2015) with 1000 classes, the same normalization steps were followed (Fig. 4-2b) to create the input images (Fig. 4-2c) for the model (Fig. 4-2d). The model had seven stages, with the first five stages containing different numbers of convolution layer combinations, batch normalization layer, ReLU activation layers, and max-pooling layers for feature extraction (Fig. 4-2d). The last two stages were average pooling and full connection layers. The details of the ResNet18 architecture have been reported previously (Feng et al., 2020). The model was trained once for each emergence parameter. In addition, our images have the color stakes used to represent the emergence date of each plant as shown in Fig. 4-2a, which may affect the feature learning from the model. Thus, feature maps (Zeiler and Fergus, 2014) in stages 3 to 5 were plotted to visualize the learned features for better interpretation of the results. The training and testing of the model and the plotting of feature maps were performed in Python (ver. 3.8.5).

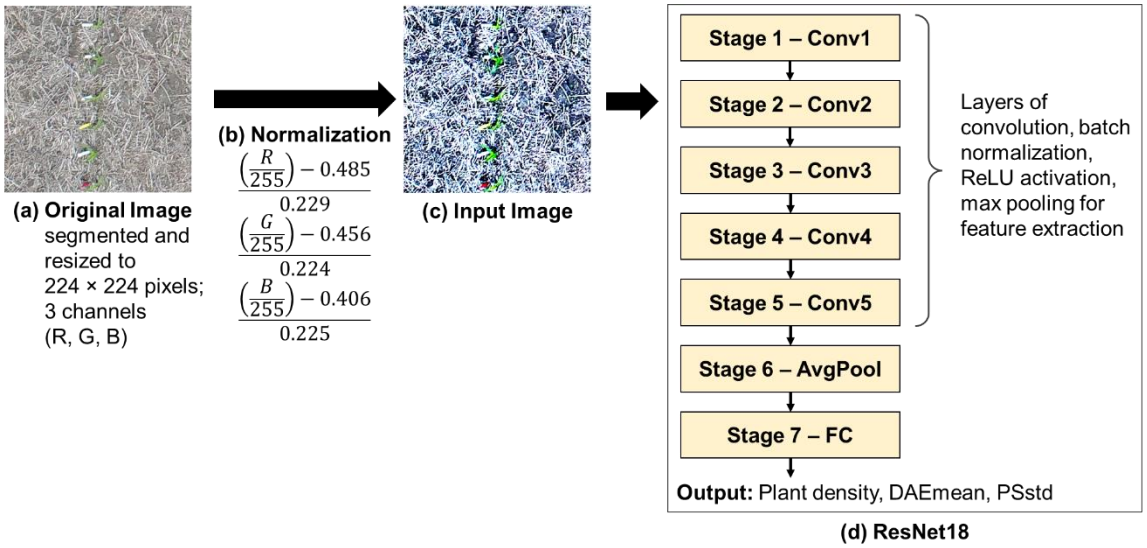

Figure 4-2. Workflow of image segmentation and normalization used to create inputd images in ResNet18 model for estimation of plant density, mean days to imaging after emergence (DAEmean), and plant spacing standard deviation (PSstd) in 1-m row segments.

To prepare the training and testing datasets for the ResNet18 model, 212 images covering the monitoring sites were selected from the series of sequential images taken by the UAV. Each image covered part of or the whole monitoring site. As the input image requires a consistent size of 224 by 224 pixels, an image size equivalent to the actual area of 1.0 m^2 was first segmented. The size was chosen for further usage in field mapping with a grid cell size of 1.0 m^2. The segmented image was then resized to the required size before normalization (Fig. 4-2a and 4-2b). The actual GSD of each image was first calculated based on the consistent plant row spacing (76.0 cm) to segment the images into an equivalent 1.0 m^2 size. The image processing steps to determine the actual GSD (Fig. A1) were conducted using Matlab 2019a (The MathWorks, Inc., Natick, MA, USA). The original image was first enhanced using decorrelation stretch (Gnädinger and Schmidhalter, 2017; Vong, Stewart, et al., 2021). Then, a threshold value of 220 (tested using a trial-and-error method and visual inspection) in the green band of the enhanced image was used to remove most of the background to create binary images. Plant rows were detected using the standard Hough transform (SHT), and the binary image was rotated using the detected angle from SHT to obtain the plant row spacing in pixels. The actual GSD in cm $pixel^{-1}$ was calculated using the division of 76.0 cm by the plant row spacing in pixels.

The detected angle by SHT was also used to rotate the original images to segment each plant row of the monitoring site. Next, plant rows of the monitoring site were segmented from the rotated binary images and region of interest (ROI), i.e., each corn plant was detected using ‘regionprops’ in Matlab. The steps for preparing the ResNet model input images included labeling each ROI, segmenting the image to an image size

equivalent of about 1.0 m^2 (ranged from 0.9 to 1.1 m^2) using the actual GSD to determine the required pixels, and computing the final labels for each segmented image (Fig. A2). There were some corn plants not being detected using the 'regionprops' and hence, the labels of the missed ROI were manually recorded. The centroid of each ROI was extracted to estimate the PS in image pixels by using the Euclidean distance between the centroid coordinates of two adjacent plants (Eq. 1, Zhang et al., 2018). The estimated PS in cm was calculated by multiplying the spacing in pixels by the GSD. To test the method's reliability, the estimated PS was compared with the ground measured PS. The final labels included the three emergence parameters of plant density, DAEmean, and PSstd in a 1-m row segment determined by calculating the total number of plants, the mean of each DAE label, and standard deviation of estimated PS in each segmented image (different color boxes in Fig. A2).

$$PS_{est} = \sqrt{(cx_{i+1} - cx_i)^2 + (cy_{i+1} - cy_i)^2} \quad (1)$$

where PS_{est} = estimated plant spacing in pixels, *cx* and *cy* = centroid coordinates of region-of-interest (ROI), and *i* = ROI ID.

A total of 7,989 images were segmented and divided into training (90%) and testing (10%) datasets, which is a commonly used split ratio for pre-trained DL models in agricultural applications (Nguyen et al., 2021; Xu et al., 2020). The performance of the model was evaluated using the estimation accuracy of the testing dataset in estimating the three parameters (plant density, DAEmean, and PSstd), as calculated using Eq. 2.

$$Accuracy = 1 - \frac{|Actual - Predict|}{Actual} \quad (2)$$

where *Actual* = actual parameter value, *Predict* = estimated parameter value. The overall workflow of image processing, model training, and testing is summarized in Fig. 4-3. The image processing as well as model training and testing were performed in a desktop configured as an Intel Core i9-9900K 3.60 Ghz CPU, a NVIDIA GeForce RTX 2060 GPU with 6 GB memory, 32 GB RAM, and 256 GB solid-state drive (SSD).

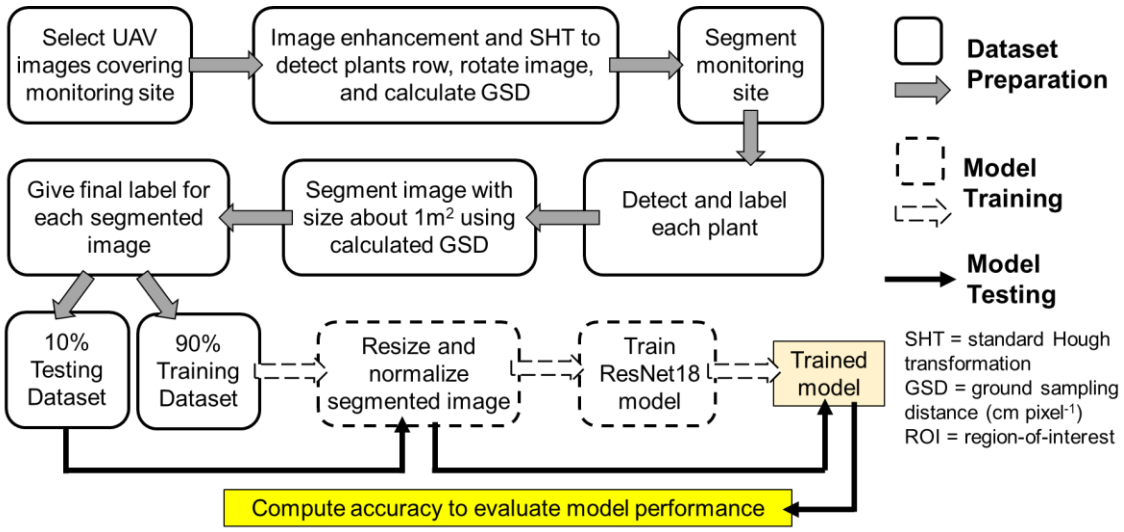

Figure 4-3. Flowchart of image processing overview, including dataset preparation as well as deep learning model training and testing.

4.3.3.2 Map and Evaluate Plant Emergence in Field Condition

An UAV image processing software Agisoft Metashape Professional (ver. 1.6.3, Agisoft LLC, St. Petersburg, Russia) was used to stitch UAV images and produce an orthomosaic of the field. The desktop for this image stitching was configured as an Intel Xeon CPU E5-1630 v4 (3.70 Ghz), a NVIDIA Quadro K1200 GPU with 20 GB memory, 32 GB RAM, and a 918 GB hard disk drive. The stitching workflow and parameters used were summarized in Table A1. The GNSS coordinates of each image pixel in the orthomosaic were extracted using the functions ‘geotiffinfo’ and ‘pixcenters’ from the Matlab Mapping Toolbox (MATLAB R2019a). The GSD of the orthomosaic was 0.28

cm pixel^{-1}. Therefore, images with a size of 357 by 357 pixels (equivalent to 1.0 m^2) were segmented for each plant row and used as the input images for the trained ResNet18 model to estimate plant density, DAEmean, and PSstd. The coordinates of each input image were determined using the center position of the input image. The maps of field plant density, DAEmean, and PSstd in 1-m row segments were overlaid on a Google map (Google, Mountain View, CA, USA) and were produced using QGIS (ver. 3.18, www.qgis.org).

Statistical analyses were conducted using Rstudio (ver. 1.2.1335, Rstudio, Boston, MA, USA) to compare the plant density, DAEmean, and PSstd distributions for the different planting depths treatments across the field. An analysis of variance (ANOVA) test (Sawyer, 2009) at a 0.05 significance level ($\alpha = 0.05$) was performed to determine significant differences in the three emergence parameters between planting depth treatments ('aov.test' function in 'stats' package). When the ANOVA test showed a significant result, Tukey's Honest Significant Difference (HSD) test (Abdi and Williams, 2010) was performed to compare the mean difference between planting depths ('TukeyHSD' function in 'stats' package).

4.4 Results and Discussion

4.4.1 Corn Emergence and Plant Spacing at Monitoring Sites

As determined by manual counts, the average number of plants that emerged at each monitoring site were 65.5, 66.2, 64.5, and 51.8 for the planting depths of 3.8, 5.1, 6.4, and 7.6 cm, respectively. For comparison, the target number of seeds planted at each monitoring site based on the target seeding rate of 81,510 seeds ha^{-1} was 74.0. Figure 4-4a shows the cumulative emergence percentage throughout the emergence window,

indicating that corn planted at both 3.8 and 5.1 cm had the first emergence 12 DAP on 2 May, while corn at 6.4- and 7.6-cm depths had the first emergence on 3 May (13 DAP). The graph also shows that the cumulative emergence percentage decreased with increasing planting depth with the difference in emergence days between plants at 3.8 and 5.1 cm was mostly 0.5 day, and 1.0 to 2.0 days for each defined depth increment from 5.1 cm. The range of emergence dates between planting depths provided variability for the DAEmean testing in this study.

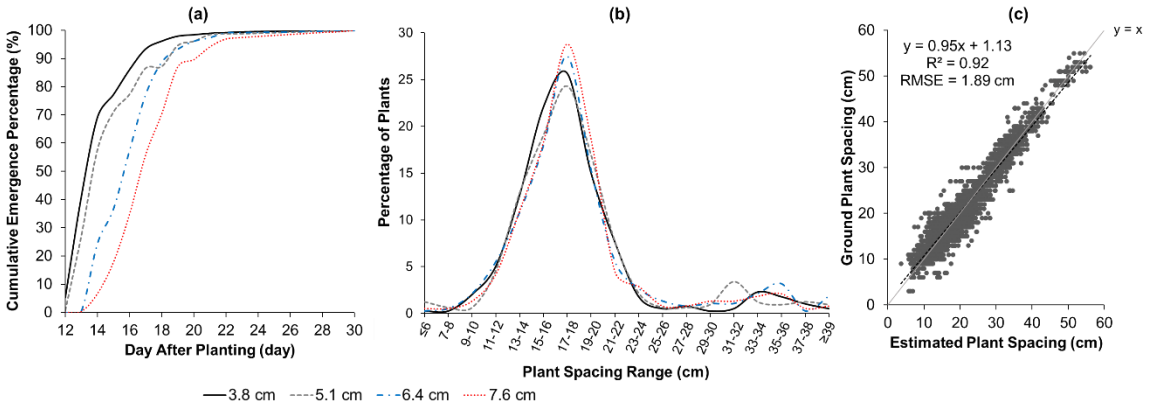

Figure 4-4. (a) Cumulative emergence percentage (%) from the first to last day of emergence and (b) plant spacing ranges at the four defined planting depths for the monitoring sites. (c) Estimated and ground measured plant spacing comparison.

The largest percentage of the PS for all the planting depths in all the monitoring sites was centered at about 15 to 19 cm, as indicated in Fig. 4-4b. For about 9% of the data, PS was centered at 31 to 37 cm (about double the average spacing), which was caused by skips between consecutive plants. The cause of skipped plants was most likely due to the seed failing to germinate and emerge. The range of PS from all the planting depths provided variability for the PSstd testing in this study. Figure 4-4c shows that the estimated PS using Eq. 1 from the UAV images was able to estimate the true measurement at an accuracy of R^2 = 0.92 and RMSE = 1.89 cm, which was similar to previous studies where R^2 ranged from 0.89 to 0.94 (Shirzadifar et al., 2020; Shuai et al.,

2019) and RMSE ranged from 1.70 to 2.56 cm (Shuai et al., 2019). This result establishes the reliability of this method for further PSstd calculation when preparing the labeled images.

4.4.2 Estimation of Emergence Parameters based on DL Model

Figures 4-5 illustrates the feature maps from stages 3 to 5 of the ResNet18 model for the three emergence parameters: plant density, PSstd, and DAEmean, with the higher color value indicating stronger features learned and passed to the next layer. Learned features for both plant density and PSstd focused on the color stakes and plants (Fig. 4-5: top and middle rows), which was evident through the higher color value of light blue to red in the middle of the images. The performance of the model in identifying plants was tested using images without color stakes. The model was still able to detect the plants (higher color values assembled in the middle of the images) from the images without color stakes (Fig. A3: top and middle rows). Conversely, for DAEmean, the learned features seemed to only focus on the colored stakes in stage 3, followed by no clear trend in stage 4, and lastly, scattered colored values in the image in stage 5 (Fig. 4-5: bottom row). A similar trend was shown when testing the model on an image without colored stakes (Fig. A3: bottom row), where the light blue to red colors were scattered in the image in all three stages.

Therefore, an additional image segmentation step was added using a U-net DL model as described by Vong, Conway, et al. (2021). The U-net DL model was built to segment images of corn within different cropping systems, which included no-tillage. The U-net model was able to segment the images with the entire background removed as demonstrated in Fig. A4 (Segmented). The segmented images were used to train the

model again, and feature maps in stages 3 to 5 with and without color stakes are shown in Fig. A4. The learned features in all of the stages focused only on the plants with higher color values that are highlighted in the middle of the images.

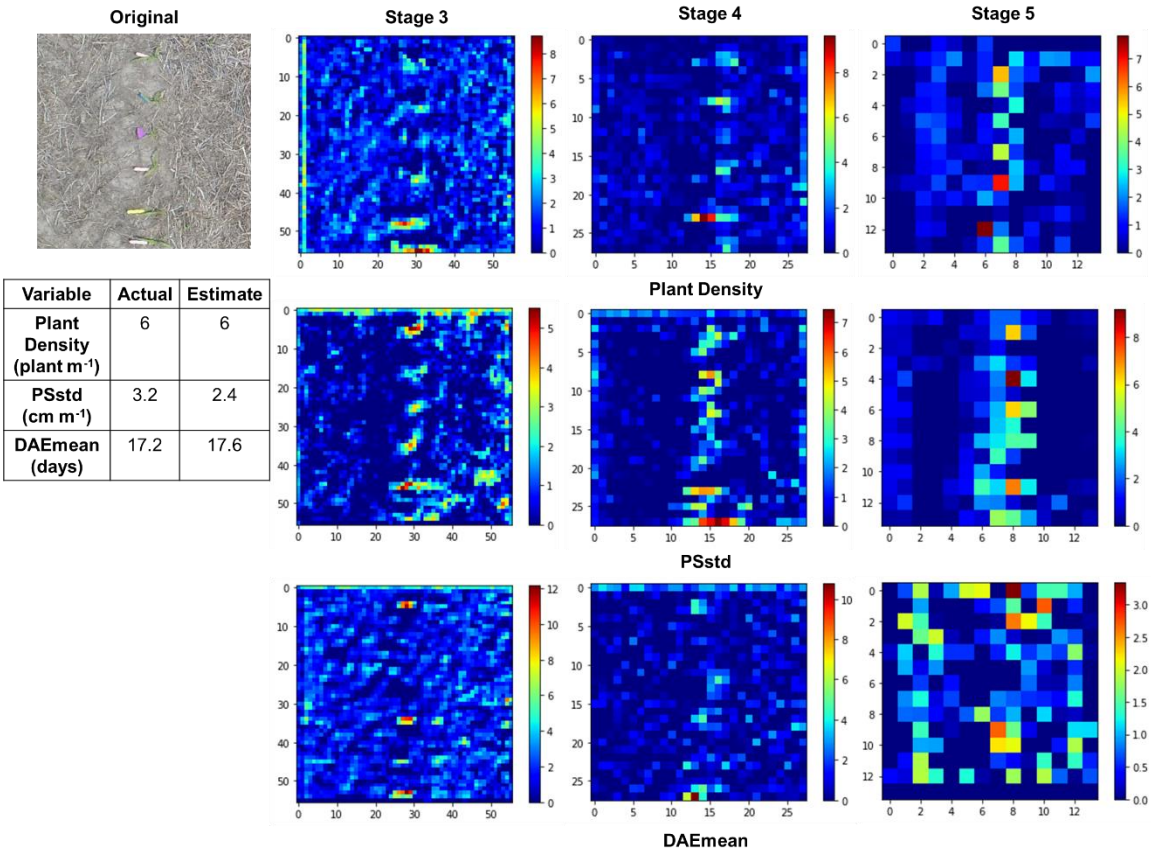

Variable	Actual	Estimate
Plant Density (plant m^{-1})	6	6
PSstd (cm m^{-1})	3.2	2.4
DAEmean (days)	17.2	17.6

Figure 4-5. Features maps of one example image from testing datasets in stages 3 to 5 of the ResNet18 model for the three emergence parameters: plant density (top row), standard deviation of plant spacing (PSstd, middle row), and mean days to imaging after emergence (DAEmean, bottom row).

The estimation accuracy of the ResNet model calculated from Eq. 2 was high for all of the emergence parameters (≥ 0.95), except PSstd, where the accuracy was 0.73 (Table 1). The accuracy of plant density (0.97) was higher than previously reported by Shirzadifer et al. (2020) with accuracy 0.91. Their UAV images were taken at about the same growth stages as this study (i.e., V2 to V4). Moreover, the RMSE = 0.39 plant m^{-1} was similar to that of a previous study with no-till management (RMSE = 0.40 plant m^{-1},

Vong, Conway, et al., 2021). Another previous study (Vong, Stewart, et al., 2021) estimated individual corn plant DAE using a random forest machine learning method and showed moderate 3-day classification accuracies of < 0.85 (-1 to +1 DAE) when estimating the DAE after two weeks of emergence (DAE 13 to DAE 20). Our study showed improved results at estimating the mean of the DAE in 1-m row segments with an accuracy of 0.95 and RMSE of 1.0 day. Although this improved result was not based on individual plants, the DAEmean per 1-m row segment was still useful in examining and mapping the temporal emergence throughout the field. These results collectively indicated that our method outperforms the previous similar methods in estimating the corn emergence uniformity.

Table 4-1. Accuracy and root mean square error (RMSE) of testing datasets for plant density, standard deviation of plant spacing (PSstd), and mean days to imaging after emergence (DAEmean).

Parameter (n = 798)	Accuracy	RMSE
Plant Density	0.97	0.39 plant m^{-1}
PSstd	0.73	2.03 cm m^{-1}
DAEmean (segmented image)	0.95	1.06 days

4.4.3 Mapping and Evaluation of Plant Emergence in Field Conditions

Figure 4-6 shows maps of the three emergence parameters (b to d) and images with planting depths for reference (a). There were a few minor portions missing at the south part of the field due to stitching errors. It was observed that the DAEmean followed a trend with planting depth, where the shallow depth had higher DAEmean as seeds emerged earlier and vice versa at the deeper depths. There were no specific trends visually apparent for plant density and PSstd among the different planting depths. However, when statistically comparing each emergence parameter between different planting depths, some significant differences were found. As indicated in Fig. 4-7, plant

density and DAEmean decreased with increasing planting depths and the opposite result was observed for PSstd. These trends were likely due to the lower soil temperature at deeper planting depths, which can reduce emergence (hence, higher PSstd, Gupta, et al., 1988). For plant density, no significant difference was found between the 3.8 and 5.1 cm planting depths and the two deepest depths had significantly lower density than that of the two shallowest depths (Fig. 4-7a). For PSstd, the deepest (7.6 cm) depth had significantly lower PSstd than all the other depths (Fig. 4-7b). Meanwhile, DAEmean for all the depths were significantly different from each other (Fig. 4-7c). Figure 4-8 shows the density distribution of PSstd (a) and DAEmean (b) at different planting depths. PSstd seemed to have a similar distribution for all the planting depths with the maximum density at 2.5 cm m^{-1}. The planting depth of 7.6 cm had a slightly higher density at PSstd > 2.5 cm m^{-1}, indicating less spatial uniformity as compared to the shallow planting depths. The DAEmean distribution showed a difference of about 0.5 days between each subsequent planting depth.

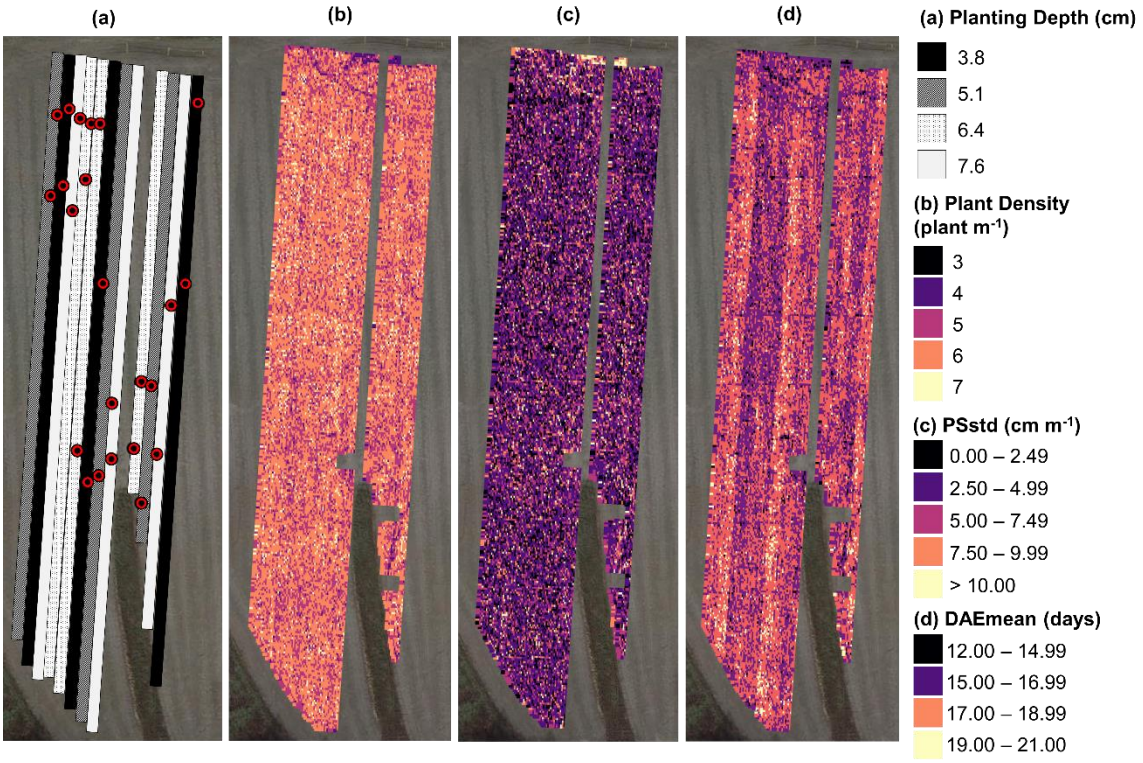

Figure 4-6. Image showing the different planting depth strips of eight plant rows (a) and maps of the three emergence parameters: (b) plant density, (c) plant spacing standard deviation (PSstd), and (d) mean days to imaging after emergence (DAEmean; earlier emerging plants have a higher DAEmean) in a 1-m row segment.

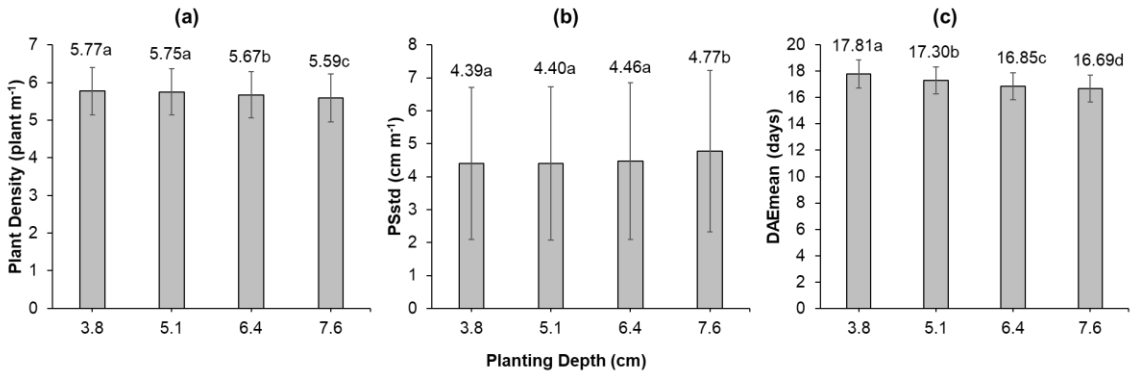

Figure 4-7. Planting depth effects on the three emergence parameters: (a) plant density, (b) plant spacing standard deviation (PSstd), and (c) mean days to imaging after emergence (DAEmean) at the four defined planting depths (earlier emerging plants have a higher DAEmean). Values at the top of each error bar show the average and different letters represent significant differences at p-value < 0.05 from Tukey HSD test.

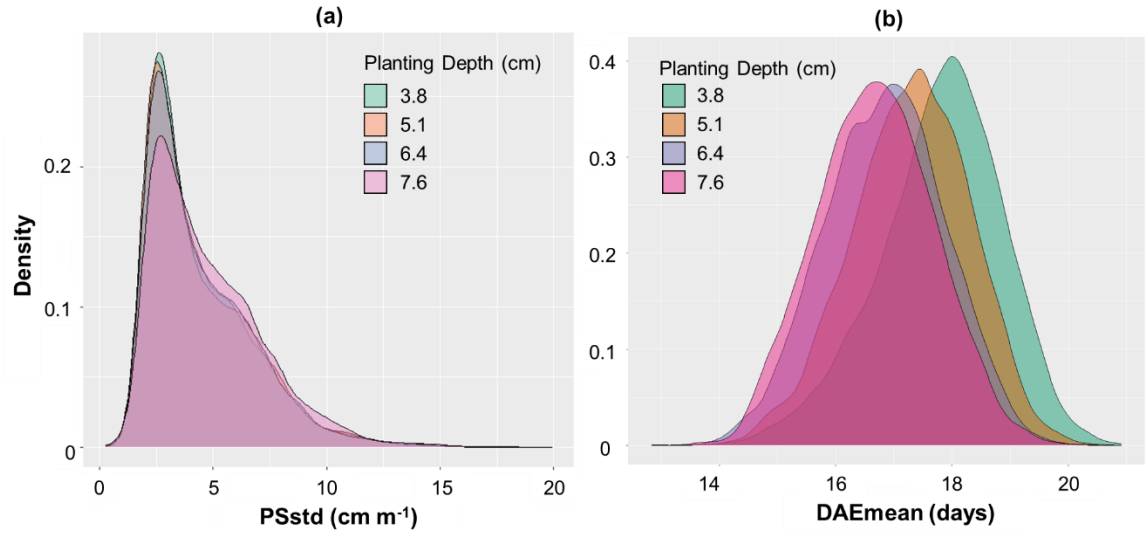

Figure 4-8. Density distribution of (a) plant spacing standard deviation (PSstd) and (b) mean days to imaging after emergence (DAEmean, earlier emerging plants have a higher DAEmean) at different planting depths.

The ability to use UAV imagery and DL model in estimating and mapping these corn emergence parameters in field condition as demonstrated could be a useful tool for other field-scale agronomic studies and commercial production. One example of applications could be to study the emergence uniformity of crops at different management practices (e.g., no-till vs. tillage, cover crops) and environment (e.g., weather, soil conditions, and topographic features). Other examples may include to access the need and performance of precision planting technologies, such as variable-rate seeding and on-the-go variable-planting depth based on real-time soil moisture sensing. Additionally, knowing the spatiotemporal emergence uniformity may help breeding programs to better understand the interactions of genotype × environment × management factors. For commercial production, the application could be aiding in replanting decision making and relating to final yield to better understand the yield variability throughout the field.

4.5 Conclusion

This study evaluated the potential of UAV imagery and a pre-trained deep learning (DL) model (ResNet18) in estimating and mapping corn temporal and spatial emergence parameters, including plant density, PSstd, and DAEmean. The DL model was able to estimate the parameters with accuracies that ranged from 0.73 to 0.97. The model performed better in estimating stand count and DAEmean than previous studies, providing higher accuracy and lower RMSE. Then, this estimation was extended to the field scale with different planting depth treatments as a case study. The DAEmean map demonstrated the expected trends of higher DAEmean at shallower planting depths as the plants emerged earlier, and therefore on the date of UAV assessment, early emerged plants would be more mature based on the growth development stage. When comparing the average emergence parameters among planting depths, the deeper planting depths had lower plant density and spatial uniformity as well as delayed emergence.

Further validation studies should be conducted to test the reliability and robustness of this workflow in estimating the same and/or other emergence parameters at other fields and different years, and to refine the workflow for more automated application. Moreover, with future technology of higher resolution cameras mounted on UAVs, flight height can be increased to cover larger fields and still achieve similar GSD. Then, this method will provide more opportunities for researchers and breeders in studying field-scale crop emergence as affected by different factors (genotype, management, and environment) as well as for producers in making better planting decision.

References

Abdi, H., & Williams, L. J. (2010). Tukey's honestly significant difference (HSD) test. Encyclopedia of Research Design, 3(1), 1-5.

Ahmad, A., Saraswat, D., Aggarwal, V., Etienne, A., & Hancock, B. (2021). Performance of deep learning models for classifying and detecting common weeds in corn and soybean production systems. Computers and Electronics in Agriculture, 184, 106081.

Andrade, F. H., & Abbate, P. E. (2005). Response of maize and soybean to variability in stand uniformity. Agronomy journal, 97(4), 1263-1269.

Badua, S., Sharda, A., Strasser, R., Ciampitti, I., & Griffin, T. (2018). Influence of planter downforce setting and ground speed on seeding depth and plant spacing uniformity of corn. In: Proceedings of 14th International Conference on Precision Agriculture.

Boomsma, C. R., Santini, J. B., West, T. D., Brewer, J. C., McIntyre, L. M., & Vyn, T. J. (2010). Maize grain yield responses to plant height variability resulting from crop rotation and tillage system in a long-term experiment. Soil and Tillage Research, 106(2), 227-240.

Corteva Agriscience, P. (2021). 2021 Agronomy research summary. Retrieved from https://www.pioneer.com/content/dam/dpagco/pioneer/na/us/en/files/agronomy/DF-PIO-2021-Agronomy-Research-Summary.pdf

Deeba, K., & Amutha, B. (2020). ResNet-deep neural network architecture for leaf disease classification. Microprocessors and Microsystems, 103364.

Espejo-Garcia, B., Mylonas, N., Athanasakos, L., & Fountas, S. (2020). Improving weeds identification with a repository of agricultural pre-trained deep neural networks. Computers and Electronics in Agriculture, 175, 105593.

Feng, A., Zhou, J., Vories, E., & Sudduth, K. A. (2020). Evaluation of cotton emergence using UAV-based imagery and deep learning. Computers and Electronics in Agriculture, 177, 105711.

Gnädinger, F., & Schmidhalter, U. (2017). Digital counts of maize plants by unmanned aerial vehicles (UAVs). Remote Sensing, 9(6), 544.

Gupta, S. C., Swan, J., & Schneider, E. (1988). Planting depth and tillage interactions on corn emergence. Soil Science Society of America Journal, 52(4), 1122-1127.

He, K., Zhang, X., Ren, S., & Sun, J. (2016). Deep residual learning for image recognition. In: Proceedings of the IEEE Conference on Computer Vision and Pattern Recognition.

Huang, G., Liu, Z., Van Der Maaten, L., & Weinberger, K. Q. (2017). Densely connected convolutional networks. In: Proceedings of the IEEE Conference on Computer Vision and Pattern Recognition.

Iacomi, C., & Popescu, O. (2015). A new concept for seed precision planting. Agriculture and Agricultural Science Procedia, 6, 38-43.

Intemational Organization for Standardization. 1984. Sowing equipment - Test methods - Part 1: Single seed drills (precision drills), 7256/1.

Jin, X., Liu, S., Baret, F., Hemerlé, M., & Comar, A. (2017). Estimates of plant density of wheat crops at emergence from very low altitude UAV imagery. Remote Sensing of Environment, 198, 105-114.

Kachman, S., & Smith, J. (1995). Alternative measures of accuracy in plant spacing for planters using single seed metering. Transactions of the ASAE, 38(2), 379-387.

Karayel, D., & Özmerzi, A. (2008). Evaluation of three depth-control components on seed placement accuracy and emergence for a precision planter. Applied Engineering in Agriculture, 24(3), 271-276.

Kitano, B. T., Mendes, C. C., Geus, A. R., Oliveira, H. C., & Souza, J. R. (2019). Corn plant counting using deep learning and UAV images. IEEE Geoscience and Remote Sensing Letters.

Kovács, P., & Vyn, T. J. (2014). Full-season retrospectives on causes of plant-to-plant variability in maize grain yield response to nitrogen and tillage. Agronomy Journal, 106(5), 1746-1757.

Krizhevsky, A. (2014). One weird trick for parallelizing convolutional neural networks. arXiv preprint arXiv:1404.5997.

Lauer, J. G., & Rankin, M. (2004). Corn response to within row plant spacing variation. Agronomy Journal, 96(5), 1464-1468.

Lawles, K., Raun, W., Desta, K., & Freeman, K. (2012). Effect of delayed emergence on corn grain yields. Journal of Plant Nutrition, 35(3), 480-496.

Lewontin, R. C. (1966). On the measurement of relative variability. Systematic Zoology, 15(2), 141-142.

Li, B., Xu, X., Han, J., Zhang, L., Bian, C., Jin, L., & Liu, J. (2019). The estimation of crop emergence in potatoes by UAV RGB imagery. Plant Methods, 15(1), 1-13.

Liu, T., Li, R., Jin, X., Ding, J., Zhu, X., Sun, C., & Guo, W. (2017). Evaluation of seed emergence uniformity of mechanically sown wheat with UAV RGB imagery. Remote Sensing, 9(12), 1241.

Liu, W., Tollenaar, M., Stewart, G., & Deen, W. (2004a). Impact of planter type, planting speed, and tillage on stand uniformity and yield of corn. Agronomy Journal, 96(6), 1668-1672.

Liu, W., Tollenaar, M., Stewart, G., & Deen, W. (2004b). Within-row plant spacing variability does not affect corn yield. Agronomy Journal, 96(1), 275-280.

Luce, G. A. (2016). Optimum corn Planting depth - "don't plant your corn too shallow". Retrieved from https://ipm.missouri.edu/IPCM/2016/4/Optimum_Corn_Planting_Depth-Dont_Plant_Your_Corn_Too_Shallow/

Milioto, A., Lottes, P., & Stachniss, C. (2017). Real-time blob-wise sugar beets vs weeds classification for monitoring fields using convolutional neural networks. ISPRS Annals of Photogrammetry, Remote Sensing & Spatial Information Sciences, 4.

Nafziger, E. D., Carter, P. R., & Graham, E. E. (1991). Response of corn to uneven emergence. Crop Science, 31(3), 811-815.

Nguyen, T. T., Vien, Q.-T., & Sellahewa, H. (2021). An efficient pest classification in smart agriculture using transfer learning. EAI Endorsed Transactions on Industrial Networks and Intelligent Systems, 8(26), 1-8.

Otsu, N. (1979). A threshold selection method from gray-level histograms. IEEE Transactions on Systems, Man, and Cybernetics, 9(1), 62-66.

Pan, S. J., & Yang, Q. (2009). A survey on transfer learning. IEEE Transactions on Knowledge and Data Engineering, 22(10), 1345-1359.

Pommel, B., Mouraux, D., Cappellen, O., & Ledent, J.-F. (2002). Influence of delayed emergence and canopy skips on the growth and development of maize plants: a plant scale approach with CERES-Maize. European Journal of Agronomy, 16(4), 263-277.

Poncet, A. M., Fulton, J. P., McDonald, T. P., Knappenberger, T., & Shaw, J. N. (2019). Corn emergence and yield response to row-unit depth and downforce for varying field conditions. Applied Engineering in Agriculture, 35(3), 399-408.

Poncet, A. M., Fulton, J. P., McDonald, T. P., Knappenberger, T., Shaw, J. N., & Bridges, R. W. (2018). Effect of heterogeneous field conditions on corn seeding depth accuracy and uniformity. Applied Engineering in Agriculture, 34(5), 819-830.

Precision Planting. (2019). Precision planting announces SmartDepth. Tremont, IL: Precision Planting, https://www.precisionplanting.com/agronomy/news/precision-planting-announces-smartdepth.

Russakovsky, O., Deng, J., Su, H., Krause, J., Satheesh, S., Ma, S., . . . Bernstein, M. (2015). Imagenet large scale visual recognition challenge. International Journal of Computer Vision, 115(3), 211-252.

Rutto, E., Daft, C., Kelly, J., Chim, B. K., Mullock, J., Torres, G., & Raun, W. (2014). Effect of delayed emergence on corn (Zea mays L.) grain yield. Journal of Plant Nutrition, 37(2), 198-208.

Sawyer, S. F. (2009). Analysis of variance: the fundamental concepts. Journal of Manual & Manipulative Therapy, 17(2), 27E-38E.

Schneider, E., & Gupta, S. (1985). Corn emergence as influenced by soil temperature, matric potential, and aggregate size distribution. Soil Science Society of America Journal, 49(2), 415-422.

Shirzadifar, A., Maharlooei, M., Bajwa, S. G., Oduor, P. G., & Nowatzki, J. F. (2020). Mapping crop stand count and planting uniformity using high resolution imagery in a maize crop. Biosystems Engineering, 200, 377-390.

Shuai, G., Martinez-Feria, R. A., Zhang, J., Li, S., Price, R., & Basso, B. (2019). Capturing Maize Stand Heterogeneity Across Yield-Stability Zones Using Unmanned Aerial Vehicles (UAV). Sensors, 19(20), 4446.

Silva, E. E. d., Baio, F. H. R., Kolling, D. F., Júnior, R. S., Zanin, A. R. A., Neves, D. C., . . . Teodoro, P. E. (2021). Variable-rate in corn sowing for maximizing grain yield. Scientific Reports, 11(1), 1-10.

Simonyan, K., & Zisserman, A. (2014). Very deep convolutional networks for large-scale image recognition. arXiv preprint arXiv:1409.1556.

Singh, R., Singh, G., & Saraswat, D. (2005). Optimisation of design and operational parameters of a pneumatic seed metering device for planting cottonseeds. Biosystems Engineering, 92(4), 429-438.

Sona, G., Passoni, D., Pinto, L., Pagliari, D., Masseroni, D., Ortuani, B., & Facchi, A. (2016). UAV multispectral survey to map soil and crop for precision farming applications. In: Proceedings of Remote Sensing and Spatial Information Sciences

Congress: International Archives of the Photogrammetry Remote Sensing and Spatial Information Sciences Congress.

Subetha, T., Khilar, R., & Christo, M. S. (2021). A comparative analysis on plant pathology classification using deep learning architecture–Resnet and VGG19. Materials Today: Proceedings.

Szegedy, C., Liu, W., Jia, Y., Sermanet, P., Reed, S., Anguelov, D., . . . Rabinovich, A. (2015). Going deeper with convolutions. In: Proceedings of the IEEE Conference on Computer Vision and Pattern Recognition.

Torres-Sánchez, J., Pena, J. M., de Castro, A. I., & López-Granados, F. (2014). Multi-temporal mapping of the vegetation fraction in early-season wheat fields using images from UAV. Computers and Electronics in Agriculture, 103, 104-113.

Varela, S., Dhodda, P., Hsu, W., Prasad, P., Assefa, Y., Peralta, N., . . . Ciampitti, I. (2018). Early-season stand count determination in corn via integration of imagery from unmanned aerial systems (UAS) and supervised learning techniques. Remote Sensing, 10(2), 343.

Vong, C. N., Conway, L. S., Zhou, J., Kitchen, N. R., & Sudduth, K. A. (2021). Early corn stand count of different cropping systems using UAV-imagery and deep learning. Computers and Electronics in Agriculture, 186, 106214.

Vong, C. N., Stewart, S. A., Zhou, J., Kitchen, N. R., & Sudduth, K. A. (2021). Estimation of corn emergence date using UAV imagery. Transactions of the ASABE, 64(4), 1173-1183.

Xu, W., Yu, G., Zare, A., Zurweller, B., Rowland, D. L., Reyes-Cabrera, J., . . . Juenger, T. E. (2020). Overcoming small minirhizotron datasets using transfer learning. Computers and Electronics in Agriculture, 175, 105466.

Yalcin, H. (2019). An approximation for a relative crop yield estimate from field images using deep learning. In: Proceedings of 2019 8th International Conference on Agro-Geoinformatics.

Zeiler, M. D., & Fergus, R. (2014). Visualizing and understanding convolutional networks. In: Proceedings of European Conference on Computer Vision.

Zhang, J., Basso, B., Price, R. F., Putman, G., & Shuai, G. (2018). Estimating plant distance in maize using Unmanned Aerial Vehicle (UAV). PloS One, 13(4), e0195223.

Zhang, X., Fu, L., Karkee, M., Whiting, M. D., & Zhang, Q. (2019). Canopy segmentation using ResNet for mechanical harvesting of apples. IFAC-PapersOnLine, 52(30), 300-305.

CHAPTER FIVE

CASE STUDIES: EARLY CORN EMERGENCE UNIFORMITY AT DIFFERENT PLANTING DEPTHS AND YIELD ESTIMATION USING UAV IMAGERY

5.1 Abstract

Uniform corn emergence is critical for maintaining optimum yield. Conventional studies relating plant emergence and early growth to yield for different treatments and management were based on small plots as limited by labor and time for in-field evaluation. Precision agriculture technologies such as proximal sensors, yield monitors, and UAV-based remote sensing have now enabled field-scale evaluation. The goal of this study was to demonstrate the applications of UAV imagery in corn production at field-scale level with two case studies: 1) investigating corn emergence spatial variability at different planting depths; 2) estimating corn yield using image features. Images taken at a corn field planted with four planting depths (i.e., 3.8, 5.1, 6.4, and 7.6 cm) by a red-green-blue camera and multispectral camera mounted on a UAV were used to determine corn emergence parameters and different vegetation indices (VIs) for early plant growth (V4, V6, V7) indicators. For case study 1, the average emergence parameters in 1.0 m × 6.1 m transects along the N-S direction of the field and coefficient of variation were computed to examine the emergence parameters for each planting depth and replication. Meanwhile, for case study 2, a random forest machine learning approach was used to estimate the yield with different feature datasets (i.e., only emergence data, each vegetative growth stage VIs, and their combination). Results demonstrated that there was spatial variability within the planting depth treatments at different replications along the transects as affected by elevation (and/or other soil and landscape environmental factors).

Emergence data alone could not explain variation in yield with R^2 of 0.01 while the combination of all growth stages VIs could estimate yield with R^2 of 0.34. The maps of the two most important VIs (V6VIREmax and V4NormRstd) showed some parts with lowest values similar with yield map. The case studies demonstrated the usage of UAV imagery in studying crop emergence variability and estimating yield at the field-scale level. Future studies should include more timely UAV data along the growing season at different fields and years to develop a more robust model.

5.2 Introduction

Seedling emergence is the initial most crucial phenological event determining the success of an annual plant (Forcella et al., 2000). Seedling emergence can be defined as the point of time when a seedling is independent of its seed's nutrient reserves and produces its own food through photosynthesis. Meanwhile, crop emergence can be defined as the appearance of the first leaf, which is an important input for crop development and biomass accumulation models (Gao et al., 2020). The emergence is influenced by both environmental factors (e.g., soil properties and weather) and the farmer's management (e.g., planting equipment, planting time, tillage, and cropping system). In corn, temporally and spatially uniform emergence is also critical to maintain optimum yield (Karayel & Özmerzi, 2008).

Many studies have investigated the effect of these factors on corn emergence, growth, and yield such as planting depth, tillage, cover crop implementation, crop rotation, seed size/shape, soil variability, landscape position, and interaction between two or three of these factors (Al‐Darby & Lowery, 1986; Drury et al., 1999; Gupta et al., 1988; Molatudi & Mariga, 2009; Nemergut et al., 2021; Stewart et al., 2021). Conventionally,

the studies were performed in a randomized complete block design with small plots and evaluation of corn emergence, growth, and yield would be in smaller monitoring sites within the plots. The evaluation of the whole plots or fields is not possible as limited by labor and time.

The advent of technologies in precision agriculture (PA, field management based on field spatial variability (Mulla, 2013)) such as remote sensing, proximal sensing, and yield monitoring have now made whole-plot or field-scale evaluation feasible. For example, apparent soil electrical conductivity (EC_a) measured by proximal soil sensors and yearly yield maps from yield monitors were related with field-scale soil properties to create crop management zones in PA (Anderson-Cook et al., 2002; King et al., 2005; Kitchen et al., 2003; Singh et al., 2016; Sudduth et al., 2005). The results showed high correlations of EC_a with clay content and cation exchange capacity (CEC) (Sudduth et al., 2005). Soil types were classified accurately with classification accuracy > 85% when using only EC_a data and > 90% when combining it with yield data (Anderson-Cook et al., 2002).

Recently, remote sensing technology based on unmanned aerial vehicle (UAV) imagery was extensively used to estimate emergence of different crops, including stand count, plant density, emergence rate, spacing uniformity, canopy cover in corn, wheat, cotton, and potato (Chen et al., 2018; Feng et al., 2020; Jin et al., 2017; Liu et al., 2017; Mhango et al., 2021; Shirzadifar et al., 2020; Shuai et al., 2019; Varela et al., 2018). The results showed R^2 of >0.80 when comparing the estimated and actual crop emergence parameters. Furthermore, the mapping of these crop emergence parameters was achievable using orthomosaics generated from continuous images captured in the field (Feng et al., 2020; Mhango et al., 2021; Shirzadifar et al., 2020).

Besides crop emergence, UAV imagery was also used to estimate crop growth and status including leaf area index (LAI), biomass, plant height, leaf nitrogen (N) content, canopy cover, and relative water content (dos Santos et al., 2021; Herrmann et al., 2020; Maresma et al., 2016; Xu et al., 2021) as well as final yield (Herrmann et al., 2020; Maresma et al., 2016; Olson et al., 2019) by determining the crop reflectance (i.e., vegetation indices, VIs). Results indicated R^2 ranged from 0.29 to 0.91 when estimating corn LAI, biomass, and plant height (dos Santos et al., 2021), 0.40 to 0.59 when estimating corn leaf N content (Xu et al., 2021), and 0.00 to 0.92 when estimating corn and sugarbeet yield (Herrmann et al., 2020; Maresma et al., 2016; Olson et al., 2019). The wide ranges of R^2 in estimating yield were due to images captured at different growth stages and at different locations.

These previous studies illustrated the feasibility of UAV imagery in estimating crop emergence, growth, and field-scale mapping. Hence, the goal of this study was to demonstrate the applications of UAV imagery in corn production at the field-scale level. Two case studies were examined: 1) corn emergence spatial variability investigation at different planting depths and 2) corn yield estimation using UAV image features.

5.3 Materials and Methodology

5.3.1 Study Site

Figure 5-1a shows the study site, which is the same as that in Chapter 4 with the same experiment setup and ground data collection. The site has notable landscape variability, as illustrated in the elevation map retrieved from the John Deere StarFire 3000 receiver (Deere & Co., Moline, IL, USA) that was mounted on the tractor during the planting operation (Fig. 5-1b). Corn was harvested on 22 October 2020 using a 4-row

combine harvester, equipped with an Ag Leader yield monitor (Ag Leader Technology, Ames, IA, USA). The harvester speed was about 1.5 ms^{-1} and the yield monitor recorded the geo-referenced grain yield every 2 s, resulting in approximately 3 m of 4-rows plants (3 m) for each yield data point. The yield data were pre-processed using Yield Editor software (Sudduth et al., 2012) to remove data artefacts. For the first case study (emergence spatial variability among planting depths), data from all the replications (Rs) were used. Yield data was missing (16 plants rows in 5.1 cm depth) in R3 while the yield in western rows of R1 (5.1 cm depth) was not reliable due to different nitrogen treatments applied at the plants row beside them. Hence, only R2 data was used in the second case study (estimating yield using UAV image features).

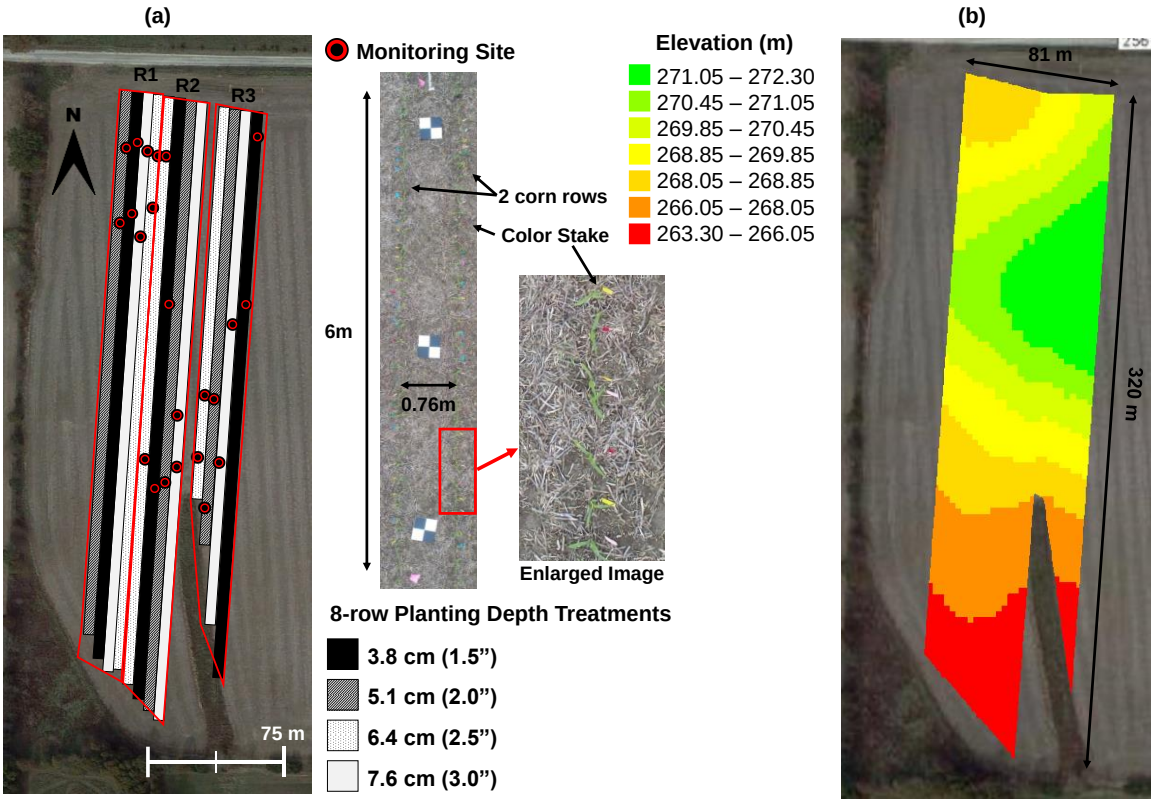

Figure 5-1. (a) Study site with a schematic diagram of 8-row corn planting depth treatments (R1 to R3 = replication 1 to 3) and an example image of a monitoring site taken on 22 May 2020; (b) Elevation map from Global Positioning System receiver mounted on the tractor used during planting.

5.3.2 UAV Data Collection

For corn emergence uniformity estimation, a Phantom 4 Advanced UAV imaging system (DJI, Shenzhen, Guangdong, China) with an onboard RGB camera was used to acquire aerial images on 22 May 2020. The details of this data collection were reported in Chapter 4. For corn early growth estimation, a multispectral camera (RedEdge-M, MicaSense, Seattle, WA, USA) mounted on a DJI Matrice 600 Pro UAV (DJI, Shenzhen, China) was used to capture multispectral images for the study field on 12 and 25 June, and 2 July 2020, corresponding to V4, V6, and V7 growth stages, respectively. These images were taken between 10 am to 2 pm (i.e., at minimum changes in the solar zenith angle). The multispectral images comprised of five bands: blue, green, red, red-edge, and near-infrared with the resolution of 1260 by 960 pixels. The frame rate used was 1 frame per second. Images of a calibration reflectance panel were taken before each flight for later image processing to convert the raw pixel values into reflectance. Autopilot (Hangar Technology, Austin, TX, USA) was used to define the flight settings and paths for the UAV. The flight speed and height were set as 2.0 m s^{-1} and 30 m, respectively, which corresponded to a calculated ground sampling distance (GSD) of 2.1 cm $pixel^{-1}$. These settings were used to ensure sufficient forward and side overlaps (at least 75%).

5.3.3 Image Processing and Data Analysis

5.3.3.1 Case Study 1: Corn Emergence Spatial Variability at Different Planting Depths

The procedures for RGB images processing and corn emergence estimation using DL model were detailed in Chapter 4. The emergence parameters estimated included plant density, mean days to imaging after emergence (DAEmean), and plant spacing standard deviation (PSstd) in 1-m by 1-m (each plant row) resolution. Each emergence

parameter was averaged across all treatment rows, resulting in a spatial resolution of 1.0 m × 6.1 m in transects along the N-S direction. Subsequently, a moving average was fitted to these data, where each point was calculated as the mean of ten adjacent points to better represent the trend in each emergence parameter along the N-S direction. The CV, which is the division of standard deviation by the mean and multiplied by 100 (Lewontin, 1966), was also calculated at the same spatial resolution to examine the relative variability of the three emergence parameters for each planting depth and replication.

5.3.3.2 Case Study 2: Corn Yield Estimation using UAV Image Features

Multispectral images were first stitched using Pix4D Mapper (Pix4D, Lausanne, Switzerland) to generate orthomosaics of each band for the study field. The template "Ag Multispectral processing" was selected for the image stitching. The orthomosaic of each band for each data collection was exported as a .tif image.

There were three data sets as tabulated in Table 5-1, which were different in data type and resolution, QGIS (ver. 3.18, www.qgis.org) was used to merge the three layers. Firstly, a multispectral orthomosaic from each growth stage was geo-referenced using 'Georeferencer' so that they aligned to each other. Then, each four plant rows were segmented from all the aligned orthomosaics by first creating a polygon for every four rows and clipping the orthomosaic based on the polygon ('Clip Raster by Mask Layer'). For both emergence and yield vector data, each 4-row data was also exported and saved as separate vector files. Each 4-row data was processed separately to ensure all of the data types aligned to each other. For some data points which did not align well, 'Move Feature' and 'Rotate Feature' were used to align them. Then, a polygon based on each yield point (yield polygon) was created and all the emergence points within the yield polygon were

assigned to the same yield value in kg ha^{-1} (Fig. 5-2a) by joining both the vector data using 'Join Attributes by Location'. Next, a polygon for each emergence point was created using 'Buffer' (Fig. 5-2b). These polygons were used to segment the orthomosaic for further VIs extraction.

Table 5-1. Data type and resolution of the three data sets in this study.

Data Set	Data Type	Resolution
UAV RGB – Emergence	Vector	1 m by 1 m (each plant row)
UAV Multispectral – Growth	Raster	1.95 cm $pixel^{-1}$
Yield	Vector	3 m by 3 m (4 plant rows)

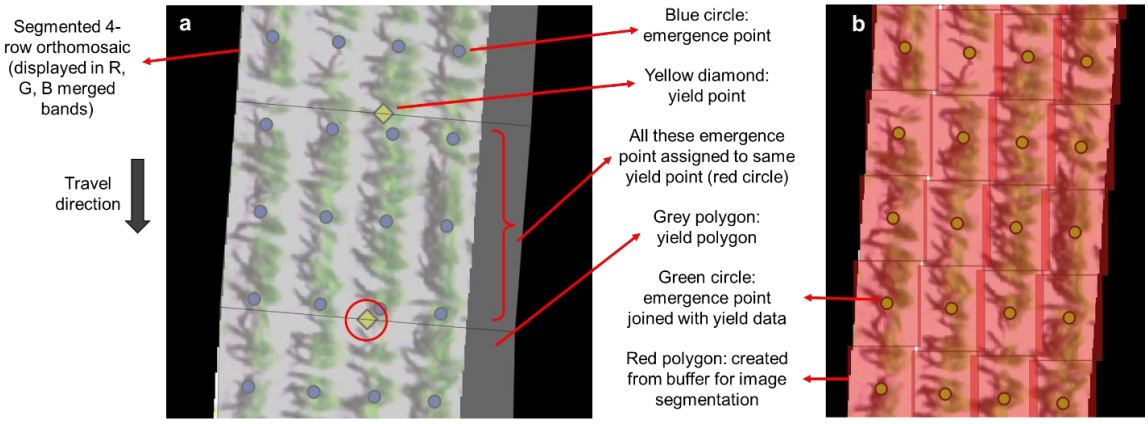

Figure 5-2. a) Example of a 4-row data with emergence and yield points, segmented orthomosaic, and created yield polygon to join yield point to emergence point; b) polygon created from buffer for further orthomosaic segmentation to extract vegetation indices.

A total of 15 VIs (Baio et al., 2018; Sripada et al., 2006) as listed in Table 5-2 were computed using Matlab 2019a (The MathWorks, Inc., Natick, MA, USA) and their average (mean), standard deviation (std), maximum (max), and minimum (min) were calculated. Different feature datasets as listed in Table 5-3 were used to estimate the yield using a random forest (RF) model. These different feature datasets were tested to investigate which components or combinations of them (emergence and early growth) could explain the variation in final yield. Furthermore, planting depth as a categorial variable was included in each dataset for the yield estimation to study the effect of planting depth on yield.

Table 5-2. Vegetation indices computed from multispectral orthomosaic.

Vegetation Index	Equation	Reference
Normalized difference vegetation index (NDVI)	$NDVI = \frac{NIR - R}{NIR + R}$	(Baio et al., 2018)
Green normalized difference vegetation index (GNDVI)	$GNDVI = \frac{NIR - G}{NIR + G}$	(Sripada et al., 2006)
Normalized difference red-edge (NDRE)	$NDRE = \frac{NIR - RE}{NIR + RE}$	(Baio et al., 2018)
Normalized red (NormR)	$NormR = \frac{R}{R + G + NIR}$	(Sripada et al., 2006)
Normalized green (NormG)	$NormG = \frac{G}{R + G + NIR}$	(Sripada et al., 2006)
Normalized near-infrared (NormNIR)	$NormNIR = \frac{NIR}{R + G + NIR}$	(Sripada et al., 2006)
Vegetation index red-edge (VIRE)	$VIRE = (lnNIR - lnRE) \times 100$	(Baio et al., 2018)
Difference vegetation index (DVI)	$DVI = NIR - R$	(Sripada et al., 2006)
Green difference vegetation index (GDVI)	$GDVI = NIR - G$	(Sripada et al., 2006)
Ratio vegetation index (RVI)	$RVI = \frac{NIR}{R}$	(Sripada et al., 2006)
Green ratio vegetation index (GRVI)	$GRVI = \frac{NIR}{G}$	(Sripada et al., 2006)
Soil adjusted vegetation index (SAVI)	$SAVI = \frac{NIR - R}{NIR + R + 0.5} \times 1.5$	(Sripada et al., 2006)
Green soil adjusted vegetation index (GSAVI)	$GSAVI = \frac{NIR - G}{NIR + G + 0.5} \times 1.5$	(Sripada et al., 2006)
Optimized soil adjusted vegetation index (OSAVI)	$OSAVI = \frac{NIR - R}{NIR + R + 0.16}$	(Sripada et al., 2006)
Green optimized soil adjusted vegetation index (GOSAVI)	$GOSAVI = \frac{NIR - R}{NIR + R + 0.16}$	(Sripada et al., 2006)

Table 5-3. Different feature datasets for yield estimation.

No.	Feature Dataset Name	Description	No. of Features	No. of Selected Features
1	Emergence	Emergence data collected from UAV RGB imagery	3	3
2	V4	Early growth data (V4) collected from UAV multispectral imagery	60	7
3	V6	Early growth data (V6) collected from UAV multispectral imagery	60	10
4	V7	Early growth data (V7) collected from UAV multispectral imagery	60	8
5	AllGrowth	Combination of no. 2 – 4	180	25
6	Emergence+V4	Combination of no. 1 and 2	63	9
7	Emergence+V6	Combination of no. 1 and 3	63	12
8	Emergence+V7	Combination of no. 1 and 4	63	10
9	AllUAV	Combination of no. 1 – 4	183	29

Statistical analysis and RF modeling were performed using Python 3.8. There are many features in the feature datasets (except emergence, Table 5-3) with multicollinearity, hence, the variance inflation factor (VIF) was calculated to remove the features with high collinearity (James et al., 2013). This is computed as a dependent variable of the coefficient of determination (R^2) of each feature against all other features. The VIF was calculated using 'variance_inflation_factor' in the 'statsmodels' module for each feature dataset (except emergence) and the variable with the highest VIF was removed. This step was repeated in a loop until all the remaining features with VIF of less than or equal to 5. Then, these remaining features were used in the RF model ('RandomForestRegressor' in the 'sklearn' module) to estimate the yield. The number of trees in the RF model was set as 100 (default value) and the maximum feature size was determined using the division of total number of features by three (James et al., 2013). The total number of datasets was 9405, divided into training (80%) and testing (20%) datasets. To test the model performance and which feature datasets contribute more to the yield, R^2 and root-mean-square error (RMSE) were calculated between the actual and estimated yield. To determine which features contributed more in estimating the yield, the importance of variables based on the mean decrease in the Gini index was calculated (James et al., 2013) with the higher the value, the more important the feature.

5.4 Results and Discussion

5.4.1 Case Study 1: Emergence Spatial Variability among Planting Depths

As shown in Fig. 5-3, the average elevation along the N-S direction varies across the site, with increasing elevation (about 269 to 272 m) from 0 to 100 m down each

replication (R1, R2 or R3) transect and decreasing elevation (about 272 to 265 m) afterward. The two deeper planting depths (6.4 and 7.6 cm) generally had a lower plant density and higher PSstd than the two shallow depths for all of the Rs along the transects (Fig. 5-3a to c, e to g). These results suggest shallower planting depths resulted in more consistent corn stands across the site. The DAEmean also decreased with increasing depths for all the Rs along the transects except R2 (Fig. 5-3j), where 6.4 cm depth had the lowest DAEmean, from 40 to 180 m. Moreover, for certain transects, some depths had similar DAEmean, such as from 60 to 100 m for 5.1- and 7.6-cm planting depths at R2 (Fig. 5-3j), as well as from 80 to 100 m for 3.8- and 5.1-cm depths, and 120 to 140 m for 6.4- and 7.6-cm depths at R3 (Fig. 5-3k). This result suggests that, in general, deeper planting depths reduced the emergence window at this study site.

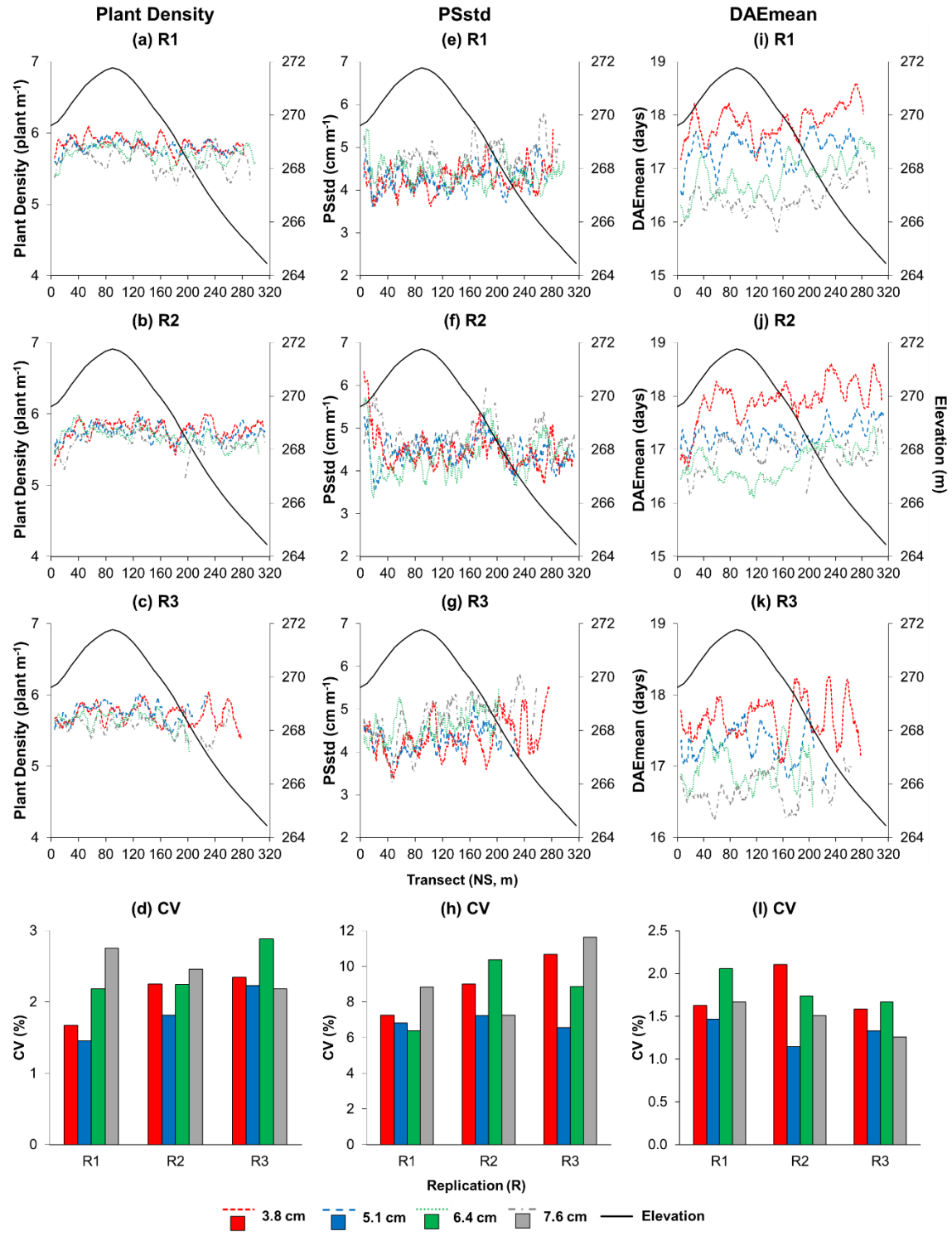

Figure 5-3. Line charts showing every 1-m transect (after a 10-m moving average) from north to south of the field with the average of the three emergence parameters at different planting depths and their coefficient of variation (bar charts) as well as average elevation: (a) to (d) plant density (plant m^{-1}), (e) to (h) plant spacing standard deviation (PSstd, cm m^{-1}), and (i) to (l) mean days to imaging after emergence (DAEmean, days) for each replication (R).

When examining the variability of each emergence parameter along the transects using CV (Fig. 5-3d, h, and l), the 5.1 cm planting depth consistently showed the lowest CV as compared to other planting depths. There were only three exceptions – R3 for plant density (Fig. 5-3d), R1 for PSstd (Fig. 5-3h), and R3 for DAEmean (Fig. 5-3l). The findings indicate that, generally, the 5.1 cm planting depth had the least variability for all the emergence parameters, which could make it an ideal depth for corn planting in this situation. The 5.1 cm planting depth was also within the recommended corn planting depth range of 4.4 to 5.7 cm, as suggested by (Luce, 2016). Moreover, the deepest depth had the highest CV for plant density and PSstd for most of the Rs, indicating their lower spatial uniformity along the transects (Fig. 5-3d and h). However, emergence uniformity (temporal) was more consistent at 7.6 cm than at the 3.8 and 6.4 cm depths (Fig. 5-3l). The higher CV for plant density and PSstd but lower CV for DAEmean for the 7.6 cm depth than other depths (most of the Rs) suggested that it had fewer emerged plants and higher PSstd variability caused by missing plants, with the emerged plants having similar emergence date.

These results collectively demonstrated spatial variability within the planting depth treatments at different Rs along the transects as affected by elevation (and/or other soil and landscape environmental factors such as aspect, wetness, encompassed by relative elevation). Furthermore, it is unlikely that these phenomena would be captured by a few monitoring sites along the N-S transects, which would be limited in numbers due to more time required for assessment. Therefore, the UAV imagery shows its practicality in capturing spatial variability of the emergence parameters at a field-scale

level with comparable accuracy but higher precision than only using monitoring sites to monitor the crop response.

5.4.2 Case Study 2: Yield Estimation using UAV Image Feature

The deepest depth (7.6 cm) had significantly lowest average yield followed by the shallowest depth (3.8 cm) as indicated in Fig. 5-4a. The 6.4 cm depth had the highest average yield of 13.59 Mg ha^{-1}, which was slightly higher than that of the 5.1 cm depth. When comparing with the emergence parameters in average (Fig. 5-4b to d), the deepest depth of 7.6 cm with the lowest plant density and highest PSstd (i.e., higher spatial variability) had the lowest yield. The 6.4 cm depth had the lowest CV (Fig. 5-4e), indicating a lower plant density variation, corresponding to the highest yield. Similarly, the deepest depth of 7.6 cm with the highest CV (i.e., highest plant density variation) had the lowest yield. As illustrated in Fig. 5-3f, the 5.1 cm depth with the lowest CV, suggesting the most uniform emergence in DAEmean had a higher average yield as compared to other depths (except 6.4 cm depth). Surprisingly, the 6.4 cm depth with the highest CV indicating more emergence variability had the highest yield. These mixed results might be caused by the effects of landscape variability and soil condition across the field (Stewart et al., 2021).

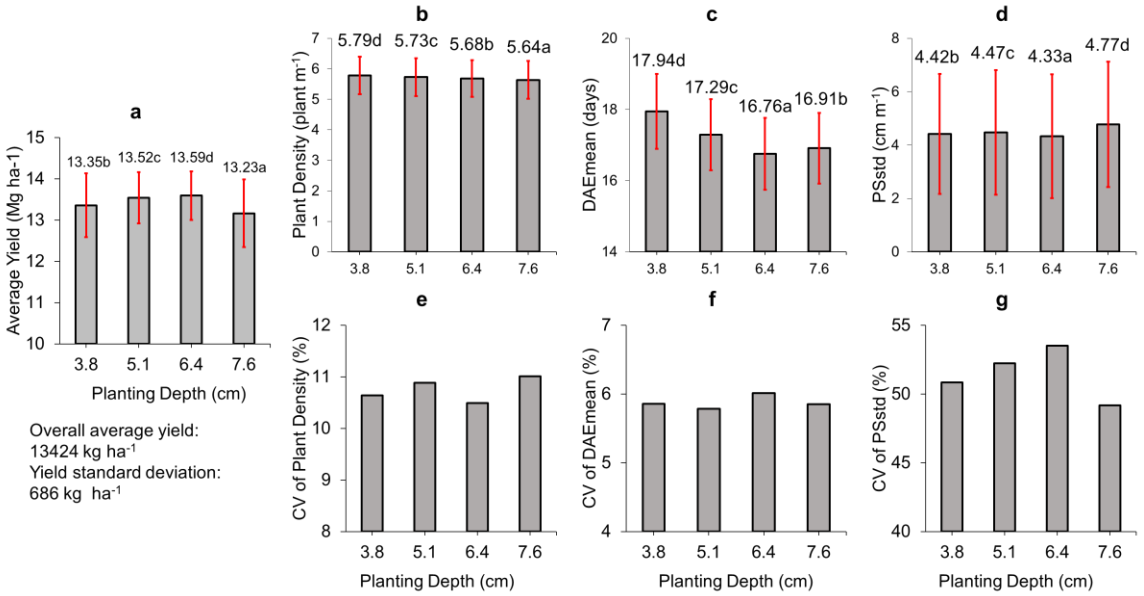

Figure 5-4. The average yield (a), emergence parameters (b – d), and their CV in percentage (e – g) at different planting depths. Different letters indicating significantly difference in average values at $p < 0.05$ for the Tukey HSD test.

After calculating VIF, only 12 to 19% of the original number of the UAV image features remained for further ML modelingfor each feature dataset except emergence (did not undergo feature selection) as indicated in Table 5-3. Most of the UAV image features with mean were removed and the remaining features were with standard deviation and maximum as illustrated in Fig. A5 and A6. As indicated in Table 5-4, the R^2 were improved when planting depths were included as features suggesting there were effects from planting depths on the final yield. The RMSE of all the feature datasets was lower than the yield standard deviation (686 kg ha^{-1}, Fig. 5-4) except for emergence datasets. The emergence did not explain any variations in yield with the lowest R^2 and highest RMSE among all the feature datasets. With the addition of emergence data to early growth data for estimating yield, the R^2 either reduced or remained the same and RMSE increased except for Emergence+V7.

Table 5-4. R^2 and RMSE of different feature datasets with and without planting depths as features in estimating yield for testing dataset.

Feature Datasets	With Planting Depth		Without Planting Depth	
	R^2	RMSE	R^2	RMSE
Emergence	0.01	720	0.00	727
V4	0.20	611	0.09	655
V6	0.18	617	0.07	659
V7	0.15	630	0.03	679
AllGrowth	0.34	560	0.24	595
Emergence+V4	0.18	618	0.08	656
Emergence+V6	0.18	617	0.07	659
Emergence+V7	0.16	627	0.04	676
AllUAV	0.34	561	0.24	596

Meanwhile, when comparing the different early growth stages (among V4, V6, and V7), V4 had the highest R^2 and lowest RMSE, indicating some yield variation could be detected as early as V4 growth stage. The feature dataset with the best performance (highest R^2 and lowest RMSE) was AllGrowth. Overall, the findings implied that emergence data had least relationship with yield. Early growth data might have a little contribution in explaining the final yield. Previous studies indicated that VIs at later vegetative growth stages (≥ V10) and early reproductive stages (R1 – R2) had higher R^2 in estimating corn yield than that of earlier grow stages (Olson et al., 2019).

Both V6VIREmax and V4NormRstd ranked as the top two important features as they have the highest mean decrease in Gini index (Fig. A5). The field maps of these two VIs were drawn in QGIS overlaid on a Google map (Google, Mountain View, CA, USA) as illustrated in Fig. 5-5b and c. with yield map included in Fig. 5-5a. Based on visual inspection, there were a few parts showing similarly low values for yield and both VIs (Fig. 5-5, black circles). However, there was also a big contrasting part specifically in V4NormRstd (Fig. 5-5, red circles), having the smallest value while V6 had the highest value and yield was mostly higher. These results implied some inconsistencies when using

these VIs in estimating the yield or further analysis involving other environmental factors such as landscape positions were needed. Overall, these maps still demonstrated some usefulness of UAV imagery in visualizing field-scale plant growth variation.

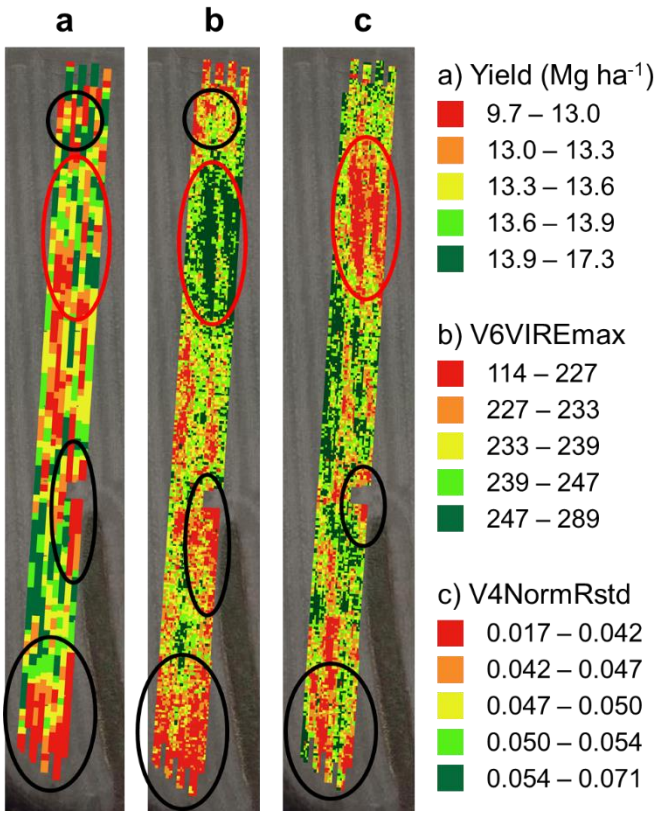

Figure 5-5. Maps of yield (a) and two top vegetation indices (VIs) determined from random forest variable importance: V6VIREmax (b) and V4NormRstd (c). Black circles indicate part with similarly low values among yield and both VIs while red circles shows the contrasting parts specifically for V4NormRstd.

5.5 Conclusion and Future Study

Both the case studies demonstrated the usage of UAV imagery in relating crop emergence uniformity to treatments such as planting depths (in this study) and estimating final yield at field-scale level. For case study 1, the spatial variability across the field in this study showed the 5.1 cm depth generally had the least variability for all the emergence parameters. The 7.6 cm depth had the highest variability for plant density and PSstd but lower variability for DAEmean than other depths except for 5.1 cm. This suggests it had

fewer emerged plants with similar emergence dates and higher PSstd variability due to missing plants. This study serves as the initial study of evaluating field-scale crop emergence at affected by planting treatments. Further studies should be conducted in multiple fields and years to further justify the usefulness of UAV imagery in evaluating emergence uniformity for different treatments such as tillage, cover crop implementation, crop rotation, landscape position, and interactions between them.

For case study 2, the average emergence parameters did not follow a trend similar in the yield at different planting depths except PSstd. When estimating the yield with UAV image features, the estimated emergence data was not able to explain final yield variation. Plant growth data as represented by UAV VIs at all the growth stages (V4, V6, and V7) was only able to represent a small amount of the variations in yield (R^2 = 0.16 – 0.34). Future studies should include weekly or biweekly UAV data to observe the growth variation along the season and relate it with the final yield. Moreover, more data collected in different fields and years integrated with environmental data such as weather and soil properties should be included to develop a more robust model for yield estimation.

References

Al‐Darby, A., & Lowery, B. (1986). Evaluation of Corn Growth and Productivity with Three Conservation Tillage Systems 1. *Agronomy Journal*, *78*(5), 901-907.

Anderson-Cook, C. M., Alley, M., Roygard, J., Khosla, R., Noble, R., & Doolittle, J. (2002). Differentiating soil types using electromagnetic conductivity and crop yield maps.

Baio, F. H. R., Silva, E. E., Vrech, M. A., Souza, F. H. Q., Zanin, A. R., & Teodoro, P. E. (2018). Vegetation indices to estimate spray application rates of crop protection products in corn. *Agronomy Journal, 110*(4), 1254-1259.

Chen, R., Chu, T., Landivar, J. A., Yang, C., & Maeda, M. M. (2018). Monitoring cotton (Gossypium hirsutum L.) germination using ultrahigh-resolution UAS images. *Precision Agriculture, 19*(1), 161-177.

dos Santos, R. A., Filgueiras, R., Mantovani, E. C., Fernandes-Filho, E. I., Almeida, T. S., Venancio, L. P., & da Silva, A. C. B. (2021). Surface reflectance calculation and predictive models of biophysical parameters of maize crop from RG-NIR sensor on board a UAV. *Precision Agriculture, 22*(5), 1535-1558.

Drury, C. F., Tan, C. S., Welacky, T. W., Oloya, T. O., Hamill, A. S., & Weaver, S. E. (1999). Red clover and tillage influence on soil temperature, water content, and corn emergence. *Agronomy Journal, 91*(1), 101-108.

Feng, A., Zhou, J., Vories, E., & Sudduth, K. A. (2020). Evaluation of cotton emergence using UAV-based imagery and deep learning. *Computers and Electronics in Agriculture, 177,* 105711.

Forcella, F., Arnold, R. L. B., Sanchez, R., & Ghersa, C. M. (2000). Modeling seedling emergence. *Field Crops Research, 67*(2), 123-139.

Gao, F., Anderson, M., Daughtry, C., Karnieli, A., Hively, D., & Kustas, W. (2020). A within-season approach for detecting early growth stages in corn and soybean using high temporal and spatial resolution imagery. *Remote Sensing of Environment, 242,* 111752.

Gupta, S. C., Swan, J., & Schneider, E. (1988). Planting depth and tillage interactions on corn emergence. *Soil Science Society of America Journal, 52*(4), 1122-1127.

Herrmann, I., Bdolach, E., Montekyo, Y., Rachmilevitch, S., Townsend, P. A., & Karnieli, A. (2020). Assessment of maize yield and phenology by drone-mounted superspectral camera. *Precision Agriculture, 21*(1), 51-76.

James, G., Witten, D., Hastie, T., & Tibshirani, R. (2013). *An introduction to statistical learning* (Vol. 112): Springer.

Jin, X., Liu, S., Baret, F., Hemerlé, M., & Comar, A. (2017). Estimates of plant density of wheat crops at emergence from very low altitude UAV imagery. *Remote Sensing of Environment, 198*, 105-114.

Karayel, D., & Özmerzi, A. (2008). Evaluation of three depth-control components on seed placement accuracy and emergence for a precision planter. *Applied Engineering in Agriculture, 24*(3), 271-276.

King, J., Dampney, P., Lark, R., Wheeler, H., Bradley, R., & Mayr, T. (2005). Mapping potential crop management zones within fields: use of yield-map series and patterns of soil physical properties identified by electromagnetic induction sensing. *Precision Agriculture, 6*(2), 167-181.

Kitchen, N., Drummond, S., Lund, E., Sudduth, K., & Buchleiter, G. (2003). Soil electrical conductivity and topography related to yield for three contrasting soil–crop systems. *Agronomy Journal, 95*(3), 483-495.

Lewontin, R. C. (1966). On the measurement of relative variability. *Systematic Zoology, 15*(2), 141-142.

Liu, T., Li, R., Jin, X., Ding, J., Zhu, X., Sun, C., & Guo, W. (2017). Evaluation of seed emergence uniformity of mechanically sown wheat with UAV RGB imagery. *Remote Sensing, 9*(12), 1241.

Luce, G. A. (2016). Optimum Corn Planting Depth - "Don't Plant Your Corn Too Shallow". Retrieved from https://ipm.missouri.edu/IPCM/2016/4/Optimum_Corn_Planting_Depth-Dont_Plant_Your_Corn_Too_Shallow/

Maresma, Á., Ariza, M., Martínez, E., Lloveras, J., & Martínez-Casasnovas, J. A. (2016). Analysis of vegetation indices to determine nitrogen application and yield prediction in maize (Zea mays L.) from a standard UAV service. *Remote Sensing, 8*(12), 973.

Mhango, J. K., Harris, E. W., Green, R., & Monaghan, J. M. (2021). Mapping potato plant density variation using aerial imagery and deep learning techniques for precision agriculture. *Remote Sensing, 13*(14), 2705.

Molatudi, R., & Mariga, I. (2009). The effect of maize seed size and depth of planting on seedling emergence and seedling vigour. *Journal of Applied Sciences Research, 5*(12), 2234-2237.

Mulla, D. J. (2013). Twenty five years of remote sensing in precision agriculture: Key advances and remaining knowledge gaps. *Biosystems engineering, 114*(4), 358-371.

Nemergut, K. T., Thomison, P. R., Carter, P. R., & Lindsey, A. J. (2021). Planting depth affects corn emergence, growth and development, and yield. *Agronomy Journal, 113*(4), 3351-3360.

Olson, D., Chatterjee, A., Franzen, D. W., & Day, S. S. (2019). Relationship of drone-based vegetation indices with corn and sugarbeet yields. *Agronomy Journal, 111*(5), 2545-2557.

Shirzadifar, A., Maharlooei, M., Bajwa, S. G., Oduor, P. G., & Nowatzki, J. F. (2020). Mapping crop stand count and planting uniformity using high resolution imagery in a maize crop. *Biosystems Engineering, 200*, 377-390.

Shuai, G., Martinez-Feria, R. A., Zhang, J., Li, S., Price, R., & Basso, B. (2019). Capturing maize stand heterogeneity across yield-stability zones using unmanned aerial vehicles (UAV). *Sensors, 19*(20), 4446.

Singh, G., Williard, K. W., & Schoonover, J. E. (2016). Spatial relation of apparent soil electrical conductivity with crop yields and soil properties at different topographic positions in a small agricultural watershed. *Agronomy, 6*(4), 57.

Sripada, R. P., Heiniger, R. W., White, J. G., & Meijer, A. D. (2006). Aerial color infrared photography for determining early in-season nitrogen requirements in corn. *Agronomy Journal, 98*(4), 968-977.

Stewart, S., Kitchen, N., Yost, M., Conway, L. S., & Carter, P. (2021). Planting depth and within-field soil variability impacts on corn stand establishment and yield. *Agrosystems, Geosciences & Environment, 4*(3), e20186.

Sudduth, K., Kitchen, N., Wiebold, W., Batchelor, W., Bollero, G., Bullock, D., . . . Schuler, R. (2005). Relating apparent electrical conductivity to soil properties across the north-central USA. *Computers and Electronics in Agriculture, 46*(1-3), 263-283.

Sudduth, K. A., Drummond, S. T., & Myers, D. B. (2012). *Yield Editor 2.0: Software for automated removal of yield map errors.* Paper presented at the 2012 Dallas, Texas, July 29-August 1, 2012.

Varela, S., Dhodda, P., Hsu, W., Prasad, P., Assefa, Y., Peralta, N., . . . Ciampitti, I. (2018). Early-season stand count determination in corn via integration of imagery from unmanned aerial systems (UAS) and supervised learning techniques. *Remote Sensing, 10*(2), 343.

Xu, X., Fan, L., Li, Z., Meng, Y., Feng, H., Yang, H., & Xu, B. (2021). Estimating leaf nitrogen content in corn based on information fusion of multiple-sensor imagery from UAV. *Remote Sensing, 13*(3), 340.

CHAPTER SIX

CONCLUSION AND FUTURE STUDIES

6.1 Summary and Conclusions

This project successfully employed a UAV-based imagery system integrated with ML and DL techniques to quantify, assess, and map corn emergence temporally and spatially. The emergence parameters estimated included DAE to determine the emergence time uniformity, plant density to determine the number of emerged plants, and PSstd to indicate the emergence spatial variability. The project comprised three specific studies (Study 1 to 3) conducted at fields practicing certain components of CA (no till, crop rotation, and/or cover crop implementation) to evaluate the capability of a UAV system, with ML and DL techniques in quantifying and estimating the emergence parameters under this practice. Meanwhile, it also consisted of a further investigation extended from the third of the specific studies for two case evaluations, demonstrating the usefulness of UAV imagery in field-scale evaluation and mapping for planting depth treatments and final yield estimation.

This project was performed gradually by first evaluating the feasibility of RGB UAV imagery in detecting corn emergence as early as the first day of emergence in Study 1. Image features extracted from UAV imagery of individual corn seedlings were used to classify the DAE with assessment time of first, second, and third weeks after the first emergence using RF ML models. The findings indicated GSD ranging from 0.55 to 0.94 mm $pixel^{-1}$ was required to detect DAE 1 and 2 seedlings. The UAV imagery and ML model were capable of classifying DAE within a 3-day window (-1 to +1 DAE) for the first two weeks after first emergence (from emergence through two-leaf stage). The

features important to be able to classify the DAE included diameter, area, and SF2 (ratio of major axis length to area).

Then, Study 2 implemented a DL model to segment RGB UAV images of early corn plants (≤ V2 growth stage) at plots and field practicing different CS (minimum-till vs no-till, crop rotation, cover crop implementation) with complex backgrounds of soil and crop residue (from a previous crop and cover crops). The results showed that the precision of image segmentation by the DL model and accuracy of plant density estimation using the segmented images reduced with increasing crop residue (more complex background). Nonetheless, the overall precision was still high for all the CS at 0.87 and the overall accuracy of plant density estimation was comparable with previous similar studies ($R^2 \geq 0.92$; RMSE ≤ 0.48 plants m^{-1}).

Next, Study 3 was conducted in a 2.6-ha field to further evaluate the potential usage of RGB UAV imagery and DL techniques for estimating and mapping corn emergence parameters at a field scale with planting depth treatments. From the first study, there were limitations in using UAV imagery and ML models in classifying the DAE, i.e., a very high GSD was required to detect newly emerged seedlings and moderate classification accuracies were obtained in classifying individual plants. On the other hand, the second study demonstrated better performance of using DL models in processing UAV imagery. Hence, this third study adapted a DL model for estimating the emergence parameters in a 1-m area instead of individual plants. Besides DAE and plant density, another parameter indicating the spatial variability, i.e., PSstd was added. Results indicated an improved accuracy (≥ 0.97) in estimating DAEmean and plant density, while for PSstd, the accuracy was 0.73. The RMSE for each parameter was low: 1.06 days, 0.39

plant m^{-1}, and 2.03 cm m^{-1} for DAEmean, plant density, and PSstd, respectively. The maps and plant emergence evaluation in field conditions indicated the expected trends of decreasing plant density and DAEmean with increasing planting depths and opposite results for PSstd.

Lastly, Study 3 was extended to additional case studies to evaluate the emergence parameters at field scale under different planting depths and replications as case study 1. Results showed that mixed trends of emergence parameters among planting depths at different replications and across the N-S direction of the field, which was mostly affected by elevation (and/or other soil and landscape environmental factors). This variability was unlikely to be captured by a few monitoring sites. Then, in case study 2, multispectral images collected at three early growth stages (V4, V6, and V7) were used to extract VIs as indicators of plant growth variation for yield estimation. The combination of VIs from all the growth stages used as features in a RF ML model was only able to estimate yield with R^2 of 0.34 and RMSE of 560 kg ha^{-1}. Emergence data alone did not show any relation with final yield (R^2 = 0.01, RMSE = 720 kg ha^{-1}).

Overall, the projects served as initial studies to quantify corn emergence date using UAV imagery and ML techniques, segmenting corn UAV imagery with complex background using DL techniques, estimating different emergence parameters for uniformity assessment temporally and spatially under field conditions. The research also evaluated the feasibility of UAV imager and DL models in mapping the emergence, plant early growth, and using VIs as indicators for yield estimation. Eestimating crop emergence and assessing their uniformity at field scale provide more opportunities for other agronomic studies to relate early crop emergence with treatments such as planting

depths, tillage, crop rotation, landscape position, soil variability, and interaction between them as well as final yield. New technologies such as precision planting to place seeds at a precise spacing and depth to ensure uniform emergence will need these emergence performance data in field conditions for further adjustments or improvements. For breeding programs, the spatiotemporal emergence uniformity data may help to better understand the interactions of genotype × environment × management factors. Furthermore, the emergence data will serve as the first information required by farmers in making replanting decisions.

6.2 Future Studies

To fully establish the usage of a UAV imagery system integrated with ML and DL techniques for quantifying and estimating emergence, future studies should be conducted to resolve the limitations of the current project. For individual plant emergence quantification, more image features (besides size and shape) including reflectance and 3D structure could be included to further differentiate plants emerged at different days. Moreover, other environmental data such as soil and weather affect plant morphological features. Hence, features such as growing degree days (calculated based on weather) as well as soil temperature and moisture data (from soil sensors inserted in the soil) should be included to further improve the classification accuracy.

For image segmentation and emergence parameter estimation using DL models, more validation studies should be conducted in fields planted with similar or other cropping systems at different locations and years to produce more robust models or used as pre-trained models for other researchers. An interactive framework can be developed to include the models as pre-trained models and users (e.g., farmers and researchers) can

input fewer images for training; thus in a shorter time obtaining final outputs of the segmented images or estimated emergence parameters maps. Meanwhile, for yield estimation, more timely UAV data will be needed to examine the growth variation along the season and environmental data such as weather and soil properties should be included. Other types of DL models such as recurrent neural networks should be explored to process and analyze these time-series data.

APPENDIX

Table A1: Stitching workflow and parameter set in Agisoft Metashape Professional to produce the orthomosaic of the field.

Stitching Workflow	Parameter
Align Photos	Accuracy: High; Generic preselection: Yes; Reference preselection: Source
Build Dense Point Cloud	Quality: High; Depth filtering: mild
Build Mesh	Source data: Dense cloud; Surface type: Height field; Depth maps quality: Medium
Build Orthomosaic	Surface: Mesh; Blending mode: Mosaic

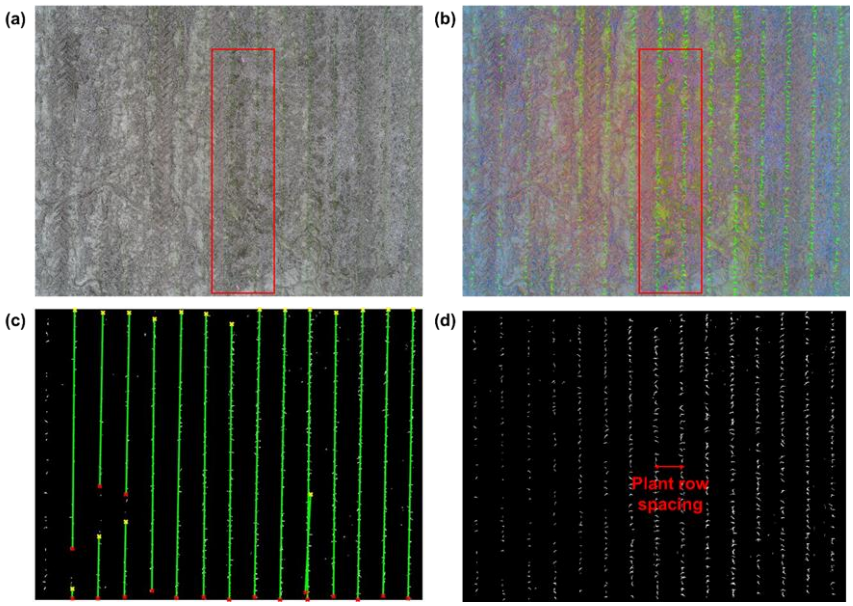

Figure A1. Demonstration of image processing steps to determine actual ground sampling distance: (a) original image; (b) enhanced image using decorrelation stretch; (c) binary image showing line detected by standard Hough transform; and (d) rotated binary image to determine the plant row spacing in pixels. The red box shows the monitoring site marked by two flags.

Bounding box of ROI × Centroid of ROI

Different colors boxes represent segmented image in image size ranged from 0.9 to 1.1 m²

(a) Label for Each ROI

ROI ID	Stand Count	DAE	cx	cy
75	1	19	442	945
76	1	19	438	1021
77	1	19	438	1132
78	1	19	440	1210
79	1	15	436	1277
80	1	18	434	1321
81	1	19	436	1382
82	1	17	442	1440
83	1	19	429	1571
84	1	18	435	1615

(b) Label for Each Segmented Image

ROI	Plant Density	DAEmean	PSstd
75 – 79	5	18.2	5.1
76 – 80	5	18.0	7.4
77 – 82	6	17.8	3.4
78 – 82	5	17.6	2.6
79 – 84	6	17.7	9.8
80 - 84	5	18.2	10.5

Figure A2. Illustration of labeled image preparation with (a) label for each ROI including the ID, stand count, days after first emergence (DAE), and centroid coordinate (cx and cy) used for plant spacing (PS) estimation; (b) final label for each segmented image (label image) for plant density, mean days to imaging after emergence (DAEmean), and standard deviation of PS (PSstd) in 1-m row segments.

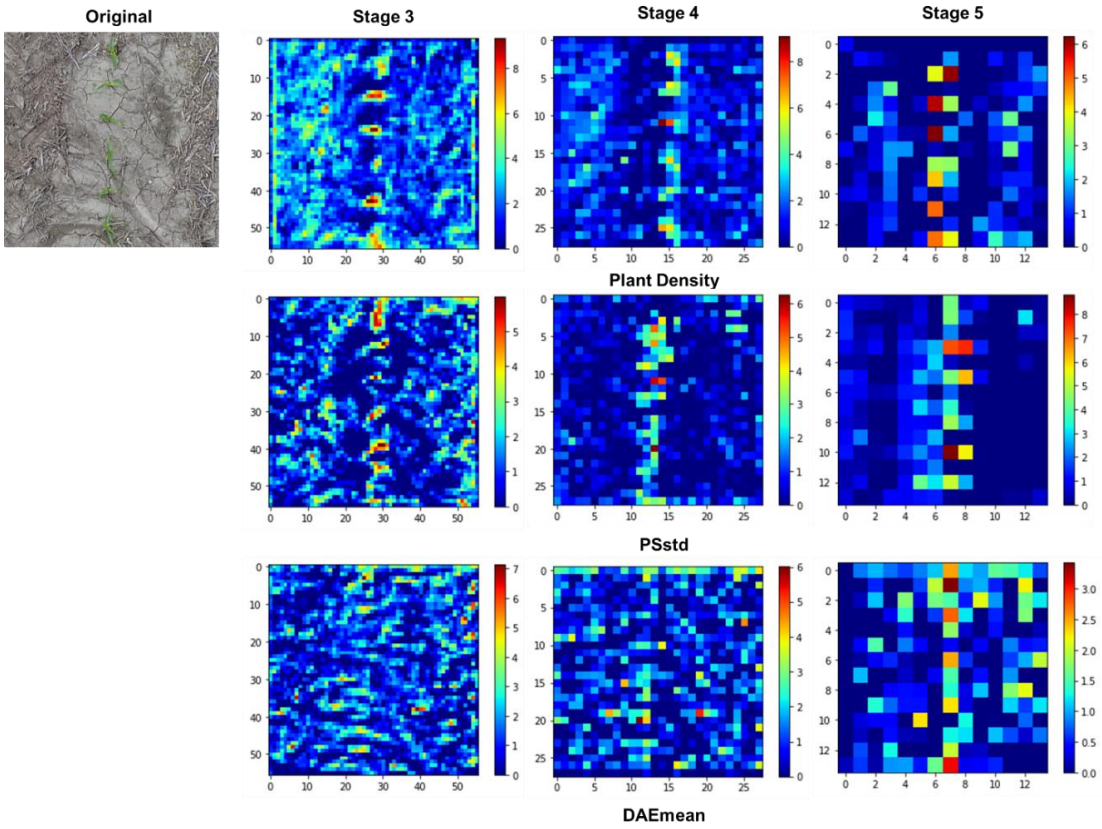

Figure A3. Features maps of one example image from the sequential UAV images collected with no color stake labeling in stages 3 to 5 of the ResNet18 model for the three emergence parameters: plant density (top row), standard deviation of plant spacing (PSstd, middle row), and mean days to imaging after emergence (DAEmean, bottom row).

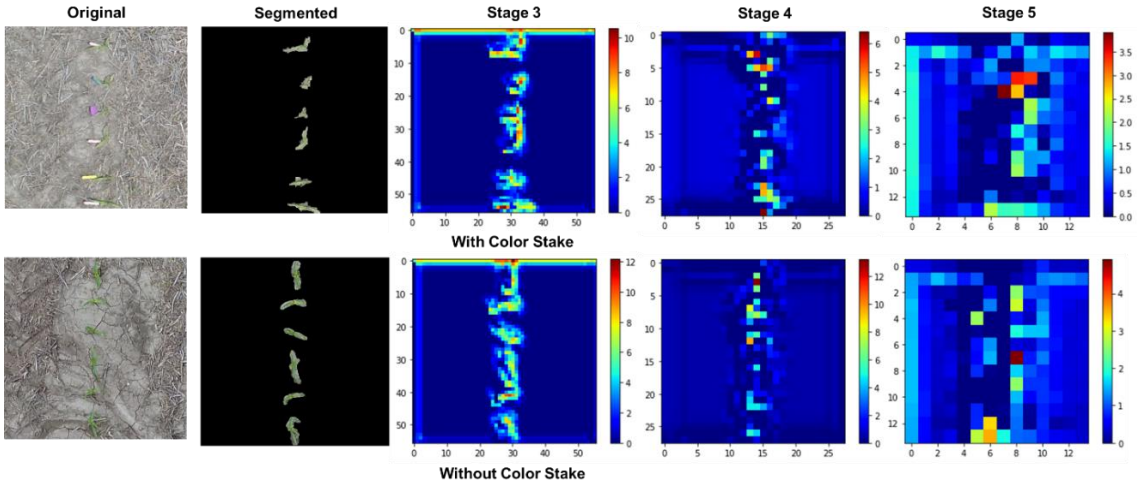

Figure A4. Features maps of segmented images with (top row) and without (bottom row) color stake labeling in stages 3 to 5 of the ResNet18 model for the parameter mean days to imaging after emergence (DAEmean). The actual and estimated DAEmean for the image with a color stake are 17.2 and 16.5 days, respectively.

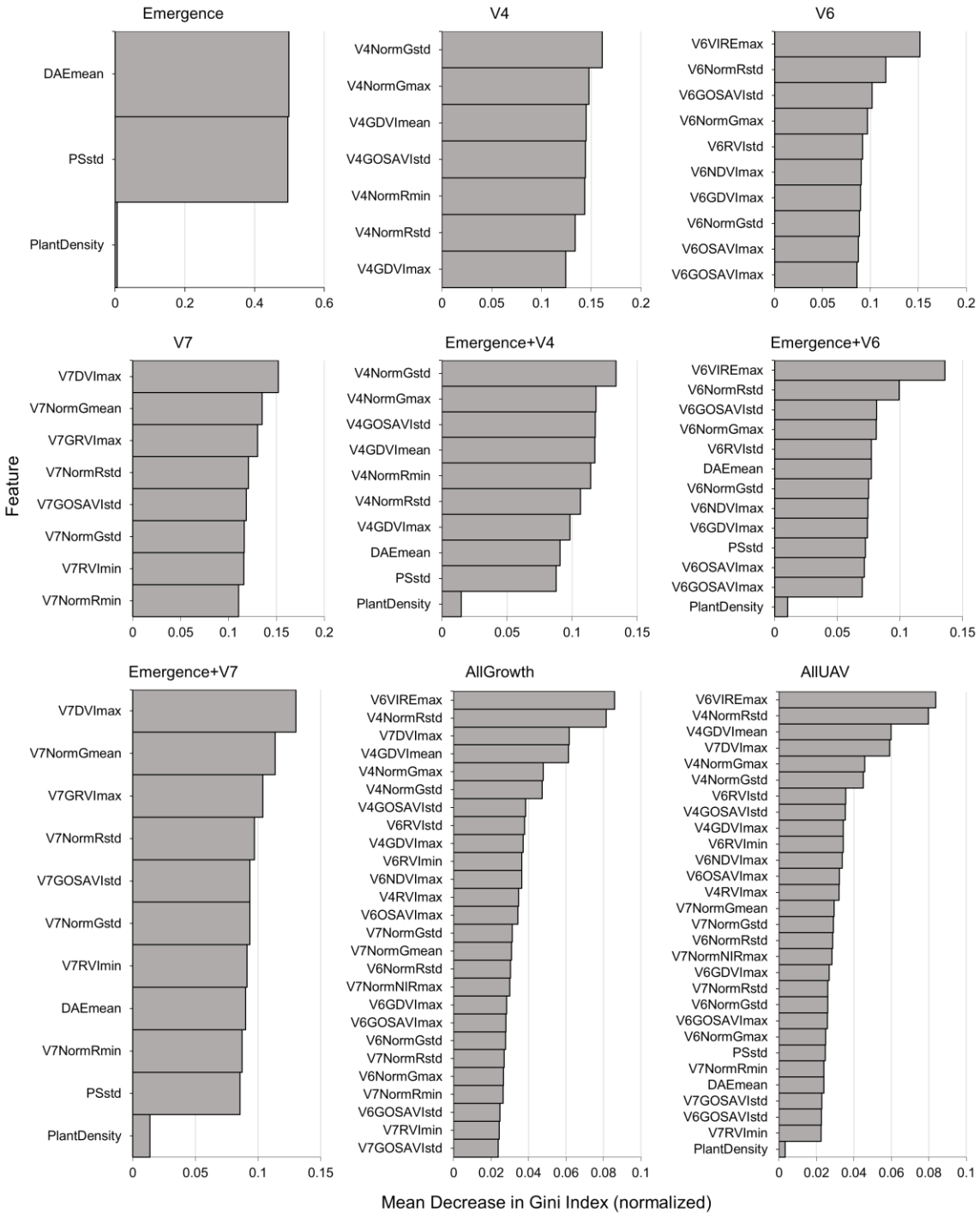

Figure A5. Variable importance plots of UAV feature datasets without planting depths.

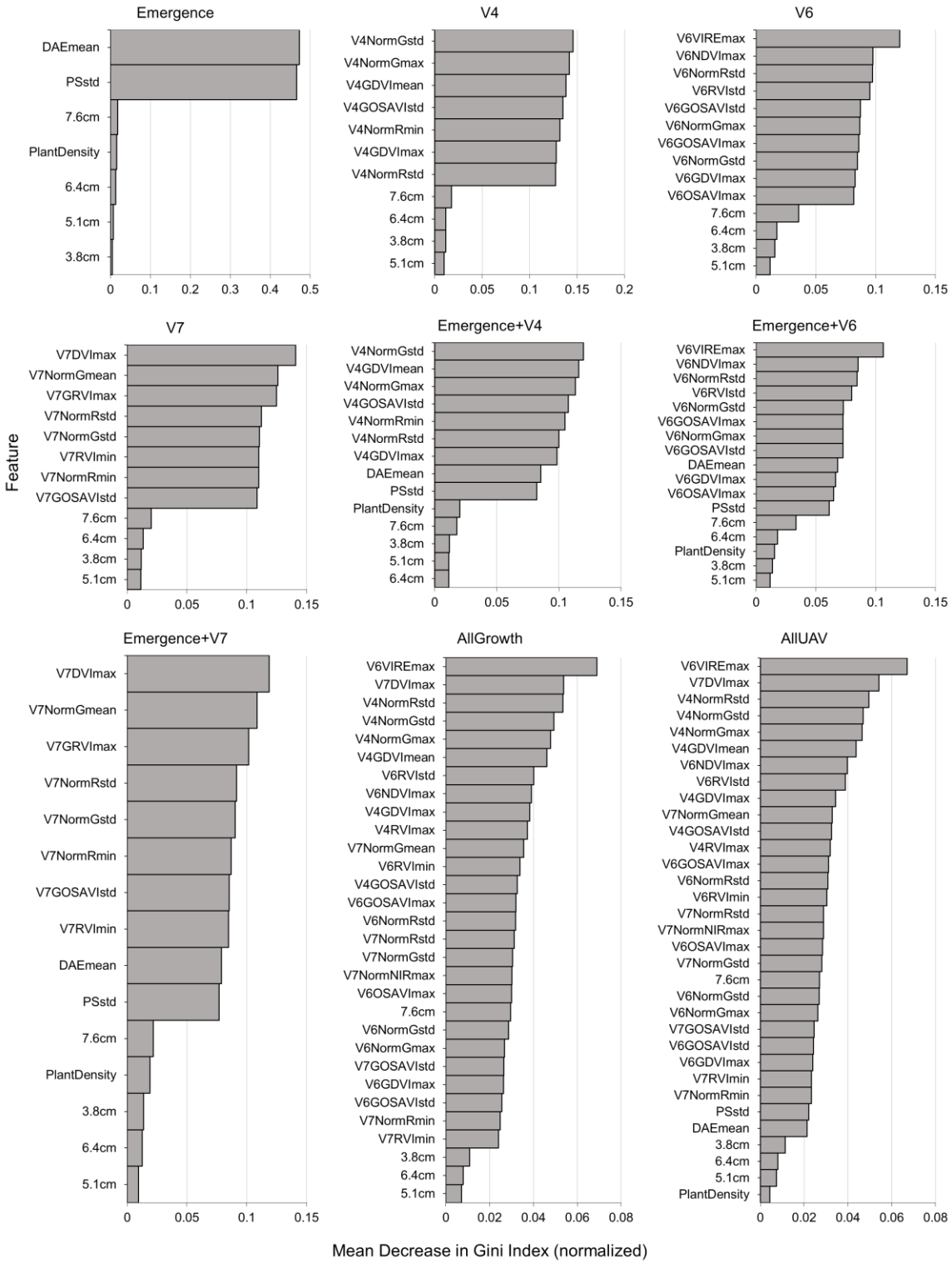

Figure A6. Variable importance plots of UAV feature datasets with planting depths.

VITA

Chin Nee Vong was born in January 1990 in Melaka, Malaysia. She obtained her Bachelor of Engineering in Agricultural and Biosystem from University Putra Malaysia (UPM) in year 2014. After working for half a year as a research assistant in UPM, she came to United State for graduate school and received her Master of Science in Agriculture (Plant and Soil Science) from Arkansas State University in year 2017. She then joined the College of Agriculture, Food & Natural Resources in University of Missouri to pursue her PhD degree in Food and Hospitality Systems (Agricultural Systems Technology) from 2018 to 2022. She has been involved in several research projects, including using unmanned aerial system (UAS/UAV) based remote sensing technology for forage quality and quantity assessment, high throughput crop phenotyping and soil organic carbon estimation. Her research focuses include remote sensing, image processing, precision agriculture, GIS application, machine learning, and deep learning. She is interested in utilizing and developing methods, techniques, and systems to address agricultural issues.